Universitat Autònoma de Barcelona

On the Longevity, Quantum Decay and the role of Oscillons in Dark Matter

Jan Ollé Aguilera

Universitat Autònoma de Barcelona

Institut de Física d'Altes Energies

A member of: BIST Barcelona Institute of Science and Technology

A center of: Institució CERCA Centres de Recerca de Catalunya

On the Longevity, Quantum Decay and the role of Oscillons in Dark Matter

A thesis presented for the degree of
Doctor of Physics by:

Jan Ollé Aguilera

Director: Prof. Oriol Pujolàs Boix
Tutor: Prof. Alex Pomarol Clotet

April 7, 2022

Acknowledgments

They say that doing a PhD is like running a marathon, and that slow and steady wins the race. The reality is that it is more like a long obstacle race, where innocently looking hurdles take much longer to surpass than what you previously thought. Indeed, a constant feeling during these four years has been that days, weeks, and even months passed without a sglimpse of progress. Yet here we are.

Getting through the finish line would not have been possible running alone, and I have benefited from a multitude of people that, in one way or another, have made this task more surmountable while also having fun in the process.

First off, I would like to thank my supervisor Oriol for his guidance and mentoring during all these years. What started as a summer project in 2015 has finally matured enough to be worth a PhD. Thank you for your constant flow of ideas and for giving me the space and the drive to pursue my own research interests.

To my collaborators of the papers included in this thesis: Fabrizio, George and Tanmay, to the ones that are not: Andreu, Axel, Dario, Jeff and Joonho, and to the ones for which our first paper together is not that far away: Evangelos, Ruth and Yaron. I am grateful for the constant stimulating exchange of ideas and for the always friendly and supportive working atmosphere.

Much part of this work has taken place at IFAE and UAB, where I have found a group of excellent people that have provided me with a wonderful environment. Special thanks to the group of IFAE PhD students, both the ones that were there when I first started in 2018 and to the ones that I leave behind today. Thank you for all those very much needed coffee breaks filled with laughter and weird stories.

I have also been able to move around the world and work in places where I had never been before. Wherever I have ended up going I have found superb human beings which I can now call friends. Tank you to Mateo, Ana, Alfredo, Uriel and all the other guys and girls that I met while my time at Trieste. Those were specially uncertain times for me and I can say I had a blast thanks to you guys. To Dario, Morena, Enea and their wonderful cats whose affection I had to earn, and to the rest of the PCS IBS staff, thank you for taking such good care of me during my time in Korea. Being able to travel once again after lockdown had never felt so great. Finally, thanks Matteo for inviting me to Madrid and for putting me in touch with the right people.

I am here today because of where I have been in the past, and before the PhD I was in Oxford, where I met some of what are now my best friends today. Despite the intensity, I only keep good memories of that year. I want to specially thank Winston, Andrea, Ragnar, Diego, Tere (and family) and Liyang for your friendship and to the rest of the 2016/17 students of the MMathphys programme for the time we spent together.

Almost as important as working is resting, without which keeping a steady pace would have been impossible. For this I am immensely grateful to the amazing *KickAss Team* of Sant Cugat, of which I am very proudly a part of. The first lockdown was bearable thanks to our everyday online workouts. Thank you for all the other countless times we've had fun together, as well as for helping me completing (real) obstacle races. Our friendship is one of the things I treasure the most.

Speaking of which, the greatest treasure of all, the *One Piece*, by Eiichiro Oda, has never failed to keeping me looking forward to next week. If you are a fan of the series you know what I'm talking about, and if you're not I urge you to read it. It's a monumental piece of fiction of our current time with more than 25 years in the making that has all my respect and appreciation.

They say that friends are the family that you choose, but I am really fortunate for the family that I didn't choose. A special thanks to my parents Sílvia and Lluís and to my brother Xavi. To my parents, thank you for always making my education a priority. I am here today thanks to your constant sacrifices and long years of work. To the rest of my family: uncles, aunts, cousins and grandparents Trini and the ones that left too early, a piece of this thesis is also yours.

Next, I want to thank my cat Sami for being such an adorable floof and an anti-stress sleeping (but sometimes also awake) bag. And last but not least, I want to thank my partner Carla for accompanying me during the latter part of this journey. My heart is yours.

Abstract

In this thesis we study several properties and applications of oscillons, localized semi-classical bound states of large numbers of bosons that appear in simple theories with attractive interactions and that are surprisingly long-lived. They have been a topic of recent interest in high energy physics due to their rather broad applications in inflation, dark matter and particle physics. The main contributions in this thesis are the following: (i) An advancement in our understanding behind the mechanisms that allow oscillons to be so remarkably long-lived, (ii) The impact that such long-lived oscillons have in dark matter models of ultra-light axion-like particles, which had been ignored before, and (iii) A calculation of the quantum radiation emmitted by oscillons using a recent method that allows to have a complete treatment of backreaction. At the more technical level and related to (i), a novel numerical method has been developed for oscillons with extreme longevity that allows to simulate them on otherwise unreachable timescales. The lifetime of oscillons is a significantly model-dependent quantity, and in the context of (i) and (ii) we provide numerical evidence for models with oscillons with lifetimes as large as 10^9 cycles, and even longer. Oscillons composed of ultra-light scalars can decay around or after matter-radiation equality and can thus act as early seeds for structure formation. In some cases, their lifetime is large enough for them to survive until today, in which case they can play a significant role in dark matter. Remarkably, the richness of their properties arise from simple physical mechanisms, which make them very interesting objects to study on their own.

Preface

This thesis is submitted for assessment in partial fulfillment of the Doctor of Physics degree of the Universitat Autònoma de Barcelona and consists of a collection of papers that I have published in peer-reviewed international scientific journals, which are listed below. Each chapter of the thesis corresponds to a different paper and is therefore self-contained.

[A] Jan Ollé, Oriol Pujolas, Tanmay Vachaspati, George Zahariade, "Quantum Evaporation of Classical Breathers", DOI:10.1103/PhysRevD.100.045011, e-Print: arXiv:1904.12962 [hep-th]. Phys.Rev. D100 (2019) no.4, 045011.

[B] Jan Ollé, Oriol Pujolas and Fabrizio Rompineve, "Oscillons and Dark Matter", DOI:10.1088/1475-7516/2020/02/006, e-Print: arXiv:1906.06352 [hep-ph]. JCAP 02 (2020), 006.

[C] Jan Ollé, Oriol Pujolas and Fabrizio Rompineve, "Recipes for Oscillon Longevity," DOI:10.1088/1475-7516/2021/09/015, e-Print: arXiv:2012.13409 [hep-ph]. JCAP, vol. 09, p. 015, 2021.

Jan Ollé Aguilera
Universitat Autònoma de Barcelona, April 7, 2022

Contents

Part I

Introduction

1 A Brief History of Bound States

The chronicle of bound states is a tale as old as physics itself, and the contemporary way of understanding them can be traced back to the Book 1, *De motu corporum* (On the motion of bodies) of Newton's *Principia*. The idea is simple: attractive interactions between two (or several) bodies lower the total energy of the system and thus the preferred state becomes localized. This energy difference is called *binding energy*.

Bound states are ubiquituous in nature: from galaxy clusters and stars to microscopic objects such as molecules and baryons. In the context of classical mechanics, the first example was perhaps the motion of the Moon around the Earth, or put in Newton's framework, on the "motion of bodies drawn to one another by centripetal forces". Let's thus begin by considering the Earth-Moon system. Both Earth and Moon will be described as classical point particles of mass M_1 and M_2 respectively. In the absence of interactions between them, each of their energies is given by the kinetic energy $T = M^2v^2/2$, and the total energy of the system becomes

$$E_{\text{free}} = \frac{1}{2}M_1^2v_1^2 + \frac{1}{2}M_2^2v_2^2 \ . \tag{1}$$

However, Newton taught us that there is an attractive force between two massive bodies that follows an inverse-square law with the distance between them. In more modern terms, there is a gravitational interaction between them, which lowers the total energy (1) to become

$$E = E_{\text{free}} - G\frac{M_1M_2}{r} \ , \tag{2}$$

where G is Newton's gravitational constant. Since $E_{\text{free}} < E$, the Earth and the Moon can never escape from one another. In other words, they form a bound state. While elementary, this example illustrates the basic pattern

$$E = E_{\text{free}} - E_b \ , \tag{3}$$

where E_b is the binding energy of the system. This pattern will remain for more complicated systems and serves as a useful picture for the logic behind the physics of bound states.

In the Newtonian descripition this bound state is stable, i.e. a state that if left unperturbed will last indefinitely. However, we now know that gravitationally bound binary systems radiate energy in the form of gravitational waves, and its energy loss $\dot{E}$ can be estimated by [1],

$$\dot{E}_{\text{GW}} \sim \frac{G^4\mu^2(M_1+M_2)^3}{R^5} \ , \tag{4}$$

where R is the distance between the Earth and the Moon and $\mu \equiv M_1M_2/(M_1+M_2)$ is the reduced mass of the system. This energy loss has to be compared with the gravitational binding energy $E_b = GM_1M_2/R$ to extract the decay rate

$$\Gamma_{\text{GW}} \sim \frac{\dot{E}_{\text{GW}}}{E_b} \sim \frac{G^3}{c^5}\frac{M_1^2M_2}{R^4} \ , \tag{5}$$

where we have restored the appropriate powers of the speed of light. Numerically, (5) gives the estimated rate $\Gamma_{\text{GW}} \sim 10^{-35}\ s^{-1}$. The inverse of this rate sets the lifetime of the Earth-Moon bound

system, and it far exceeds the age of the universe. Obviously, the death of the Sun sets a much smaller timescale ($\sim 10^{17}$ s) after which both the Earth and the Moon will cease to be. Moreover, we are modelling both objects as point particles, and other well-known phenomena such as tidal acceleration could alter this result. Here we simply want to show that even in the most simplified model of this system, gravitational interaction is both the binding mechanism *and* the responsible one for the demise of the bound state by radiation emission.

More generally, bound states come with a *lifetime* τ which is the characteristic timescale after which the system, for whatever reason, will no longer be in the original bound configuration. On the other hand are *stable* bound states and are those that have an infinite lifetime. This happens only in the cases where there is a *symmetry* that protects such a state from decaying to another one as it evolves in time. Familiar examples of stable bound states are the proton and atoms in general, which are stable by baryon number conservation. Another example to be further discussed later are topological solitons, which are protected by topological number conservation. And also related to the latter are breathers in the $(1+1)$-dimensional sine Gordon model, which are stable by the theory being integrable and thus providing an infinite number of conserved quantities. Oscillons are examples of bound states that decay, but interestingly, breathers (which are stable) are a special limiting case of oscillons.

How long-lived a bound state is can be quantified by the dimensionless quantity τ/T, where τ is the lifetime and T is the characteristic timescale of the problem. It is clear that, by definition, bound states must satisfy $\tau/T > O(1)$. In general, however, the wide diversity of bound states make their lifetimes a rather non-trivial and interesting quantity to calculate. It will be very model dependent, it will scale non-trivially with the couplings of the theory and it will depend on the particular dynamics of the system, in many cases requiring numerical simulations. For instance, in the Earth-Moon example, the ratio τ/T is ridiculously large, $\tau/T \sim 10^{28}$, which can be explained by the motion of the system being non-relativistic and by the weakness of gravity.

Another interesting example is positronium[1]: an electron and a positron forming a (Hydrogen-like) bound state in Quantum Electrodynamics (QED). There are two positronium spin states: a singlet state ($S=0,\ M_S=0$) called para-positronium and a triplet state ($S=1,\ M_S=-1,0,1$) called ortho-positronium.

Decay rates can be estimated in general by using the well-known formula

$$\Gamma \sim v\sigma n \ , \tag{6}$$

where σ is the scattering cross section associated to the proccesses that generate outgoing states energetic enough to escape from the localized region, n is the number density and v the typical velocity of the particles inside the bound state. Para-positronium can decay into any even number of photons, with 2 photons being the dominant decay channel, which gives a cross section $\sigma \sim \alpha^2/(vm_e^2)$. The v in the denominator of σ gets cancelled by the one appearing in (6) and this quantity is enhanced by three inverse powers of the Bohr radius, $n \sim {a_0}^{-3} \sim (\alpha m_e)^3$. All in all, one gets $\Gamma_p \sim \alpha^5 m_e$, which correctly matches the scaling that is observed in experiments [2] and where we have used the subscript p to denote para-positronium. On the other hand, ortho-positronium mostly decays into 3 photons (so $\sigma \sim \alpha^3$ in this case), leading now to $\Gamma_o \sim \alpha^6 m_e$, which is also matched nicely by experiment.

[1] The generic name given to a bound state of particle-antiparticle is *onium*.

In both the Earth-Moon system and positronium, both the binding mechanism and the decay channel is controlled by the same interaction: gravity in the former and QED in the latter. In general, however, these could be different, as is the case for pionium: a π^+-π^- electromagnetic bound state whose dominant decay channel is via strong interaction into two neutral pions. The cross section will now have the form $\sigma \sim \delta_s^2/m_\pi^2$, with δ_s some dimensionless quantity coming from QCD (Quantum Chromodynamics), while $n \sim (\alpha m_\pi)^3$. This leads to an estimated decay rate of $\Gamma \sim \alpha^3 m_\pi \delta_s^2$, which nicely captures the correct α^3 dependence. The unknown δ_s factor coming from QCD is usually called $a_0^0 - a_0^2$ in the literature [3, 4], it takes into account isospin breaking effects and can be computed using standard chiral perturbation theory.

In the context of field theory, the simplest models that one can consider are those of a single real scalar field ϕ, given by

$$\mathcal{L} = \frac{1}{2}\left(\partial_\mu \phi\right)^2 - V(\phi) \ , \tag{7}$$

where $V(\phi) = m^2\phi^2/2 + \dots$ defines the self-interactions of the scalar field. Within these, formation of bound states requires attractive self-interactions, which can be framed as

$$V(\phi) < \frac{1}{2} m^2 \phi^2 \ , \tag{8}$$

and then allow states with an energy following the bound state formula (3) to form. Oscillons are within these class of states, and their lifetime and other properties will depend on the particular shape of the potential $V(\phi)$, often requiring numerical simulations. In addition, oscillons are states populated by a large number of particles, making community[2] their particular survival method.

1.1 More is Different

More often than it would be desirable, knowledge of the underlying physics of a system is not enough to solve the equations that govern its behaviour. A well-known example of this was also immediately found by Newton in his Book 1 of the *Principia* when adding the Sun to the Earth-Moon system. This innocent modification lead to the inexistence of generic closed-form solutions for the dynamics of the Earth-Moon-Sun system, a phenomenon that is generic to N-body problems in general. The main reason why this happens is that there are not enough symmetries that constrain the (larger number of) degrees of freedom of the system enough to reduce its description to a closed-form formula. In these situations the dynamics of the system become chaotic for most initial conditions and numerical methods are generally required, see Fig.1.

Taking the limit of a very large number of particles often simplifies the problem dramatically. This observation has been exploited in statistical physics, with progress coming from the fact that the collective motion of such an enormous number of microscopic degrees of freedom can be correctly

[2] An unrelated but very interesting example of a similar situation is the way emperor penguins survive the long, cold and dark Antarctic winters. Emperor penguins have developed a social behaviour that when it gets cold, they cluster in groups of several thousand penguins. The surface area to volume ratio of the group is greatly reduced and lots of warmth conserved. Of course it is not so great for the individuals on the boundary of the group as they are quite exposed to the extreme cold. So, to survive, there is a continual movement of penguins from the outside of the group to the center, displacing the warmer and more protected penguins to the outside in a continuous fashion. While a single penguin would not make it through the winter, this mechanism allows the group to remain at an impressive constant 38°C body temperature all winter without eating, albeit they lose $\sim 40\%$ of their body fat.

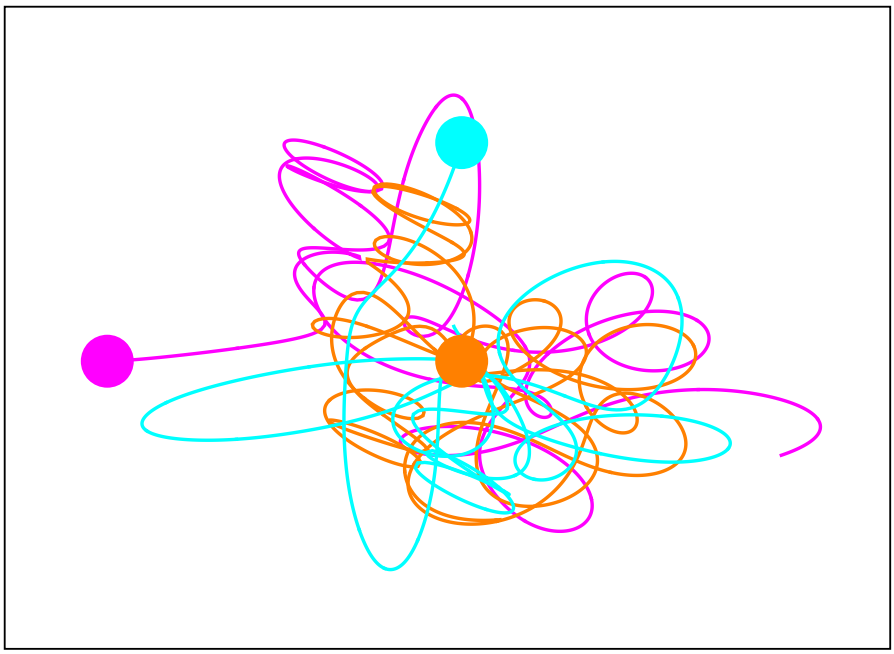

Fig. 1: Example of the trajectories for 3 equal mass bodies interacting gravitationally, generated by solving the equations of motion numerically. The filled circles indicate the initial positions of each mass, distinguished by each having a different color in the picture. A very slight modification of the initial conditions can lead to very different trajectories, a generic feature of chaotic systems.

captured from far fewer macroscopic ones that emerge as a combination of all the former. One then may treat the microscopic variables as random variables and the law of large numbers then guarantees that the macroscopic variables will hold predictive value. The point then is that by treating the number of particles N as a parameter that we can vary, this may lead to the emergence of alternative degrees of freedom that describe the system better.

In quantum systems, the average number of quanta (or occupation number) N plays an even more important role since one expects that for large enough N "quantumness" itself is lost. Here the two quantities that must be compared are the action S and $\hbar$. Typically one formally takes the classical limit as $\hbar \to 0$, but this can be alternatively seen as a high-occupation limit. Indeed, this picture emerges from how the action scales with the occupation number, which is $S \sim \hbar N$. Thus, since classical objects are in the $N \gg 1$ regime, the ratio of S and $\hbar$ is large, and the usual saddle-point approximation is well-justified. However, this intuition that there might be some "critical" N above which the dynamics "classicalizes" has been challenged since the early days of quantum mechanics with the prediction (and posterior discovery) of Bose-Einstein condensates, where quantum mechanical phenomena become apparent macroscopically. And this was just the first of many other "macroscopic" quantum effects such as superconductivity, the Quantum Hall effect or topological quantum phases of matter. More recently, the idea that the quantum properties

of black holes can be understood as arising from a large-N description where the black hole can be seen as an effective Bose-Einstein condensate of gravitons [5–7] has provided a new theoretical umbrella under which other lumps such as solitons, instantons and oscillons can be put on the same footing.

Using this corpuscular description of quantum bound states, we have been able to obtain analytic estimates of the oscillon lifetime in terms of the couplings and parameters in the potential that defines the theory. While this is one of the results of Paper C, we find it appropriate to give a summary of this method here, as the same logic can be applied to other bound states, to which we will refer generically as *lumps*. The starting point is that classical field solutions can be re-interpreted as mean-field descriptions of the (bosonic) quantum field in the Bose-Einstein condensate limit, that is when there is a large occupation number of the same state. We thus consider the simplest classical field theory with an attractive self-interaction, defined by

$$V(\phi) = \frac{1}{2}m^2\phi^2 - g_4\phi^4 + \cdots \ , \tag{9}$$

where g_4 is taken to be positive to satisfy (8) and where $\cdots$ contain higher powers of ϕ that are needed to stabilize the potential but that are unimportant for the following argument.

A large-N description requires exploring the non-linear regime of (9), which is set by the scale $\phi^2 \sim m^2/g_4$. We can thus estimate the typical energy of a spherically symmetric (oscillon) configuration of typical size $R \sim m^{-1}$ around such non-linear field value as

$$M_{\rm osc} \sim g_4 \left(\frac{m^2}{g_4}\right)^2 m^{-3} = \frac{1}{g_4}\ m \ . \tag{10}$$

Since the energy of this object scales inversely with the coupling g_4, this is a non-perturbative object. Secondly, in the weak-coupling limit $g_4 \ll 1$ this can be viewed as composed of a collection of N quanta, $M_{\rm osc} \approx Nm$. Here, despite the weakness of the coupling, a strong *collective coupling* defined as $\lambda = Ng_4$ arises [5–7], which then makes each of the N quanta to feel a strong interaction and are unable to escape from the lump.

Since the N quanta basically occupy the same state, one can identify the wavelength of the occupied quantum state with the lump radius, R, which we expect to be around[3] $1/m$. A heuristic way to obtain this result using the corpuscular description is to picture that the scalar field quanta are trapped (dynamically) inside a spherical box of radius R. This trapping then lowers the mean energy per quanta from m to

$$\omega = \sqrt{m^2 - R^{-2}} \ , \tag{11}$$

or, in the spirit of (3),

$$\omega = m - \Delta\omega \ , \tag{12}$$

with

$$\Delta\omega \approx \frac{1}{2mR^2} \ , \tag{13}$$

[3]Numerically, one typically has an oscillon radius closer to $\sim 5\ m^{-1}$, which can then be used to improve the estimate (10) to match better what is found in simulations.

which is the usual non-relativistic relation between energy $\Delta\omega$ and momentum $1/R$ that is obtained from (11) in the small binding energy regime $\Delta\omega/m \ll 1$. The way we estimate the lifetime of such a lump is by viewing it as a finite density concentration of $N \sim 1/g_4$ particles and by using the usual formula for the decay rate given by (6). The number density is simply $n = N/V \sim 1/(g_4 R^3)$. The typical speed of the quanta is also easily estimated through $v \sim p/E$, with $p \sim 1/R$ and $E \sim m$, i.e. $v \sim 1/(mR)$ in the small $\Delta\omega$ regime. The main process that endows the quanta with enough energy to escape are $3 \to 1$ conversion processes, and it has an estimated cross section $\sigma \sim N g_4^2/m^2 \sim g_4/m^2$. Collecting all the pieces, one arrives at

$$\Gamma \sim \frac{1}{mR}\frac{g_4}{m^2}\frac{1}{g_4 R^3} = \left(\frac{\Delta\omega}{m}\right)^2 m \ , \tag{14}$$

which does not depend on g_4, as expected. The reason is that the field can always be rescaled arbitrarily in (9), which then fixes the magnitude of g_4.

The lifetime τ is roughly the invserse decay rate Γ, so we end up having

$$\tau m \sim \left(\frac{m}{\Delta\omega}\right)^2 \ . \tag{15}$$

This analysis resolves the question that we raised in the previous section, namely *What is the expected value of τ/T for a generic bound state?* What we have seen here is that this ratio is given by (15) for semi-classical (bosonic) lumps in the Bose-Einstein condensate limit and that this is essentially controlled by the binding energy $\Delta\omega$.

While this is a generic estimation for lumps, oscillons in the simplest potentials typically exhibit the following numerical value,

$$\frac{\Delta\omega}{m} \sim 10^{-2} \ , \tag{16}$$

which then leads to lifetimes $\tau m > O(10^2)$. All in all, lifetimes of $O(10^3)$ are understandable using this argument. However, longer lifetimes (which do appear in some models) do not follow from this kind of simple estimate and will require numerics or more sophisticated arguments to understand their properties.

2 Oscillons

While we have motivated oscillons from a corpuscular, large$-N$ bound state perspective, the traditional framework that has been used to define and describe oscillons has been that of non-linear wave equations, which we may adopt for a while. Oscillons are then long-lived, localized and oscillating solutions of non-linear wave equations. They were originally dubed *pulsating solitons* or *pulsons* in the 1970s [8–10] and were then rediscovered by Gleiser and collaborators in the 1990s [11, 12], after which the *oscillon* terminology became standard.

The historical *pulsating soliton* name suggests they are some kind of soliton, and even though oscillons and solitons are related, there is an important distinction to be made. Let's thus briefly discuss what is a soliton. Quoting [13], the story goes as follows:

"Solitons were first discovered by a Scottish engineer, J. Scott Russell, in 1834 while riding his horse by a water channel when a boat suddenly stopped. A hump of water rolled off the prow of

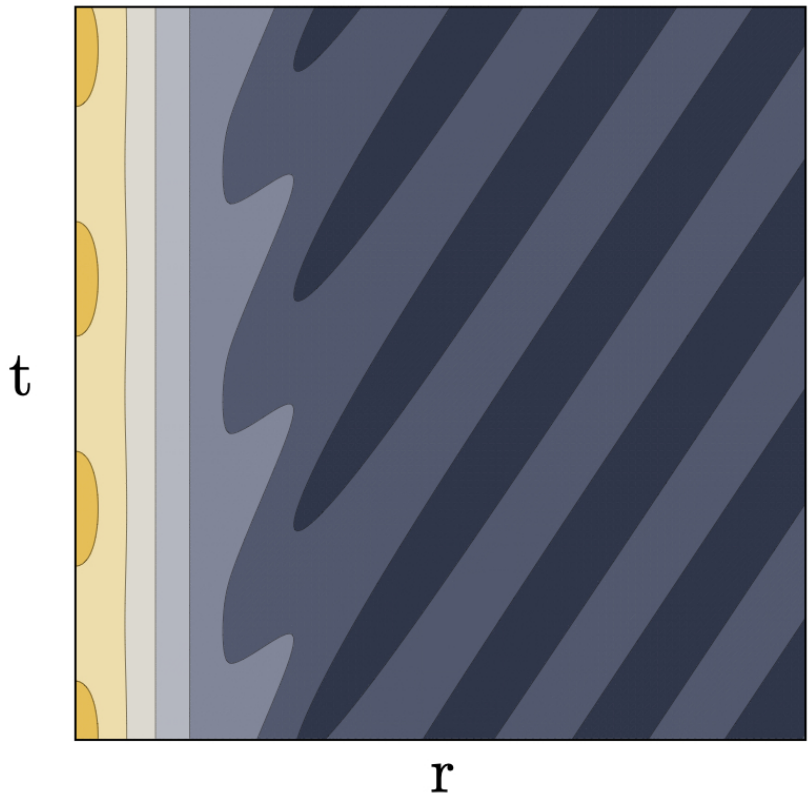

Fig. 2: Cartoon of the typical energy density distribution of an oscillon. r is the radial direction in space and t is time. One sees a clear separation between the core, here taking yellowish colours (which indicate large values) and the outgoing radiation at the tail in blue colours (which indicate small values). Radiation decays as $1/r$ but we chose to ignore this fact in this figure for pedagogical purposes.

the boat and moved rapidly down the channel for several miles, preserving its shape and speed. The observation was surprising because the hump did not rise and fall, or spread and die out, as ordinary water waves do."

Solitons are wave configurations that don't dissipate as they travel with constant velocity. Like oscillons, they are localized non-linear wave phenomena, even though strictly speaking solitons are by definition stable whereas oscillons are unstable but extremely long-lived nonetheless. Solitons are static solutions in their rest frame, while oscillons display a series of quasiperiodic oscillations around some characteristic frequency ω. Oscillons are long-lived in the sense that they decay in timescales $\tau \gg \omega^{-1}$. In more than one spatial dimension they are spherically symmetric objects and they decay by slowly emitting linear spherical waves in a very inefficient way. Since these waves carry a tiny fraction of the total energy of the system, this process can carry on over large timescales. Oscillons are thus characterized by a core and a tail. The core is the localized region where the large majority of the total energy is stored and is roughly given by $R \sim \omega^{-1}$. The tail refers to the outgoing radiation. A useful sketch of the typical energy density distribution of an oscillon is shown in Fig.2.

Many efforts in this thesis have been devoted to understanding the longevity of oscillons. More

specifically, given some model that supports oscillons, how large is the quantity τm? Is it $O(10^3)$, $O(10^8)$, or more? And why? Is there a clear dependence on the couplings of the theory? These are relevant questions on their own, but they become much more important in the context of cosmology where the energy density content of the Universe essentially dictates its evolution. We will begin by studying oscillons in the sine-Gordon theory in (1+1) dimensions. Even though this is an exceptional theory with absolutely stable oscillons, it is still useful as a theory laboratory to understand many of the generic properties of oscillons in other models and different number of dimensions. Moreover, it is the central model that we have studied in Paper A.

2.1 The sine-Gordon model in $(1+1)$ dimensions

Traditionally, the model that is used to understand many of the properties of both oscillons and solitons as well as their relationship is the $(1+1)$-dimensional sine-Gordon (sG) model. This is a field theory of a single scalar field in one spatial dimension with the following Lagrangian:

$$L = \int dx \left[\frac{1}{2}(\partial_\mu \phi)^2 - \frac{m^2}{\beta^2}\left(1 - \cos(\beta\phi)\right) \right], \tag{17}$$

where m is the mass parameter and β is a dimensionless quantity that sets the periodicity scale of ϕ. The solitons in this model are called kinks, and are configurations that interpolate between neighboring vacua $\phi_n = 2\pi n/\beta$ of the sine-Gordon potential. The kink that interpolates between the $[0, 2\pi/\beta]$ vacua is

$$\phi_k(x) = \frac{4}{\beta}\arctan\left(e^{mx}\right), \tag{18}$$

which can be checked to satisfy the Euler-Lagrange equation of motion (EoM) associated to Eq.(17). Important things to notice is that this is a non-trivial static solution of the EoM. Furthermore, it is localized in a region $\ell \approx m^{-1}$, and has an energy $E_k = 8m/\beta^2$.

Interestingly, a solution interpolating now from 2π to 0 also exists, it is called the antikink and is obtained from Eq.(18) by replacing $x \to -x$, but is otherwise identical to the kink. In general, kink states interpolate between increasing neighboring vacua, i.e. from $2\pi n$ to $2\pi(n+1)$, while antikinks do so for decreasing neighboring vacua, i.e. from $2\pi n$ to $2\pi(n-1)$.

Oscillons, called breathers in this model, emerge as a bound state between a kink and an antikink and also have an exact closed formula,

$$\phi_b(t, x) = \frac{4}{\beta}\arctan\left[\frac{\eta\sin(\omega t)}{\cosh(\eta\omega x)}\right], \tag{19}$$

where $\eta \equiv \sqrt{m^2 - \omega^2}/\omega$ and $0 < \omega < m$ is the frequency parameter. To see the breather as a bound state of a kink and an antikink, first notice that $\phi_b(t, \pm\infty) = 0$. Second, it's useful to consider the limit $\omega \ll m$. Here, $\max_t|\phi_b(t, 0)| = 2\pi$, which means that for a short period of time the breather almost separates into a kink and an antikink. A picture of the behaviour of breathers is shown in Fig.3 . Finally, the energy of the breather is

$$E_b = \frac{16m}{\beta^2}\sqrt{1 - \frac{\omega^2}{m^2}} = 2E_k\sqrt{1 - \frac{\omega^2}{m^2}}. \tag{20}$$

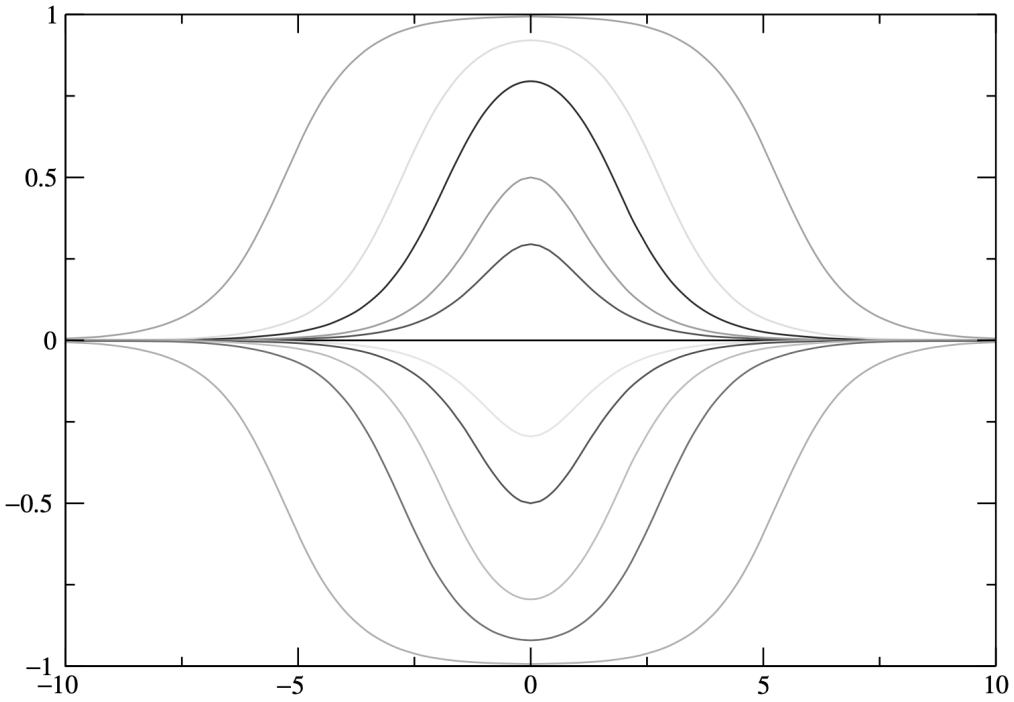

Fig. 3: Reproduced from [13]. The sG breather profile shown at different time slices during one oscillation period as given by (19). It can be seen that at certain times it almost separates into a kink and an antikink at the center, giving visual evidence that a breather is a kink-antikink bound state. Units in this figure are $m = 1$, $\beta = 2\pi$. An oscillon profile would display small wiggles outside of the core corresponding to outgoing radiation.

Since $E_b < 2E_k$, this means that there is a binding energy between the kink and the antikink that makes them bound into a stable breather state. Also, in the static limit $\omega \to 0$, $E_b \to 2E_k$, as expected. It is also worth mentioning that even though the equations of motion to be solved are non-linear, there is a well-defined mathematical prescription to obtain general solutions to these kind of equations that goes under the name of Bäcklund transformations [14] or inverse scattering transformations [15].

Breathers are a very special kind of oscillon. While oscillons end up decaying, albeit in a timescale $\tau \gg \omega^{-1}$, breathers are eternal. This is due to the sine-Gordon model in $(1+1)$ dimensions being integrable, which is equivalent to the statement that its equation of motion admits solutions that are separable, i.e. $\phi(t,x) = f(t)g(x)$. The kink and the antikink are protected from decay by a conserved topological charge Q that arises from the following current:

$$j^\mu = \frac{\beta}{4\pi}\epsilon^{\mu\nu}\partial_\nu\phi \ , \tag{21}$$

where $\mu, \nu = 0, 1$ and $\epsilon^{\mu\nu}$ is the antisymmetric symbol in two dimensions ($\epsilon^{01} = 1$). By antisymmetry

of $\epsilon^{\mu\nu}$, the current j^μ is conserved, i.e. $\partial_\mu j^\mu = 0$, and its zeroth component defines the conserved topological charge

$$Q \equiv \int_{-\infty}^{+\infty} dx\ j^0 = \frac{\beta}{4\pi}\left[\phi(t,+\infty) - \phi(t,-\infty)\right]\ . \tag{22}$$

For the kink, substitution of (18) in (22) gives $Q_k = 1$, while for the antikink we have $Q_{\overline{k}} = -1$. Since stability of kinks (antikinks) are guaranteed by conservation of a topological charge, these are inside the class of topological solitons. The breather, on the other hand, has the same topological charge as the vacuum $\phi = 0$ and it is in principle not guaranteed from this argument alone that it will be stable. However, the sG theory in $(1+1)$ dimensions enjoys from an infinite number of conserved charges [16] which can be seen to arise from a conserved covariant fourth rank tensor current $J_{\mu\alpha\beta\gamma}$ in particular [17].

While so far we have been discussing the properties of kinks and breathers at a classical level, much is also known at the quantum level. However, before jumping into the quantum swimming pool, let's discuss the role of β. Going back to the sine-Gordon Lagrangian (17), by defining a rescaled field $\tilde{\phi} \equiv \beta\phi$, the Lagrangian (17) becomes

$$L = \frac{1}{\beta^2}\int dx\left[\frac{1}{2}\left(\partial_\mu\tilde{\phi}\right)^2 - m^2\left(1-\cos\tilde{\phi}\right)\right]\ , \tag{23}$$

β becomes a global multiplicative factor in the action and thus β plays no role classically. This is no longer true in the quantum version of this theory, as a field rescaling affects the path integral measure $[D\phi]$. In the weak coupling limit $\beta \to 0$, kinks and breathers are non-perturbative (semi-classical) objects since both their energies scale as $\sim \beta^{-2}$. Classical equations of motion, however, lose significance in the quantum regime and it is in principle no longer clear that kinks and breathers will be stable to quantum fluctuations.

For $\beta < \sqrt{4\pi}$ the theory is under perturbative control and the spectrum of single-particle excitations consists of solitons, anti-solitons and breathers. Quite remarkably, these remain stable. The mass of the kink gets renormalized and the breather spectrum becomes quantized with a sequence of energies that depend on an integer $n = 1, 2, \ldots, \lfloor 8\pi/\beta'^2 \rfloor$,

$$E_n = 2E'_k \sin\left(\frac{\beta'^2 n}{16}\right), \tag{24}$$

where $E'_k = E'_k(\beta)$ is the renormalized kink mass, which we shall not write down, and

$$\beta'^2 = \frac{\beta^2}{1-\beta^2/8\pi}. \tag{25}$$

Eq. (24) is exact, and each of these states has an infinite lifetime. Moreover, notice that the sequence stops at $\beta^2 \geq 4\pi$, where the maximal n that can be reached is 0.

Finally, we may add a last entry in the list of remarkable properties of the sG model in $(1+1)$ dimensions, which is the fact that it can be seen to be dual to the massive Thirring model [18]: the unique $(1+1)-$dimensional model of a Dirac fermion with a local self-interaction. This duality is of the strong-weak coupling type, meaning that the strong coupling limit on one side of the duality corresponds to the weak coupling of the other. This allows to map the kink (antikink) with

the fermion (antifermion) of the Thirring model and the breather to a bound state of two massive Thirring fermions. Moreover, the range of β^2 for which the theory is under control can be further extended above 4π ($\beta^2 = 4\pi$ corresponds to the free fermion case) and up to $\beta^2 = 8\pi$, above which the sG theory does not have a well-defined ground state [13].

All in all, due to its remarkable properties, the sG theory is an ideal toy model to test our knowledge on non-perturbative aspects of QFTs. In particular, an exciting new direction that I have explored but that will not be included in this thesis is the use of quantum superconducting circuits to build a faithful quantum simulator of the sG model. This is possible since the potential governing Josephson junctions (which are the elementary building blocks of superconducting quantum circuits) feature a cosine potential. Theoretical proposals in this direction have only very recently appeared in the literature [19], and it is certainly a new avenue very much worth pursuing.

2.2 Oscillons in other models

In the previous section, we have seen how breathers are a very special kind of oscillon, which is something that stems from the fact that the sine-Gordon model in $(1+1)$ dimensions is integrable. This is both a combination of it having an infinite number of equivalent degenerate vacua and the ambient spacetime being $(1+1)$-dimensional. For instance, another model that is well known for having degenerate vacua is the "Mexican hat" ($\lambda\phi^4$) potential,

$$V(\phi) = \frac{\lambda}{4}(\phi^2 - \eta^2)^2 \ , \tag{26}$$

which we, again, will consider in $(1+1)$ dimensions and thus the mass dimension of λ is $[\lambda] = 2$. Here there are also kink (and antikink) solutions,

$$\phi_k(x) = \eta \tanh\left(\sqrt{\frac{\lambda}{2}}\eta x\right) \ , \tag{27}$$

with the antikink obtained again from $\phi_{\overline{k}}(x) = \phi_k(-x)$ and with a total energy that scales as $E_k \sim m^3/\lambda$, with $m^2 \equiv \lambda\eta^2$ setting the width of the kink.

Breather solutions are known to not exist in the $\lambda\phi^4$ model [20]. However, even the earliest numerical kink-antikink scattering studies revealed the existence of extremely long-lived, oscillating bound states of kinks and antikinks [8]: oscillons. The simplest hypothesis for such a difference is that between the two neighboring vacua the sG and the $\lambda\phi^4$ potentials have very similar shapes, and thus the oscillons of the $\lambda\phi^4$ theory can be thought of as being approximate breather solutions. However, and rather importantly, the stability of breathers is controlled by the coefficients in front of *higher dimensional operators* ϕ^6, $\phi^8, \ldots$ whose particular values in the sG make the theory integrable, thus making the breather eternal.

To be fair, however, QFTs in $(1+1)$ dimensions are rather special theories. In the more familiar $(3+1)$-dimensional space, there is a scaling argument known as Derrick's Theorem [21] that forbids the existence of static localized solutions held together by self-interactions alone. Oscillons then become spherically symmetric localized objects[4] and avoid Derrick's Theorem by being time-dependent, while they also slowly decay by sheding away energy in the form of scalar radiation.

[4]Oscillons have been seen to form in numerical simulations that are initialized from randomly chosen and non-spherically symmetric initial data [22–24]. They are also stable to elliptical perturbations [23, 25]

As such, their oscillating frequency also slowly increases until a threshold value is reached and the remaining energy is radiated away in the form of a "burst", or wave packet, a process that we call the death of an oscillon.

How long-lived an oscillon is is both model and dimension-dependent and is one of the main focuses of this thesis. We have already given a rough estimate of their lifetime through (15), with potentially important modifications coming from the coefficients in front of *higher dimensional operators* ϕ^6, $\phi^8, \ldots$. Moreover, the ambient space-time dimension also plays a crucial role[5]. A dramatic example of this is again seen in the sG theory when extended to more than one spatial dimension. The integrability properties are lost and the would-be breather, now an oscillon, has a lifetime of "just" $\tau_{sG} \sim 10^3\ m^{-1}$ in (3+1) dimensions. Moreover, the $\lambda\phi^4$ oscillon in (3+1) dimensions, contrary to what happens in $(1+1)$, is now more long-lived than the sG one with $\tau_{\lambda\phi^4} \sim 10^4\ m^{-1}$.

While the examples we have been considering involve a degenerate vacuum, this is not necessary for oscillon existence in a theory. What is really the only necessary condition for the existence of oscillons is an attractive interaction channel, which is expressed in terms of having a potential *more open than quadratic around one of its minima*,

$$V(\phi) = \frac{1}{2}m^2\phi^2 - m^2F^2\ v(\phi/F)\ , \tag{28}$$

with $v > 0$. Thus, a field configuration oscillating about this minimum with a large enough amplitude to notice the presence of non-linearities will do so at a frequency $\omega \lesssim m$. As we have seen, the mean energy per quanta in such a state is therefore slightly less than m and as a result a bound state is formed due to the field's own self-interactions.

Once the oscillon has formed, it slowly radiates away individual quanta mainly through relativistic $3\phi \to 1\phi$ processes, thereby increasing its oscillating frequency (alternatively reducing the collective coupling λ) until a critical frequency (critical collective coupling) value is reached where it cannot be self-sustained anymore and the remaining quanta in the condensate disperse as a wave packet.

The interest in oscillons has also risen by the fact that these are not exceptional states, but are quite generically found by initializing the system with an inhomogeneous field profile that has enough energy. Oscillons can then be produced rather easily by evolving numerically such an initial inhomogeneous profile[6]. This means that they are attractors in the space of inhomogeneous field configurations, see Fig.4.

A model without degenerate vacua that plays an important role in Papers B and C with relevant applications to dark matter is a family of potentials parametrized by a parameter p that is motivated from string theory constructions and receive the *axion monodromy* name. These are commonly written as

$$V(\phi) = \frac{m^2F^2}{2p}\left[\left(1+\frac{\phi^2}{F^2}\right)^p - 1\right]\ , \tag{29}$$

which asymptotes to ϕ^{2p} for $p > 0$ but that saturates at a plateau for $p < 0$. Importantly, this potential satisfies the necessary condition for oscillon existence (28) for $p < 1$, see Fig.5. Quite

[5] In [26] the authors studied the lifetimes of oscillons in different $(D+1)$-spacetime dimensions, reporting an apparent absence of oscillons for $D > 5$.

[6] Common choices are Gaussian-shaped or sech profiles, but which precise shape one choses is not so important.

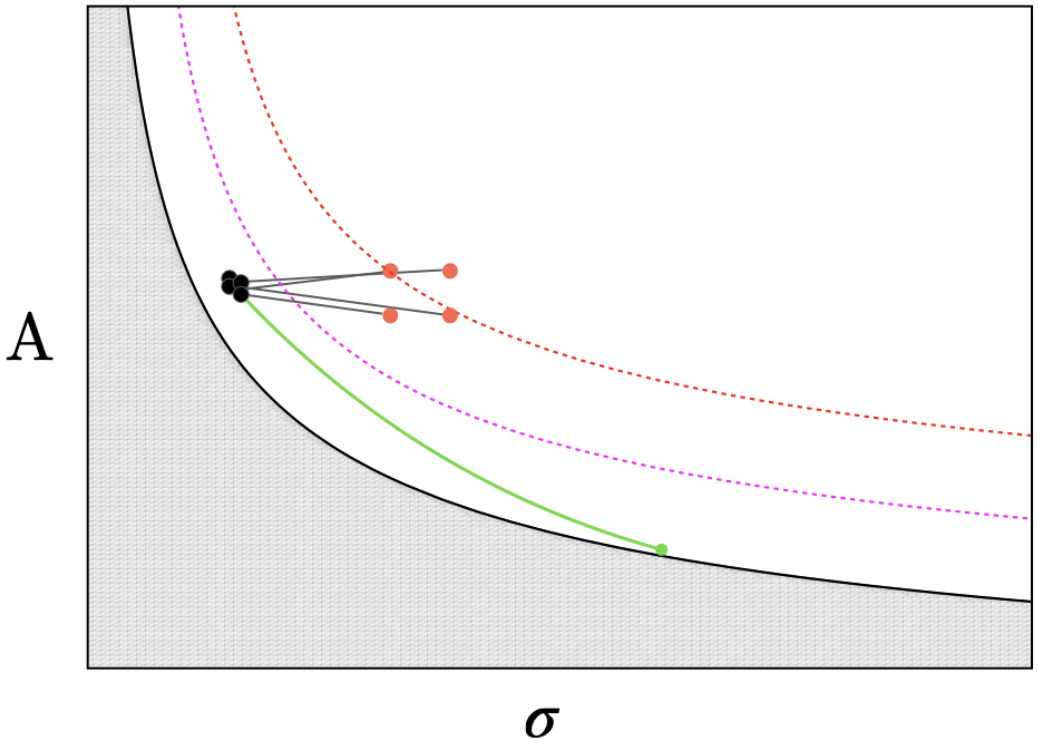

Fig. 4: Sketch of the time evolution of inhomogeneous configurations parametrized by a field amplitude A and size σ ($\phi = A\exp(-r^2/\sigma^2)$, for instance). Initially separated configurations (red dots) cluster (black dots) after a rather small relaxation time. They all then evolve following the green line (oscillon configuration) until they eventually decay (green dot) once they reach a threshold energy. The black solid, magenta and red dashed curves represent equal-energy lines, with the black solid curve being the threshold (minmal) energy curve. Configurations initialized below this energy (gray region) will decay without forming an oscillon.

importantly, potential (29) displays the following two limiting cases:

(i) $p \to -\infty$

Here, the potential (29) becomes

$$V(\phi) = \frac{m^2\tilde{F}^2}{2}\left(1 - e^{-\phi^2/\tilde{F}^2}\right) + \mathcal{O}\left(\frac{1}{p}\right) \ , \tag{30}$$

with $\tilde{F} \equiv F/\sqrt{1-p}$. Therefore, the properties of oscillons should be insensitive to variation of p in the large negative p limit.

(ii) $p \to 1$

Potential (29) now becomes

$$V(\phi) = \frac{m^2}{2}\left\{\phi^2 - (1-p)\left[(\phi^2+F^2)\log\left(1+\frac{\phi^2}{F^2}\right) - \phi^2\right] + \dots\right\} \ , \tag{31}$$

where $\cdots = \mathcal{O}\left[(1-p)^2\log^2\left(1+\phi^2/F^2\right)\right]$ are the leading order corrections.

The second limiting case ($p \to 1$) is important since it asymptotes at large field values to the *exceptional* potential

$$V_{\log}(\phi) = \frac{1}{2}(1+\epsilon)m^2\phi^2 - \frac{1}{2}\epsilon m^2\phi^2\log\left(\frac{\phi^2}{F^2}\right) \ , \tag{32}$$

with ϵ an arbitrarily small (positive) parameter. In the context of oscillons, this potential is exceptional since it was shown in [27] that this is the only potential in 3 spatial dimensions with eternal oscillons. The main reason behind this is the fact that the equation of motion associated to (32) is factorizable, $\phi(t,r) = A(t)B(r)$, [27, 28], and this leads to stable localized solutions with a Gaussian profile

$$B(r) = e^{-(r/R)^2} \quad \text{with} \quad R = \frac{2}{\epsilon}m^{-1} \tag{33}$$

provided that the overall amplitude $A(t)$ satisfies

$$\ddot{A} = -m^2 A\left[1 + 3\epsilon - \epsilon\log(A^2/F^2)\right] \ , \tag{34}$$

whose solution is a periodic function. An extended analysis is given in Paper C. The relevant point for now is that one expects the lifetime of oscillons to grow indefinitely as one approaches $p \to 1$ from below.

More than often the only tool available for the study of oscillons is explicit numerical evolution of some initial field configuration. For instance, in [29] the authors followed the oscillons of both the sG and the $\lambda\phi^4$ theories in 2 spatial dimensions during an evolution time $10^8\ m^{-1}$ without seeing them deccay, and with timescales $\sim 10^9\ m^{-1}$ out of reach for explicit numerical simulations. At the core of this thesis also lies numerical simulations for the study of oscillons. However, we have been able to surpass the $\sim 10^9\ m^{-1}$ barrier by means of a new algorithm we called the *relax and fast-forward* method that avoids explicit time evolution altogether but that allows us to determine oscillon lifetimes very precisely. This development has been possible by exploiting the fact that oscillons are attractors of lump-like configurations (see Fig.4) and is one of the main results of Paper C.

Other methods to study the properties of oscillons are semi-analytic. An important one is the so-called ϵ-*expansion* or *small-amplitude* formalism, which is a perturbative expansion in a small parameter ϵ that originated from early studies of the sG breather [20, 30] and is useful to study small-amplitude oscillons whose non-linearities are felt by their size R being $R \gg m^{-1}$. The relation between the oscillon's frequency ω and the expansion (amplitude) parameter ϵ is $\omega^2 = m^2(1-\epsilon^2)$ and a nice review of the topic can be found in [31]. Another one is a non-relativistic limit in which the oscillon (there called an I-ball) carries a global $U(1)$ charge that is adiabatically conserved [27, 32–34], meaning that it is slowly lost during time evolution. If the scalar field ϕ were a complex variable

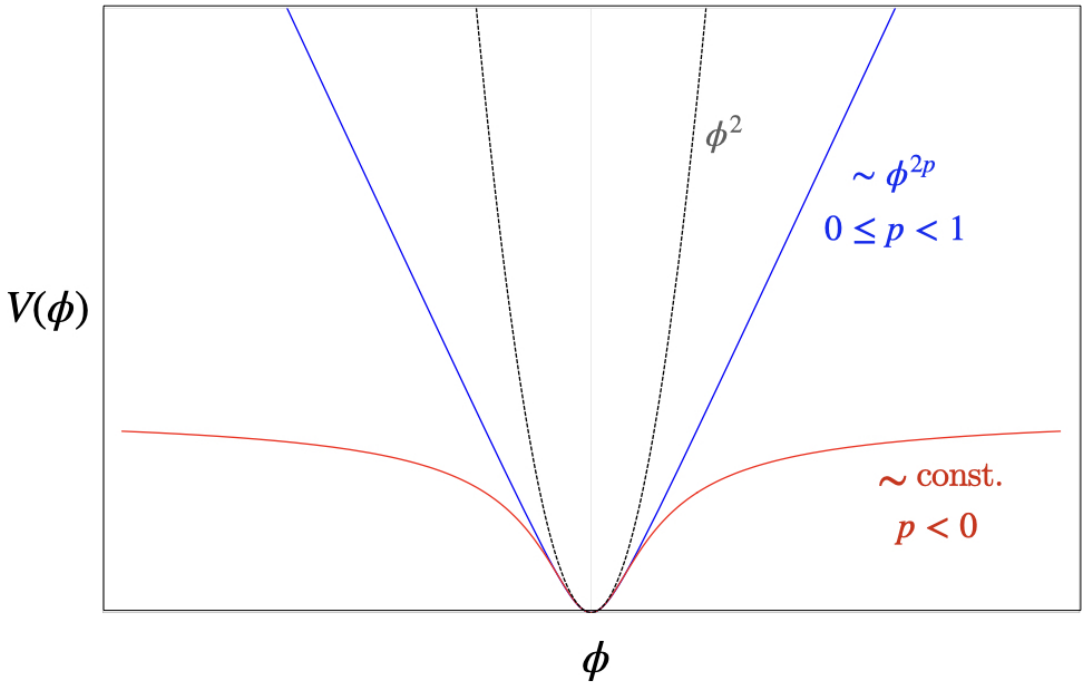

Fig. 5: Sketch of the behaviour of the family of potentials (29) parametrized by p. While the potential plateaus for $p < 0$, it grows as a power law for $p > 0$. The condition $p < 1$ makes the potential more open than quadratic, which is a necessary condition for oscillon existence, (28).

instead of a real one, such global charge conservation is exact and the resulting object is called a Q-ball, originally discovered by Coleman in [35]. Oscillons can also be found outside high energy physics. In particular, oscillons are expected to be formed in Bose-Einstein condensate setups [36–38].

Finally, oscillons also exist in models with more than one field. Examples are two-field oscillons arising after hybrid inflation [39], in an SU(2) gauged Higgs model [40, 41], an Abelian Higgs model [42, 43] and in an SU(2)×U(1) model [44, 45]. However, it is known that rather special conditions are needed for multi-field oscillons to arise. In the case of the SU(2) gauged Higgs model, for instance, the Higgs mass needs to be almost twice the W mass for the resulting oscillons to be long-lived. More recent works are [46, 47] as well as some work in progress of this author related to the possibility that bound states of a large number of pions (π^0 and $\pi^\pm$) exist in nature [48]. Even though this work is not part of this thesis we found it worth mentioning.

3 Dark Matter

The 20th century has seen the rise of cosmology as a sound scientific discipline. Driven by dramatic improvements in observational equipment, theories that were considered short from science fiction are today rigorously scrutinized. One of the most well established and perhaps surprising fact about our universe is that approximately 25% of its energy density must be in the form of dark matter (DM) [49]. Even though this was established as long ago as the 1970s, its true composition still remains a mystery. From the context of particle physics, one expects DM to be composed of (at least) a novel particle that is not included in the Standard Model of Particle Physics (SM) and that is electrically neutral, weakly-interacting, uncolored and stable.

In the context of cosmology, flat models with cold dark matter (CDM) are both consistent with standard inflationary cosmology and agree with observations on large scales ($\gg$ 1 kpc). However, CDM models have repeatedly failed to give accurate predictions on shorther scales ($\lesssim$ 10kpc) [50]. The cleanest place to look for DM effects at short scales is inside dwarf spheroidal (dSph) galaxies. These are small, low-luminosity galaxies with very little dust and rather old stellar populations. Their internal dynamics are thus mostly dominated by DM and their properties (uniformity of their central masses, $M_{\rm central} \sim 10^7 M_\odot$ and shallow density profiles) are very hard to understand using standard CDM models: these predict the existence of galaxies with much lower masses than dSph galaxies, with steeper, singular density profiles. In fact, a generic prediction of cosmological CDM N-body simulations is that dark matter halos develop "cuspy" density profiles at their center, with a density scaling as $\rho(r)\ \alpha\ r^{-1}$ [51, 52]. However, flatter distributions are preferred from observations, generating an important tension between theory and observation. An interesting resolution to this so-called *core-cusp* problem is that DM displays a wave-like behavior at short distances ($\lesssim$ 10kpc). This is achieved if DM is composed of very light scalar bosons (or axions) with mass $m \sim 10^{-22}$ eV, meaning their de Broglie wavelength is $\lambda \sim 1$ kpc. In this way, one can both keep the successful large-scale predictions of standard CDM models while "smoothing out" the cusp at the core of DM halos, as seen in modern high resolution cosmological simulations [53] (see Figs.6,7). This is the so-called fuzzy dark matter (FDM), wavelike dark matter (ψDM) or ultra-light dark matter (ULDM) scenario, and it was first proposed in [54] a bit more than 20 years ago. In the following we will review the original motivation in [54] behind these models as well as which kind of particle physics models could realize this scenario.

3.1 Cold and Fuzzy Dark Matter

The otherwise widely successful CDM model for structure formation suffers from small scale shortcomings: cuspy energy density profiles at the core of DM halos as well as an abundance of low mass halos that are in tension with observations. Even though these tensions could still be potentially solved within the baryonic sector through astrophysical processes, a solution within the CDM framework alone can also be provided. Dark Matter can be kept cold and very weakly interacting while simultaneously changing its small scale behaviour if it is made of ultra-light particles with $m \sim 10^{-22}$ eV. Under this scenario, the wave nature of DM becomes noticeable on an astrophysical scale set by their de Broglie wavelength and DM halos become stable on small scales due to large gradients costing large amounts of energy for wave-like systems. Cuspy profiles thus become energetically disfavored and DM halos get their core profile smoothened out.

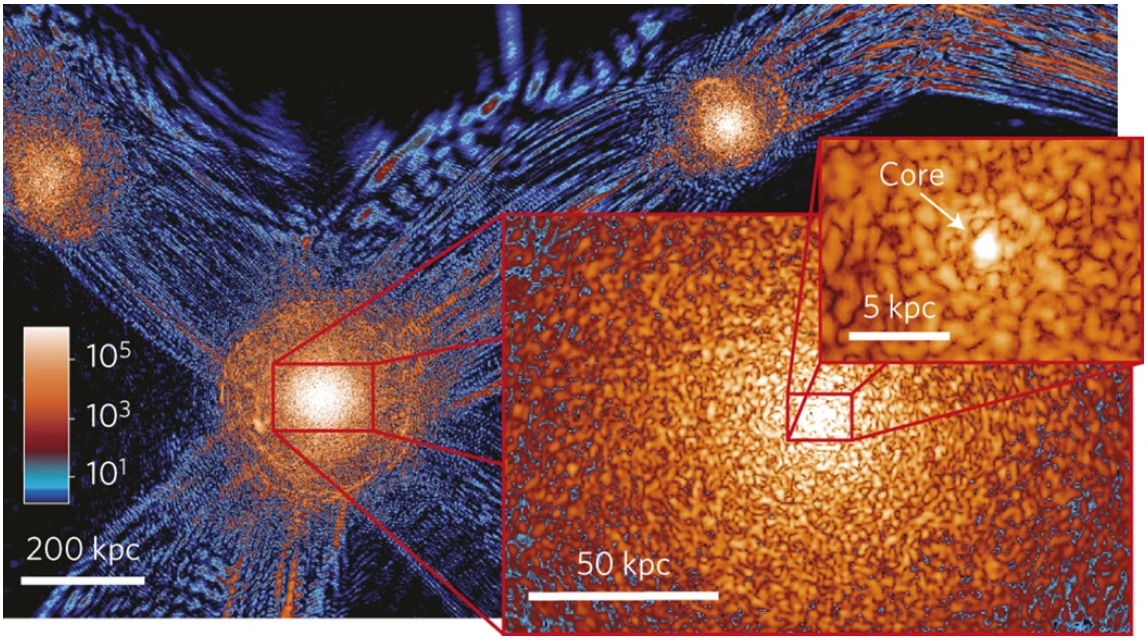

Fig. 6: Reproduced from Fig.2 of [53]. We reproduce the original caption: "**A slice of the density field of the ψDM simulation on various scales at** $z = 0.1$: This scaled sequence (each of thickness 60 pc) shows how quantum interference patterns can be clearly seen everywhere from the large-scale filaments, tangential fringes near the virial boundaries, to the granular structure inside the haloes. Distinct solitonic cores with radii $\sim 0.3 - 1.6$ kpc are found within collapsed haloes (which have virial masses $M_{\rm vir} \sim 10^9 - 10^{11} M_\odot$). The density shown here spans over nine orders of magnitude, from 10^{-1} to 10^8 (normalized to the cosmic mean density). The colour map scales logarithmically, with cyan corresponding to density $\lesssim 10$."

DM halos are very heavy objects in comparison to $m = 10^{-22}$ eV, and as such the occupation number of such ultra-light (assumed scalar) particles in DM halos is huge, which means that a mean field description is justified. As a classical field, and ignoring self-interactions, it then obeys the Klein-Gordon equation of motion

$$(\Box + m^2)\phi = 0 \ . \tag{35}$$

At distances much larger than m^{-1} but much smaller than the horizon scale, one can work within the Newtonian approximation of the gravitational interaction and use a (cold assumption) non-relativistic dispersion relation for the ϕ field. This leads to the following Schrödinger-Poisson equation:

$$i\partial_t \psi = \left(-\frac{\nabla^2}{2m} + m\Phi \right) \psi \ , \tag{36}$$

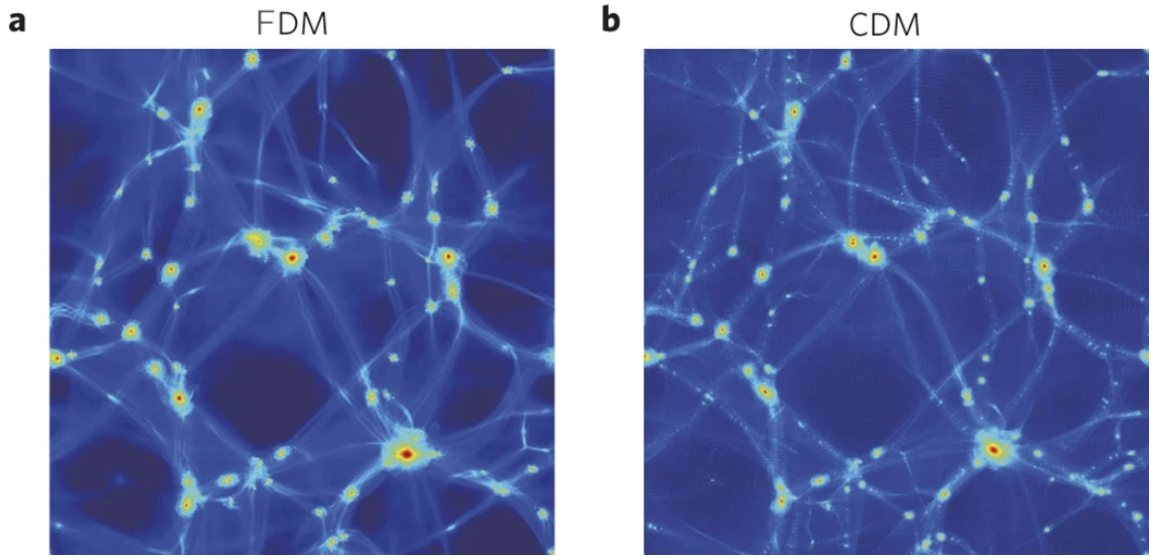

Fig. 7: Adapted from Fig.1 of [53]. **a** High precision simulation results for the structure created by FDM. **b** Same as in **a** but with CDM N-body simulations. These results show a clear indistinguishability between both models at large scales.

where the wavefunction ψ is basically the amplitude of the field, defined through

$$\phi(t, \mathbf{x}) = \frac{\psi(t, \mathbf{x})}{m} \cos(mt) \ , \tag{37}$$

and Φ is the Newtonian gravitational potential,

$$\nabla^2 \Phi = 4\pi G \rho \ . \tag{38}$$

The implicit assumption is that DM dominates the energy density content of the universe and as such $\rho \sim m^2 \psi^2$. In addition, we have neglected the effect of the expansion of the Universe in (36) so it is valid for a time evolution shorter than the expansion time timescale.

At the time when [54] was published it was already known that N-body simulations of CDM [52] predicted equilibrium density profiles of halos that were well fit by

$$\frac{\rho(r)}{\rho_{\rm crit}} = \frac{\delta_c}{(r/r_s)(1 + r/r_s)^2} \ , \tag{39}$$

where r_s is a scale radius, δ_c is a characteristic (dimensionless) density, and $\rho_{\rm crit} = 3H^2/8\pi G$ is the critical density for closure, displaying a cuspy r^{-1} profile below r_s and a r^{-3} behaviour at large scales.

The cuspy profile is specially problematic due to the existence of the Jeans instability, a process under which gravitationally bound systems collapse under their own gravity. The realization of [54] is that the Jeans scale of this condensate corresponds to the de Broglie wavelength of the ground state of a particle in the gravitational potential well generated by the condensate. As such, stability below the Jeans scale is guaranteed by the wave uncertainty principle since any attempt to confine the particle further results in its momentum increasing. This wave nature modifies the halo density profile (39) below r_s and therefore avoids the cuspy r^{-1} behaviour.

The coupled Schrödinger-Poisson Eqs.(36),(38) admit a family of localized solutions [55] known as *gravitational solitons*, which are bound by gravity and with typical masses and sizes of

$$M_{\rm sol} = \lambda M_1 \ , \ \text{with} \ M_1 \approx 2.79 \times 10^{12} \left(\frac{m}{10^{-22}\ {\rm eV}}\right)^{-1} M_\odot \ , \tag{40}$$

$$R_{\rm sol} = \lambda^{-1} R_1 \ , \ \text{with} \ R_1 \approx 0.082 \left(\frac{m}{10^{-22}\ {\rm eV}}\right)^{-1} \ {\rm pc} \ , \tag{41}$$

where $\lambda < 1$ is a positive dimensionless parameter that is determined from initial conditions and $M_\odot$ is a solar mass. These can be seen at the core of Fig.6.

In contrast, condensates can also form in the absence of gravity with the binding mechanism provided by their own self-interactions, oscillons. This is precisely the scenario that we studied in Paper B, which then lead to similar relations to (40) and (41). These are

$$M_{\rm osc} \approx 10^8 \left(\frac{F}{10^{16}\ {\rm GeV}}\right)^2 \left(\frac{m}{10^{-22}\ {\rm eV}}\right)^{-1} M_\odot \ , \tag{42}$$

$$R_{\rm osc} \approx 0.3 \left(\frac{m}{10^{-22}\ {\rm eV}}\right)^{-1} \ {\rm pc} \ , \tag{43}$$

which can work as seeds for the later formation of gravitational solitons, see Paper B. In particular, it would be interesting to include the effects of self-interactions in future cosmological N-body simulations to see how the results shown in Figs.6,7 change.

Since [54], many subsequent works on FDM have been published and it has received lots of attention more recently. In the following, we will give a motivation from a particle physics point of view to expect the existence of light scalar particles in our universe, with masses as small as $m \sim 10^{-22}$ eV. These are often known as axion-like particles (ALPs).

3.2 Cosmology of Light Scalar Particles

The simplest mechanism for providing light spin-0 bosons is the well known Goldstone Theorem: for every spontaneously broken generator of a continuous symmetry there is an associated massless spin-0 particle in the spectrum of the theory known as a Nambu-Goldstone boson (NGB). For a spontaneously broken $U(1)$ invariant theory, the associated NGB appears in the phase of the unbroken field, it enjoys a continuous shift symmetry and is therefore massless. If there is an additional small

explicit breaking, then the NGB acquires a potential and a mass proportional to the strength of the explicit breaking.

The QCD axion [56–59] is a relevant example of a NGB of this kind, with non-perturbative QCD effects providing the source of explicit symmetry breaking. Even though its original motivation was to provide a solution to the strong CP problem, it was later realized that oscillations of the axion field about the minimum of the effective potential – the misalignment mechanism [60–62] – could provide a cosmological population of cold axions that could account for dark matter. Later, with the advent of string theory, it was realized that the effective field theories derived from string theory that are relevant for cosmology almost universally feature several ALPs. The number of ALPs descending from string theory is determined by the topology of the compactified internal space, and the richness of such topologies often give rise to a large number ($O(100)$) of axions distributed over a wide range of mass scales, which led to the *string axiverse* [63].

ALP models have two mass parameters Λ and F, and can be largely described by the action

$$S = \int d^4x \left(\frac{1}{2}(\partial_\mu \phi)^2 - \Lambda^4 \left[1 - \cos\left(\frac{\phi}{F} \right) \right] \right) \ , \tag{44}$$

which displays the shift symmetry $\phi \to \phi + 2\pi F$ descending from the phase character of the axion being a NGB. Strictly speaking, the potential may be any periodic function of ϕ, but we chose a cosine potential for simplicity. This behaviour is determined by two physical processes: a spontaneous symmetry breaking occuring at the energy scale F that sets the axion as a NGB, and an explicit symmetry breaking by non-perturbative effects at a scale Λ that provide the periodic potential for the axion. The combination

$$m = \frac{\Lambda^2}{F} \tag{45}$$

sets the mass of ϕ, which for FDM models one wants this to be $m \sim 10^{-22} - 10^{-21}$eV. Masses so small can thus be achieved if there is a separation of scales $F \gg \Lambda$. Let's consider some examples for these scales. The QCD axion, for instance, has $\Lambda^4 \approx \Lambda_{QCD}^3 m_u$ with $\Lambda_{QCD} \approx 200$MeV and m_u the up-quark mass, and a range for F not excluded by experiments $10^9\text{GeV} \lesssim F \lesssim 10^{17}\text{GeV}$, see [64]. This leads to a QCD axion mass in the range $10^{-10}\text{eV} \lesssim m \lesssim 10^{-2}\text{eV}$. In string-theory-motivated FDM models, these scales are much more uncertain, even though F takes values near the GUT scale but below the Planck scale [64], $10^{16}\text{GeV} \lesssim F \lesssim 10^{18}\text{GeV}$. The point is that masses as small as 10^{-22}eV are theoretically reasonable from a particle physics modelling point of view. Moreover, contrary to the Higgs, ALP masses are protected from quantum corrections due to all of them breaking the underlying shift symmetry and thus coming suppressed by powers of F. For the same reason, both self-interactions and interactions with SM fields also come with a suppression by powers of F. All in all, ALPs are very attractive DM candidates as they are light, weakly interacting and long-lived particles. Also, it's easy to make them electrically neutral and uncolored.

Now, we may ask what value of F would make ultralight ALP models work as DM models. From the point of view of cosmology, one assumes that the very early universe underwent a period of inflation followed by a reheating epoch under which the inflaton field decayed into SM particles plus any other BSM particles, amongst which would be the ALPs from our models. In this situation, the field ϕ can be assumed to start from a random value different from its ground state, but constant everywhere, and one then follows its cosmological evolution in an expanding FLRW universe [65].

The Friedmann equation for the dimensionless field $a \equiv \phi/F$ is

$$\ddot{a} + 3H\dot{a} + m^2 \sin a = 0, \tag{46}$$

where $H = \dot{R}/R$ is the Hubble constant and we have assumed that a depends only on time. As a classical equation of motion, this is the equation describing a simple pendulum with a friction term, which will only start oscillating once $H \lesssim m$. The standard picture[7] is then that a will oscillate at frequency m and the oscillations are damped as $R^{-3/2}$. Oscillating at frequency m, the field is in the non-relativistic regime and one can think that it is made of a collection of cold axions, also called an axion condensate, and since it is a source of matter its energy density decays as R^{-3}.

As explained, the axion field a will not start to oscillate until $H \sim m$. This is roughly achieved at a temperature T_0,

$$T_0^2 = mM_{Pl}. \tag{47}$$

At that temperature, the DM energy density is of order Λ^4, while the universe is radiation-dominated with a radiation energy density of roughly T_0^4. Ignoring dark energy, as the universe keeps expanding the energy density decays as

$$\rho = \rho_{dust} R^{-3} + \rho_{rad} R^{-4} \ , \tag{48}$$

where "dust" englobes both DM and baryonic matter, but that for our estimations we will approximate it to be DM only. This means that the ratio of DM to radiation density grows as T^{-1}, until they become equal at the matter-radiation equality temperature $T_1 \sim 1\text{eV}$. This gives the estimate

$$\frac{T_0}{T_1} \sim \frac{T_0^4}{\Lambda^4} \ . \tag{49}$$

We finally make use of (45) and (47) and end up obtaining

$$F \sim \frac{T_1^{1/2} M_{Pl}^{3/4}}{m^{1/4}} \sim 10^{17}\text{GeV} \tag{50}$$

for the FDM mass $m = 10^{-22}\text{eV}$. Interestingly, this lies within the range of values for F provided by the string-theory-motivated FDM models and such coincidence has sparked a lot of interest in the community.

The idea that even the weakest of self-interactions can form bound states of a large number of particles in scalar models is a central piece in this thesis, and this also happens for models with ALPs. In particular, the main motivation of Paper B was to understand how self-interactions affect the usual picture of FDM, finding that oscillons inevitably arise at some point as part of the dark sector in these models. Another important characteristic that we have seen about oscillons is the fact their lifetime can be very model-dependent, and in the string-theory-descending zoo of models that give rise to ultra-light scalars there is a rich catalog of potentials to be considered. We have focused in the so-called axion monodromy models, where the family of potentials that have been found can be parametrized by (29).

[7] This picture is only correct if $a \lesssim 1$. If not, nonlinearities dominate and inhomogeneities start to grow, leading to oscillon formation. This has been discussed for the QCD axion in [66] and is one of the main results of Paper B for FDM.

Before closing this section, we also want to mention that the study of oscillons in cosmology is certainly not restricted to DM. Historically, the first place where oscillons were studied in cosmology was in early universe inflationary models, see e.g. [39, 67–72]. This is due to the mechanism underlying inflation being a single scalar field slowly rolling in a class of potentials that support oscillons. The details of the transition from the inflationary epoch to the hot big-bang, a radiation dominated epoch as required by big bang nucleosynthesis is still under debate, and oscillons could provide a transitory matter-dominated epoch in the early universe. More recently, oscillon formation after inflation is attracting increasing attention partly because they can be a powerful source of gravitational waves (GWs) [73–80], which could then be useful for discriminating between different inflationary models.

4 Quantum Evaporation of Oscillons

There are no truly classical systems in our quantum universe, and oscillons are certainly no exception. An important question is thus *how do oscillons evaporate as one includes quantum corrections?*. Even though important, there are not many studies in the literature on this particular topic. The reason is that oscillons are both space-and-time dependent objects and the lack of an exact closed analytic formula to describe them makes standard quantization techniques on such backgrounds hard. In addition, modelling correctly how the growth of quantum fluctuations backreact on the oscillon background is also a delicate issue. There are thus both conceptual and technical limitations that hinder progress in this area.

The first study on the quantum evaporation of oscillons is [81], where a semiclassical method for the calculation of quantum radiation of oscillons was developed using the *small-amplitude* formalism for oscillons. In [82] the authors studied the stability of oscillons in $2+1$ spacetime dimensions in the presence of quantum fluctuations using a inhomogeneous Hartree approximation and numerical simulations. Both studies reported a decrease in oscillon lifetimes as compared to a purely classical evolution, an effect that can be more dramatic if the oscillon is coupled to other fields, a form of parametric resonance.

Paper A of this thesis is a new study in the direction of forming a better understanding on the quantum evaporation of oscillons. The central tool in our study is a newly discovered classical-quantum correspondence (CQC) put forward in a sequence of papers [83–85] by our collaborators. In them, they developed a concrete mapping between quantum degrees of freedom and some corresponding classical degrees of freedom in a different number of dimensions. The original goal was that of capturing the backreaction of quantum systems on classical background dynamical systems. These situations are specially relevant in cosmological inflationary physics and in Hawking evaporation of black holes, but also in the study of the quantum evaporation of oscillons. However, the formalism is general enough to be applied to quantum systems that can be accurately described as a set of quantum harmonic oscillators with a time-dependent frequency provided by a classical background. In the following, we will present a review of the CQC that will serve as a useful introduction to Paper A.

The simplest derivation of the CQC is that of a single quantum harmonic oscillator (QHO) with

a time-dependent frequency in the Heisenberg picture [84]. The Hamiltonian reads

$$H(t) = \frac{p^2}{2m} + \frac{mx^2}{2}\omega(t)^2, \tag{51}$$

with $\omega(t)$ an arbitrary function. The standard treatment of the QHO involves diagonalization through (now time-dependent) ladder operators a and $a^\dagger$,

$$a(t) = \frac{p - imx\omega(t)}{\sqrt{2m\omega(t)}}, \quad a^\dagger(t) = \frac{p + imx\omega(t)}{\sqrt{2m\omega(t)}}. \tag{52}$$

These follow the usual commutation relations $[a(t), a^\dagger(t)] = 1$. The QHO Hamiltonian (51) can be brought to the diagonal form

$$H(t) = \omega(t)\left(a^\dagger(t)a(t) + \frac{1}{2}\right). \tag{53}$$

The time evolution of a and $a^\dagger$ are determined by their Heisenberg equation of motion, which are

$$\begin{aligned} \frac{da}{dt} &= -i[a, H] + \frac{\partial a}{\partial t} = -i\omega a - \frac{\dot\omega}{2\omega}a^\dagger, \\ \frac{da^\dagger}{dt} &= i\omega a^\dagger - \frac{\dot\omega}{2\omega}a. \end{aligned} \tag{54}$$

Complementarily, their time evolution can be moved from operators to c-numbers $\alpha(t)$ and $\beta(t)$ through a standard Bogoliubov transformation,

$$\begin{aligned} a(t) &= \alpha(t)a_0 + \beta(t)a_0^\dagger, \\ a^\dagger(t) &= \alpha^*(t)a_0^\dagger + \beta^*(t)a_0, \end{aligned} \tag{55}$$

where $a_0 \equiv a(t = 0)$ (and correspondingly for $a_0^\dagger$). Substitution of (55) into (54) leads to the following equations of motion for $\alpha(t)$ and $\beta(t)$:

$$\begin{aligned} \dot\alpha &= -i\omega\alpha - \frac{\dot\omega}{2\omega}\beta^*, \\ \dot\beta &= -i\omega\beta - \frac{\dot\omega}{2\omega}\alpha^*, \end{aligned} \tag{56}$$

and the expectation value of the Hamiltonian (53) in the vacuum state $|\Omega\rangle$ becomes

$$E_q(t) \equiv \langle H\rangle_\Omega = \omega(t)\left(|\beta|^2 + \frac{1}{2}\right). \tag{57}$$

The CQC is a reinterpretation of the EOMs (56) for α and β as a single complex classical degree of freedom. This is made explicit through the following change of variables:

$$\begin{aligned} \alpha &= \sqrt{\frac{m}{2\omega}}(\dot z^* - i\omega z^*)\ , \\ \beta &= \sqrt{\frac{m}{2\omega}}(\dot z - i\omega z)\ , \end{aligned} \tag{58}$$

where $z \equiv \xi + i\chi$ is complex, and ξ and χ are its real and imaginary parts respectively. Through this change of variables, (56) become a single EOM for z:

$$\ddot{z} + \omega^2(t) z = 0 \ , \tag{59}$$

i.e. both its real part ξ and its imaginary part χ follow a classical harmonic oscillator (CHO) equation of motion, albeit with a time-dependent frequency $\omega(t)$. All in all, (59) describes the dynamics of a *two*-dimensional classical harmonic oscillator with time-dependent frequency $\omega(t)$.

To complete the CQC we must map the initial operator a_0 condition to a corresponding one for z. This is done by noticing that the condition $a(0) = a_0$ corresponds to $\alpha(0) = 1$ and $\beta(0) = 0$. These imply

$$\begin{aligned} z(0) &= \frac{-i}{\sqrt{2m\omega_0}} \ , \\ \dot{z}(0) &= \sqrt{\frac{\omega_0}{2m}} \ , \end{aligned} \tag{60}$$

where $\omega_0 = \omega(0)$. Finally, we want to make explicit that the expected value of the quantum energy given by (57) can now also be written in terms of the *classical* variables ξ, χ as

$$E_q = \frac{m}{2}\left(\dot{\xi}^2 + \omega^2\xi^2\right) + \frac{m}{2}\left(\dot{\chi}^2 + \omega^2\chi^2\right). \tag{61}$$

The remarkable connection is therefore completed: the dynamics of *any* time-dependent simple quantum harmonic oscillator can be computed using two classical harmonic oscillators. The initial state of the QHO is then mapped to certain initial conditions for the two CHOs that have the same energy as the quantum expected value of the Hamiltonian.

The CQC is thus a new entry in the list of mathematical dualities between quantum and classical theories. The great value of the CQC is that we can trade off a complicated quantum calculation by a purely classical one, and this is specially well suited to deal with those situations in which backreaction of quantum degrees of freedom on a classical background are non-negligible, like in inflation, black hole evaporation or Schwinger particle production.

In [85], the CQC was extended to fields by treating quantum fields as a collection of QHOs. The most salient new feature of this version of the CQC is that it now maps N quantum degrees of freedom into $2N^2$ CHOs after regularization. Paper A of this thesis is an improvement of the CQC for fields together with the first explicit example calculation: the quantum evaporation of the sine-Gordon breather. Further work using this method has been inflation-inspired calculations of a rolling classical scalar field in a linear potential coupled to a quantum field [86] and of a coupled Einstein-Klein-Gordon system [87]. Related to oscillons, [47] has studied kink-antikink scattering in the sG model coupled to an additional scalar field starting off in its vacuum state.

5 Results and Discussion

5.1 Paper A

Even though breathers of the $(1+1)$-dimensional sG model are stable, this is no longer true once a coupling to an extra quantum field is introduced. In this situation, the integrability properties of the

model are lost and the breathers are no longer protected from decaying. The quantum evaporation of breathers can be studied in the limit where the breather itself is treated classically and provides a space-and-time-dependent background causing the other field to get excited, thereby losing energy and slowly decaying. Even though this phenomenon has been studied before, the backreaction of the extra quantum field on the classical breather background has not been fully taken into account.

In Paper A we apply the CQC to the study of quantum evaporation of breathers in the setup that has been described in the previous paragraph, providing a full treatment of backreaction of quantum modes on a classical breather. In the context of the CQC, this is the first application of this formalism to a field theoretical example. In particular, the model that we consider is given by

$$L = \int dx \left[\frac{1}{2}(\partial_\mu \phi)^2 - m_\phi^2(1-\cos\phi) + \frac{1}{2}(\partial_\mu \psi)^2 - \frac{\lambda}{2}\phi^2\psi^2\right], \tag{62}$$

where $\mu = 0, 1$ is the spacetime index and λ is the coupling constant, with mass dimension $[\lambda] = 2$. The classical breather solution (see Eq.(19)) $\phi = \phi_b,\ \psi = 0$ is an exact solution to the classical equations of motion derived from (62), but in a quantum treatment we expect ψ to get excited and the breather to evaporate. This can be seen in Fig.A.2, which indeed shows that the breather evaporates by depletion of energy into the quantum field ψ and that the breather oscillation frequency increases with time, similarly to what happens with oscillons.

We emphasize that computing such an effect is hard: one has to implement a semi-classical iterative procedure where one starts with the classical breather solution, computes the quantum radiation in this background, uses it to calculate the first semi-classical correction to the background and repeats this process *ad infinitum*. Usually, only the first iteration of this semi-classical procedure is carried out, but our calculation using the CQC is a calculation that automatically takes all iterations into account.

No method is perfect, and the one we present has its own limitations. These are important to discuss because the success of exporting this method to other field theory models depends on understanding these, which I will briefly mention. The most important one is that the CQC is most accurate in the limit where the background field can be treated classically, which then sets a timescale over which the CQC gives accurate results. The second limitation is more easily surmountable and is a quadratic computational complexity cost in the size of the lattice, which can be easily improved by using parallelization methods, for instance.

Further work using this method has been inflation-inspired calculations of a rolling classical scalar field in a linear potential coupled to a quantum field [86] and of a coupled Einstein-Klein-Gordon system [87]. Related to oscillons, [47] has studied kink-antikink scattering in the sG model coupled to an additional scalar field starting off in its vacuum state, very much in spirit with our work.

5.2 Paper B

Even though we have considered periodic potentials for FDM models, these are not the only options. The most notable ones are the so-called *axion monodromy* models, parametrized by the family of potentials (29).

The goal of Paper B is to study to which extent do self-interactions in generic scalar models parametrized by (29) modify the standard predictions of FDM. The most dramatic change is the generic birth and persistence of very long-lived oscillons. We discus the role these oscillons play in

a biographical way: we first explain their formation (birth) mechanism, compute their properties while they are alive (lifetime) and the universe they leave behind (legacy).

Regarding their birth, we show that the family of potentials (29) have a built-in oscillon formation mechanism (parametric resonance instability) that evolve homogeneous oscillating configurations of ϕ into a highly inhomogeneous ones that then settle into an oscillon, a phenomenon similar to [88] and dubbed "the large-misalignment mechanism" in [66]. We then perform explicit numerical simulations of the time evolution dictated by the equation of motion derived from (29) to compute the most relevant properties of the oscillons in (29) for DM: mass $M_{\rm osc}$, size $R_{\rm osc}$ and lifetime τ. The most striking result is their lifetime: while the lifetime of QCD axion oscillons last for $\sim 10^3\ m^{-1}$, we find lifetimes of the order of $\sim 10^8\ m^{-1}$ and even larger. The scalings of $M_{\rm osc}$, $R_{\rm osc}$ with the parameters of the model are given by (42) and (43).

Oscillons die through emmission of (warm) axion waves of momentum $k \approx R_{\rm osc}^{-1} \lesssim m$. These waves lose energy by Hubble friction and can organize in a gravitational soliton structure by falling into their own gravitational potential well. Thus, these oscillons can act as *parents* for gravitational solitons. Due to their extremely long lifetime, however, the legacy of these oscillons depends on whether they decay before or after matter-radiation equality, which depends on m.

By assuming that the energy density of the axion field is equally distributed into the original oscillating homogeneous background and a population of massive oscillons, we extract some observational consequences of oscillons as part of DM in the family of models (29). These are summarized in Figs.B.10,B.11 (separated by whether they decay before or after matter-radiation equality) as a function of the model parameters m, F. The most important constraints in Figs.B.10,B.11 are: (i) DM overproduction, (ii) Warm DM by emission of axion waves, and (iii) CMB anisotropies. Of most relevance to FDM is the scenario where oscillons survive up to (or past) matter-radiation equality, which favors axion masses in the ultra-light regime $m \sim 10^{-22}$ eV. In this case, the allowed parameter space is 10^{14} GeV $\lesssim F \lesssim 10^{16}$ GeV, leading to oscillons with a typical size $R_{\rm osc} \sim 10^{-1}\ pc$ and masses in the range $10^4 M_\odot \lesssim M_{\rm osc} \lesssim 10^8 M_\odot$ and survival past matter-radiation equality.

The purpose of this work was to study the impact that self-interactions alone have in FDM, which is consistent for $F \ll M_{Pl}$. Subsequent works [89–91] have considered the case $F \lesssim M_{Pl}$ in which both gravity and self-interactions are comparable, showing that oscillons can collapse to black holes in some cases. The surprisingly large lifetimes of the oscillons we found in (29) pioneered a group of other works focusing on understanding the longevity of oscillons [34, 92–95] and Paper C, all of them agreeing with our results. Other works [66, 88, 96–98] have also studied and confirmed that oscillon formation happens through a resonance instability that drives homogeneous configurations into highly inhomogeneous ones, together with the potentially interesting observables that can be extracted from this process. Finally, several observational prospects have been drawn from the presence of oscillons in DM: through a resonant conversion to photons by interacting with pulsar magnetospheres [99, 100] and other interesting electromagnetic conversion processes [101–104], a potential signal in the observation of the 21cm line [105, 106], and a deflection in the geodesic motion of test particles around oscillons [107].

5.3 Paper C

As we have discussed, the lifetime of oscillons in (29) is surprisingly large. The data we gathered for $p = -1/2$ in Paper B suggested that it could be various orders of magnitude above $10^8\ m^{-1}$,

making explicit time evolution by numerically solving the equation of motion unfeasible. Moreover, a systematic and complete analysis of the lifetimes of oscillons as a function of the family parameter p was lacking. Using (29) as a benchmark family of potentials, we study how the shape of a (general) potential $V(\phi)$ determines the lifetime of its oscillons.

There are two main results:

(i) Two properties of $V(\phi)$ at the non-perturbative level can enhance the lifetime significantly: the flattening of $V(\phi)$ and the positivity of $V''(\phi)$.

(ii) The development of a new *fast-forward* numerical algorithm that allows to evolve in time to stages that cannot be reached through explicit time evolution of the equations of motion.

Item (i) is related to oscillons being a bound state of a large number of particles. In order to form, the total energy of the condensate must be lowered by a binding energy, which can be roughly measured by *how much does* $V(\phi)$ *deviate from being quadratic*. It is clear that potentials $V(\phi)$ that flatten allow ϕ to explore larger values without increasing the energy of the system further, thereby giving a larger binding energy. Then, once an oscillon has formed, its lifetime is dictated by its (in)efficiency to radiate classical scalar waves. In this respect, it is well known that fluctuations of an homogeneous oscillating field can undergo resonant enhancement. The same can happen in the localized oscillon configuration, i.e. the amplitude of modes whose wavelength is smaller than the oscillon size can be potentially enhanced. When this happens, the oscillon configuration is quickly disrupted. In analogy with the homogeneous case, the efficiency of such a resonant enhancement is expected to be controlled by the effective mass, $V''(\phi_{\rm osc}(t,r))$, experienced by the field fluctuations over the oscillon background. Thus, models with non-negative $V''(\phi)$ are less prompt to enhance field fluctuations resonantly.

The method presented in (ii) exploits the attractor properties of the oscillons and fully accounts for nonlinearities. The idea is to compute the decay rate $\Gamma = \dot{E}/E$ (E being the total mass of the oscillon) and then integrate it to obtain the lifetime. Explicit numerical evolution of the equations motion for timescales of the order the lifetime τ of the oscillon can be avoided by sampling initial conditions. The strategy then is to choose a set of N inhomogeneous different initial configurations and evolve each of them a relaxation time $t_{\rm relax}$ until the oscillon configuration is found, for which the data $\{\omega, \Gamma, E\}$ are then computed. A numerical advantage is obtained if $Nt_{\rm relax} \ll \tau$, which indeed happens, allowing time evolution past the $10^9\ m^{-1}$ barrier. Results of $\Gamma(\omega)$ can be found in Fig.C.3 and the lifetimes as a function of p can be found in Fig.C.4.

Paper C nicely completes the study that was started in Paper B for all values of p and strengthens further the observational implications of oscillons as part of DM, which strongly depend on their lifetime. In particular, for $m \sim 10^{-19}\ eV$ and p close to unity, we find that oscillons can survive until today, making them part of DM.

Similar methods were proposed simultaneously [92–94] when this paper was published to compute the lifetime. However, in these works a certain profile with a single oscillation frequency is assumed and the decay rate Γ is computed by linearizing the field equation of the perturbations around such profile and computing the emitted power perturbatively in the small scalar waves, which typically tends to overestimate the actual value of Γ. Another relevant subsequent study that investigates the internal mechanisms responsible for oscillon longevity is [95].

5.4 Concluding Remarks

In this thesis we have studied how several aspects of oscillons impact our understanding of modern theories of dark matter, how lump-like objects decay by emission of quantum radiation and the physical mechanisms responsible for the semi-classical stability of generic highly populated bosonic quantum states.

Before closing, however, we want to mention what we think could be interesting new research avenues related to the topics covered in this thesis.

The first one is related to how the lifetime of oscillons depends sensitively on the number of space dimensions the theory is embedded in. In particular, the exact lifetimes of oscillons in two spatial dimensions are not known [29] due to their lifetimes being well above $\tau = 10^8\ m^{-1}$, and our *relax and fast-forward* method could be valuable in this study. The application of these oscillons would be in condensed matter physics systems [36–38], which are known to display several scalar (pseudo)particles in the spectrum of their theories.

The second one is related to further DM-related studies and, as we have seen, these are already part of ongoing research programs of several research groups [66, 88, 90, 91, 96–107]. The interesting part is that oscillons being DM overdensities can provide an ehancement of signals with respect to free particles which, when considering the axion coupling to photons can lead to observable effects in the near future. Moreover, oscillon formation is a powerful source of GWs [73–80] and if F is close to M_{Pl}, other interesting gravitational effects such as oscillon collapse to a black hole [90].

Related to the CQC method, it should be mentioned that this technique should be readily applicable to more complicated field theory scenarios such as backreaction of quantum radiation on a gravitationally collapsing background or Schwinger pair creation. In the context of gravity, the CQC is amongst the very few tools available to solve important problems such as black hole evaporation.

We have also mentioned how quantum technologies are on the verge of being capable of performing faithful quantum simulations of the quantum sG model [19], which will open an entirely new methodology to study non-perturbative aspects of QFTs.

Finally, we want remark again that oscillons also exist in multi-field models, and a specially relevant case with applications in particle physics is an oscillon made of pions (π^0 and $\pi^\pm$), which is part of an ongoing work in progress.

References

[1] B. Schutz, *A first course in general relativity.* Cambridge university press, 2009.

[2] S. G. Karshenboim, "Precision study of positronium: Testing bound state QED theory," *Int. J. Mod. Phys. A*, vol. 19, pp. 3879–3896, 2004.

[3] H. Jallouli and H. Sazdjian, "Relativistic effects in the pionium lifetime," *Physical Review D*, vol. 58, no. 1, p. 014011, 1998.

[4] D. Eiras and J. Soto, "Effective field theory approach to pionium," *Physical Review D*, vol. 61, no. 11, p. 114027, 2000.

[5] G. Dvali and C. Gomez, "Black Hole's Quantum N-Portrait," *Fortsch. Phys.*, vol. 61, pp. 742–767, 2013.

[6] ——, "Landau–Ginzburg limit of black hole's quantum portrait: Self-similarity and critical exponent," *Phys. Lett. B*, vol. 716, pp. 240–242, 2012.

[7] ——, "Black Hole's 1/N Hair," *Phys. Lett. B*, vol. 719, pp. 419–423, 2013.

[8] I. Bogolyubsky and V. Makhankov, "Lifetime of Pulsating Solitons in Some Classical Models," *Pisma Zh. Eksp. Teor. Fiz.*, vol. 24, pp. 15–18, 1976.

[9] I. Bogolubsky, "Cascade evolution of spherically symmetric pulsons in multivacuum field theory models," *Physics Letters A*, vol. 61, no. 4, pp. 205–206, 1977. [Online]. Available: https://www.sciencedirect.com/science/article/pii/0375960177901384

[10] I. Bogolyubskii and V. Makhan'kov, "Dynamics of spherically symmetrical pulsons of large amplitude," *JETP Lett.(USSR)(Engl. Transl.);(United States)*, vol. 25, no. 2, 1977.

[11] M. Gleiser, "Pseudostable bubbles," *Phys. Rev. D*, vol. 49, pp. 2978–2981, 1994.

[12] E. J. Copeland, M. Gleiser, and H.-R. Muller, "Oscillons: Resonant configurations during bubble collapse," *Phys. Rev. D*, vol. 52, pp. 1920–1933, 1995.

[13] T. Vachaspati, *Kinks and domain walls: An introduction to classical and quantum solitons.* Cambridge University Press, 4 2010.

[14] R. Hermann, *The geometry of non-linear differential equations, Bäcklund transformations, and solitons.* Math Science Press, 1976.

[15] M. J. Ablowitz, M. Ablowitz, P. Clarkson, and P. A. Clarkson, *Solitons, nonlinear evolution equations and inverse scattering.* Cambridge university press, 1991, vol. 149.

[16] L. Faddeev and L. Takhtajan, *Hamiltonian methods in the theory of solitons.* Springer Science & Business Media, 2007.

[17] D. Z. Freedman, A. Lerda, and S. Penati, "Covariant form for the conserved currents of the sine-gordon and liouville theories," *Physics Letters B*, vol. 250, no. 1-2, pp. 102–106, 1990.

[18] S. Coleman, *Aspects of Symmetry*. Cambridge, U.K.: Cambridge University Press, 1985.

[19] A. Roy, D. Schuricht, J. Hauschild, F. Pollmann, and H. Saleur, "The quantum sine-Gordon model with quantum circuits," *Nucl. Phys. B*, vol. 968, p. 115445, 2021.

[20] H. Segur and M. D. Kruskal, "Nonexistence of small-amplitude breather solutions in phi^4 theory," *Phys. Rev. Lett.*, vol. 58, pp. 747–750, Feb 1987. [Online]. Available: https://link.aps.org/doi/10.1103/PhysRevLett.58.747

[21] G. H. Derrick, "Comments on nonlinear wave equations as models for elementary particles," *Journal of Mathematical Physics*, vol. 5, no. 9, pp. 1252–1254, 1964. [Online]. Available: https://doi.org/10.1063/1.1704233

[22] E. W. Kolb and I. I. Tkachev, "Large amplitude isothermal fluctuations and high density dark matter clumps," *Phys. Rev. D*, vol. 50, pp. 769–773, 1994.

[23] M. Hindmarsh and P. Salmi, "Numerical investigations of oscillons in 2 dimensions," *Phys. Rev. D*, vol. 74, p. 105005, 2006.

[24] M. A. Amin, R. Easther, and H. Finkel, "Inflaton fragmentation and oscillon formation in three dimensions," *Journal of Cosmology and Astroparticle Physics*, vol. 2010, no. 12, pp. 001–001, dec 2010. [Online]. Available: https://doi.org/10.1088/1475-7516/2010/12/001

[25] A. B. Adib, M. Gleiser, and C. A. S. Almeida, "Long-lived oscillons from asymmetric bubbles: Existence and stability," *Phys. Rev. D*, vol. 66, p. 085011, Oct 2002. [Online]. Available: https://link.aps.org/doi/10.1103/PhysRevD.66.085011

[26] P. M. Saffin and A. Tranberg, "Oscillons and quasi-breathers in D+1 dimensions," *JHEP*, vol. 01, p. 030, 2007.

[27] M. Kawasaki, F. Takahashi, and N. Takeda, "Adiabatic Invariance of Oscillons/I-balls," *Phys. Rev. D*, vol. 92, no. 10, p. 105024, 2015.

[28] G. Dvali and A. Vilenkin, "Solitonic D-branes and brane annihilation," *Phys. Rev. D*, vol. 67, p. 046002, 2003.

[29] P. Salmi and M. Hindmarsh, "Radiation and Relaxation of Oscillons," *Phys. Rev. D*, vol. 85, p. 085033, 2012.

[30] A. Kosevich and A. Kovalev, "Selflocalization of vibrations in a one-dimensional anharmonic chain," *Sov. Phys. JETP*, vol. 67, p. 1793, 1974.

[31] G. Fodor, "A review on radiation of oscillons and oscillatons," Ph.D. dissertation, Wigner RCP, Budapest, 2019.

[32] S. Kasuya, M. Kawasaki, and F. Takahashi, "I-balls," *Phys. Lett. B*, vol. 559, pp. 99–106, 2003.

[33] K. Mukaida, M. Takimoto, and M. Yamada, "On Longevity of I-ball/Oscillon," *JHEP*, vol. 03, p. 122, 2017.

[34] M. Ibe, M. Kawasaki, W. Nakano, and E. Sonomoto, "Fragileness of Exact I-ball/Oscillon," *Phys. Rev. D*, vol. 100, no. 12, p. 125021, 2020.

[35] S. R. Coleman, "Q-balls," *Nucl. Phys. B*, vol. 262, no. 2, p. 263, 1985, [Addendum: Nucl.Phys.B 269, 744 (1986)].

[36] S.-W. Su, S.-C. Gou, I.-K. Liu, A. S. Bradley, O. Fialko, and J. Brand, "Oscillons in coupled bose-einstein condensates," *Physical Review A*, vol. 91, no. 2, p. 023631, 2015.

[37] M. Charukhchyan, E. Sedov, S. Arakelian, and A. Alodjants, "Spatially localized structures and oscillons in atomic bose-einstein condensates confined in optical lattices," *Physical Review A*, vol. 89, no. 6, p. 063624, 2014.

[38] L. D. M. Villari, I. Galbraith, and F. Biancalana, "Long-lived nonlinear oscillatory states in interacting relativistic bose-einstein condensates," *Physical Review A*, vol. 102, no. 3, p. 033321, 2020.

[39] M. Gleiser, N. Graham, and N. Stamatopoulos, "Generation of Coherent Structures After Cosmic Inflation," *Phys. Rev. D*, vol. 83, p. 096010, 2011.

[40] E. Farhi, N. Graham, V. Khemani, R. Markov, and R. Rosales, "An Oscillon in the SU(2) gauged Higgs model," *Phys. Rev. D*, vol. 72, p. 101701, 2005.

[41] E. I. Sfakianakis, "Analysis of Oscillons in the SU(2) Gauged Higgs Model," 10 2012.

[42] V. Achilleos, F. K. Diakonos, D. J. Frantzeskakis, G. C. Katsimiga, X. N. Maintas, E. Manousakis, C. E. Tsagkarakis, and A. Tsapalis, "Oscillons and oscillating kinks in the Abelian-Higgs model," *Phys. Rev. D*, vol. 88, p. 045015, 2013.

[43] F. K. Diakonos, G. C. Katsimiga, X. N. Maintas, and C. E. Tsagkarakis, "Symmetric solitonic excitations of the (1 + 1)-dimensional Abelian-Higgs classical vacuum," *Phys. Rev. E*, vol. 91, no. 2, p. 023202, 2015.

[44] N. Graham, "An Electroweak oscillon," *Phys. Rev. Lett.*, vol. 98, p. 101801, 2007, [Erratum: Phys.Rev.Lett. 98, 189904 (2007)].

[45] ——, "Numerical Simulation of an Electroweak Oscillon," *Phys. Rev. D*, vol. 76, p. 085017, 2007.

[46] F. Van Dissel and E. I. Sfakianakis, "Symmetric multi-field oscillons," 10 2020.

[47] M. Mukhopadhyay, E. I. Sfakianakis, T. Vachaspati, and G. Zahariade, "Kink-antikink scattering in a quantum vacuum," 10 2021.

[48] J. Hormuzdiar and S. D. Hsu, "Isospin fluctuations from multiple domains of disoriented chiral condensates," *Physical Review C*, vol. 58, no. 2, p. 1165, 1998.

[49] N. Aghanim, Y. Akrami, M. Ashdown, J. Aumont, C. Baccigalupi, M. Ballardini, A. Banday, R. Barreiro, N. Bartolo, S. Basak *et al.*, "Planck 2018 results-vi. cosmological parameters," *Astronomy & Astrophysics*, vol. 641, p. A6, 2020.

[50] L. Hui, J. P. Ostriker, S. Tremaine, and E. Witten, "Ultralight scalars as cosmological dark matter," *Phys. Rev. D*, vol. 95, no. 4, p. 043541, 2017.

[51] J. Dubinski and R. G. Carlberg, "The Structure of Cold Dark Matter Halos," *APJ*, vol. 378, p. 496, Sep. 1991.

[52] J. F. Navarro, C. S. Frenk, and S. D. M. White, "A Universal density profile from hierarchical clustering," *Astrophys. J.*, vol. 490, pp. 493–508, 1997.

[53] H.-Y. Schive, T. Chiueh, and T. Broadhurst, "Cosmic Structure as the Quantum Interference of a Coherent Dark Wave," *Nature Phys.*, vol. 10, pp. 496–499, 2014.

[54] W. Hu, R. Barkana, and A. Gruzinov, "Cold and fuzzy dark matter," *Phys. Rev. Lett.*, vol. 85, pp. 1158–1161, 2000.

[55] N. Bar, D. Blas, K. Blum, and S. Sibiryakov, "Galactic rotation curves versus ultralight dark matter: Implications of the soliton-host halo relation," *Phys. Rev. D*, vol. 98, no. 8, p. 083027, 2018.

[56] R. D. Peccei and H. R. Quinn, "CP Conservation in the Presence of Instantons," *Phys. Rev. Lett.*, vol. 38, pp. 1440–1443, 1977.

[57] ——, "Constraints Imposed by CP Conservation in the Presence of Instantons," *Phys. Rev. D*, vol. 16, pp. 1791–1797, 1977.

[58] S. Weinberg, "A New Light Boson?" *Phys. Rev. Lett.*, vol. 40, pp. 223–226, 1978.

[59] F. Wilczek, "Problem of Strong P and T Invariance in the Presence of Instantons," *Phys. Rev. Lett.*, vol. 40, pp. 279–282, 1978.

[60] J. Preskill, M. B. Wise, and F. Wilczek, "Cosmology of the Invisible Axion," *Phys. Lett. B*, vol. 120, pp. 127–132, 1983.

[61] M. Dine and W. Fischler, "The Not So Harmless Axion," *Phys. Lett. B*, vol. 120, pp. 137–141, 1983.

[62] L. F. Abbott and P. Sikivie, "A Cosmological Bound on the Invisible Axion," *Phys. Lett. B*, vol. 120, pp. 133–136, 1983.

[63] A. Arvanitaki, S. Dimopoulos, S. Dubovsky, N. Kaloper, and J. March-Russell, "String Axiverse," *Phys. Rev. D*, vol. 81, p. 123530, 2010.

[64] D. J. Marsh, "Axion cosmology," *Physics Reports*, vol. 643, pp. 1–79, 2016, axion cosmology. [Online]. Available: https://www.sciencedirect.com/science/article/pii/S0370157316301557

[65] L. Di Luzio, M. Giannotti, E. Nardi, and L. Visinelli, "The landscape of QCD axion models," *Phys. Rept.*, vol. 870, pp. 1–117, 2020.

[66] A. Arvanitaki, S. Dimopoulos, M. Galanis, L. Lehner, J. O. Thompson, and K. Van Tilburg, "Large-misalignment mechanism for the formation of compact axion structures: Signatures from the QCD axion to fuzzy dark matter," *Phys. Rev. D*, vol. 101, no. 8, p. 083014, 2020.

[67] J. McDonald, "Inflaton condensate fragmentation in hybrid inflation models," *Phys. Rev. D*, vol. 66, p. 043525, 2002.

[68] E. J. Copeland, S. Pascoli, and A. Rajantie, "Dynamics of tachyonic preheating after hybrid inflation," *Phys. Rev. D*, vol. 65, p. 103517, 2002.

[69] M. A. Amin, "Inflaton fragmentation: Emergence of pseudo-stable inflaton lumps (oscillons) after inflation," 6 2010.

[70] M. A. Amin, R. Easther, and H. Finkel, "Inflaton Fragmentation and Oscillon Formation in Three Dimensions," *JCAP*, vol. 12, p. 001, 2010.

[71] M. A. Amin, R. Easther, H. Finkel, R. Flauger, and M. P. Hertzberg, "Oscillons After Inflation," *Phys. Rev. Lett.*, vol. 108, p. 241302, 2012.

[72] S. Antusch, F. Cefala, S. Krippendorf, F. Muia, S. Orani, and F. Quevedo, "Oscillons from String Moduli," *JHEP*, vol. 01, p. 083, 2018.

[73] S.-Y. Zhou, E. J. Copeland, R. Easther, H. Finkel, Z.-G. Mou, and P. M. Saffin, "Gravitational Waves from Oscillon Preheating," *JHEP*, vol. 10, p. 026, 2013.

[74] S. Antusch, F. Cefala, and S. Orani, "Gravitational waves from oscillons after inflation," *Phys. Rev. Lett.*, vol. 118, no. 1, p. 011303, 2017, [Erratum: Phys.Rev.Lett. 120, 219901 (2018)].

[75] J. Liu, Z.-K. Guo, R.-G. Cai, and G. Shiu, "Gravitational wave production after inflation with cuspy potentials," *Phys. Rev. D*, vol. 99, no. 10, p. 103506, 2019.

[76] K. D. Lozanov and M. A. Amin, "Self-resonance after inflation: oscillons, transients and radiation domination," *Phys. Rev. D*, vol. 97, no. 2, p. 023533, 2018.

[77] M. A. Amin, J. Braden, E. J. Copeland, J. T. Giblin, C. Solorio, Z. J. Weiner, and S.-Y. Zhou, "Gravitational waves from asymmetric oscillon dynamics?" *Phys. Rev. D*, vol. 98, p. 024040, 2018.

[78] N. Kitajima, J. Soda, and Y. Urakawa, "Gravitational wave forest from string axiverse," *JCAP*, vol. 10, p. 008, 2018.

[79] K. D. Lozanov and M. A. Amin, "Gravitational perturbations from oscillons and transients after inflation," *Phys. Rev. D*, vol. 99, no. 12, p. 123504, 2019.

[80] T. Hiramatsu, E. I. Sfakianakis, and M. Yamaguchi, "Gravitational wave spectra from oscillon formation after inflation," *JHEP*, vol. 03, p. 021, 2021.

[81] M. P. Hertzberg, "Quantum Radiation of Oscillons," *Phys. Rev. D*, vol. 82, p. 045022, 2010.

[82] P. M. Saffin, P. Tognarelli, and A. Tranberg, "Oscillon Lifetime in the Presence of Quantum Fluctuations," *JHEP*, vol. 08, p. 125, 2014.

[83] T. Vachaspati and G. Zahariade, "Classical Hawking Radiation," 2018.

[84] ——, "Classical-quantum correspondence and backreaction," *Phys. Rev.*, vol. D98, no. 6, p. 065002, 2018.

[85] ——, "Classical-Quantum Correspondence for Fields," 2018.

[86] M. Mukhopadhyay and T. Vachaspati, "Rolling classical scalar field in a linear potential coupled to a quantum field," *Phys. Rev. D*, vol. 100, no. 9, p. 096018, 2019.

[87] R. C. Bernardo, "Inflationary quantum dynamics and backreaction using a classical-quantum correspondence," *Eur. Phys. J. C*, vol. 81, no. 11, p. 994, 2021.

[88] H. Fukunaga, N. Kitajima, and Y. Urakawa, "Efficient self-resonance instability from axions," *JCAP*, vol. 06, p. 055, 2019.

[89] F. Muia, M. Cicoli, K. Clough, F. Pedro, F. Quevedo, and G. P. Vacca, "The Fate of Dense Scalar Stars," *JCAP*, vol. 07, p. 044, 2019.

[90] Z. Nazari, M. Cicoli, K. Clough, and F. Muia, "Oscillon collapse to black holes," *JCAP*, vol. 05, p. 027, 2021.

[91] H.-Y. Zhang, "Gravitational effects on oscillon lifetimes," 11 2020.

[92] M. Kawasaki, W. Nakano, and E. Sonomoto, "Oscillon of Ultra-Light Axion-like Particle," *JCAP*, vol. 01, p. 047, 2020.

[93] H.-Y. Zhang, M. A. Amin, E. J. Copeland, P. M. Saffin, and K. D. Lozanov, "Classical Decay Rates of Oscillons," *JCAP*, vol. 07, p. 055, 2020.

[94] M. Kawasaki, W. Nakano, H. Nakatsuka, and E. Sonomoto, "Oscillons of Axion-Like Particle: Mass distribution and power spectrum," 10 2020.

[95] D. Cyncynates and T. Giurgica-Tiron, "Structure of the oscillon: The dynamics of attractive self-interaction," *Phys. Rev. D*, vol. 103, no. 11, p. 116011, 2021.

[96] N. Fonseca, E. Morgante, R. Sato, and G. Servant, "Axion fragmentation," *JHEP*, vol. 04, p. 010, 2020.

[97] H. Fukunaga, N. Kitajima, and Y. Urakawa, "Can axion clumps be formed in a pre-inflationary scenario?" *JCAP*, vol. 02, p. 015, 2021.

[98] P. Brax, J. A. R. Cembranos, and P. Valageas, "Nonrelativistic formation of scalar clumps as a candidate for dark matter," *Phys. Rev. D*, vol. 102, no. 8, p. 083012, 2020.

[99] J. H. Buckley, P. S. B. Dev, F. Ferrer, and F. P. Huang, "Fast radio bursts from axion stars moving through pulsar magnetospheres," *Phys. Rev. D*, vol. 103, no. 4, p. 043015, 2021.

[100] A. Prabhu and N. M. Rapidis, "Resonant Conversion of Dark Matter Oscillons in Pulsar Magnetospheres," *JCAP*, vol. 10, p. 054, 2020.

[101] N. Blinov, M. J. Dolan, and P. Draper, "Imprints of the Early Universe on Axion Dark Matter Substructure," *Phys. Rev. D*, vol. 101, no. 3, p. 035002, 2020.

[102] A. Prabhu, "Optical Lensing by Axion Stars: Observational Prospects with Radio Astrometry," 6 2020.

[103] M. A. Amin and Z.-G. Mou, "Electromagnetic Bursts from Mergers of Oscillons in Axion-like Fields," *JCAP*, vol. 02, p. 024, 2021.

[104] M. A. Amin, A. J. Long, Z.-G. Mou, and P. Saffin, "Dipole radiation and beyond from axion stars in electromagnetic fields," *JHEP*, vol. 06, p. 182, 2021.

[105] M. Kawasaki, W. Nakano, H. Nakatsuka, and E. Sonomoto, "Probing Oscillons of Ultra-Light Axion-like Particle by 21cm Forest," 10 2020.

[106] M. Kawasaki, K. Miyazaki, K. Murai, H. Nakatsuka, and E. Sonomoto, "Anisotropies in Cosmological 21 cm Background by Oscillons/I-balls of Ultra-light Axion-like Particle," 12 2021.

[107] V. A. Koutvitsky and E. M. Maslov, "Passage of test particles through oscillating spherically symmetric dark matter configurations," *Phys. Rev. D*, vol. 104, no. 12, p. 124046, 2021.

Part II

Papers

Paper A

Quantum Evaporation of Classical Breathers

Jan Ollé[*], Oriol Pujolàs[*], Tanmay Vachaspati[†], George Zahariade[†♯]

[*] *Institut de Física d'Altes Energies, Universitat Autònoma de Barcelona, E-08193 Bellaterra, Spain*
[†] *Physics Department, Arizona State University, Tempe, AZ 85287, USA.*
[♯] *Beyond Center for Fundamental Concepts in Science, Arizona State University, Tempe, AZ 85287, USA.*

This paper has been published in *Phys.Rev.D* 100 (2019) 4, 045011.

The layout has been revised.

Abstract

We apply the recently discovered classical-quantum correspondence (CQC) to study the quantum evaporation of breathers in an extended sine-Gordon model. We present numerical results for the decay rate of the breather as a function of the coupling strength in the model. This is a complete treatment of the backreaction of quantum radiation on the classical dynamics of oscillons.

1 Introduction

Oscillons are long-lived localized oscillating solutions of non-linear wave equations. They occur in many different fields of physics, such as condensed matter theory [1] or cosmology [2], and have been studied extensively. A particularly interesting example of such a solution is the so-called breather solution of the sine-Gordon model [3]. It is well-known that this model possesses soliton and antisoliton solutions interpolating between two consecutive vacua, which are non-perturbative, stable and stationary. In this context breather solutions can be interpreted as soliton-antisoliton bound state solutions which are time-periodic and perfectly stable.

It is of course understood that breathers are purely classical solutions but their stability properties can be shown to extend into the quantum realm [4]. This however ceases to hold when one introduces a coupling to a quantum radiative field. The quantum evaporation of breathers can be studied in the limit where the breather itself is treated classically and provides a time-dependent background causing the radiation field to get excited, thereby losing energy and slowly decaying. The classical breather thus becomes a "quantum oscillon". This radiative phenomenon is analogous to particle production during gravitational collapse (Hawking radiation) [5] or pair creation in electric fields (Schwinger pair production) [6].

This radiative phenomenon has been studied in detail by Hertzberg in Ref. [7] but there the backreaction of the quantum radiation on the classical breather background was not fully taken into account. In this work we provide a full treatment of the classical breather decay under the effect of quantum radiation *i.e.* fully incorporating backreaction effects. We do this by using the recently developed classical-quantum correspondence (CQC) described at length in Refs. [8–10]. The CQC method is identical to the "mode function method" used previously in the literature (see *e.g.*, [11–14]). In [11] the technique was used to study fermion production and backreaction in classical scalar plus gauge field backgrounds; in [12–14] particle production and backreaction in solitonic backgrounds were treated but also including other assumptions because of particle interactions.

Quantum backreaction on classical backgrounds is generally calculated in the semiclassical approximation. This is an iterative procedure and usually only the first iteration is carried out as continuing the iterations is quite laborious. Within the CQC however, the quantum fields are replaced by corresponding complexified classical variables. The dynamics of these classical variables together with the classical background defines a new entirely classical dynamics problem that can be solved by numerical or other means. The resulting solution for the classical background is precisely the backreacted solution we are seeking. Application of this technique to a quantum mechanical example, where the full solution can also be calculated, shows excellent agreement [8].

In Sec. 2 we start by introducing the notations pertaining to the particular evaporating breather model we will be studying. The $1+1$ dimensional model will involve a classical sine-Gordon field

$\phi(t,x)$ and a quantum massless scalar field $\psi(t,x)$ coupled together via a bi-quadratic interaction term. In Sec. 3 we discretize this mixed classical-quantum model on a lattice and map it to a fully classical system with well-defined initial conditions that exactly mimics the full backreacted dynamics. This mapping is achieved via the CQC which we briefly describe in this particular context. In Secs. 4 and 5 we set up the numerical simulation of the dynamics and describe its results. We conclude with Sec. 6 where we discuss the validity of our analysis and compare it to previous work.

2 Field theory model

We consider the sine-Gordon model plus an extra real scalar field with bi-quadratic coupling:

$$L = \int dx \left[\frac{1}{2}\dot{\phi}^2 - \frac{1}{2}\phi'^2 - m_\phi^2(1-\cos\phi) + \frac{1}{2}\dot{\psi}^2 - \frac{1}{2}\psi'^2 - \frac{\lambda}{2}\phi^2\psi^2 \right]. \tag{A.1}$$

Here dotted (*resp.* primed) quantities denote time (*resp.* spatial) derivatives, m_ϕ is the mass of the excitations about the vacua, and we use natural units where $\hbar = c = 1$. The classical breather solution,

$$\phi_b(t,x) = 4\,\tan^{-1}\left[\frac{\eta\sin(\omega t)}{\cosh(\eta\omega x)}\right], \quad \psi = 0 \tag{A.2}$$

with $\eta = \sqrt{m_\phi^2 - \omega^2}/\omega$, is an exact classical solution to the equations of motion that is time-dependent, periodic and non-dissipative *i.e.* it has an infinite lifetime. However at the quantum level, the ψ field will get excited and this quantum radiation will backreact on the breather and cause it to evaporate.

In general, it is difficult to couple the quantum excitations of the field ψ to the purely classical breather solution. Indeed, calculating such backreaction effects requires in principle working in the fully quantized theory and since the breather is a non-perturbative solution of the sine-Gordon model, results can only be obtained via computationally intensive lattice field theory simulations. Another avenue generally used is the semi-classical approximation whereby the dynamics of the quantum field ψ are first determined in the presence of the fixed classical background ϕ, then the classical equations of motion for the field ϕ are solved by substituting ψ^2 for its vacuum expectation value $\langle\psi^2\rangle$, and finally the procedure is reiterated in order to get better and better approximations to the backreaction.

In the following, we will choose a somewhat different path and study the evaporation of the breather using the classical-quantum correspondence (CQC) developed in Refs. [8–10]. Notice that the CQC only applies to the case of free quantum fields. To generalize the method to scenarios where the field ψ has self-interactions requires approximation methods [12].

3 Lattice version

We first discretize the theory by putting it on a spatial lattice as in Ref. [9]. More precisely, we introduce an IR regulator L for the spatial domain (physical size of the lattice) and divide the interval $[-L/2, L/2]$ into $N+1$ intervals of size $a = L/(N+1)$. For any integer i running from 0 to $N+1$ we then define

$$\phi(t, ia - L/2) = \phi_i(t)\,, \tag{A.3}$$
$$\psi(t, ia - L/2) = \psi_i(t) \tag{A.4}$$

and impose Dirichlet boundary conditions $\phi_0 = \phi_{N+1} = \psi_0 = \psi_{N+1} = 0$ at "spatial infinity." With these definitions (A.1) is well approximated by

$$\begin{aligned} L^{(N)} = \sum_{i=1}^{N} a \Bigg[& \frac{1}{2}\dot{\phi}_i^2 + \frac{1}{2a^2}\phi_i(\phi_{i-1} - 2\phi_i + \phi_{i+1}) \\ & + \frac{1}{2}\dot{\psi}_i^2 + \frac{1}{2a^2}\psi_i(\psi_{i-1} - 2\psi_i + \psi_{i+1}) \\ & - m_\phi^2(1 - \cos\phi_i) - \frac{\lambda}{2}\phi_i^2\psi_i^2 \Bigg]\,. \end{aligned} \tag{A.5}$$

Introducing the matrix Ω^2 defined by

$$\Omega^2_{ij} = \begin{cases} +2/a^2 + \lambda\phi_i^2\,, & \text{if } i = j \\ -1/a^2\,, & \text{if } i = j \pm 1\,. \end{cases} \tag{A.6}$$

we can recast the ψ dependent part of (A.5) in more compact form as

$$L_\psi^{(N)} = \sum_{i,j=1}^{N} \left[\frac{a}{2}\dot{\psi}_i\delta_{ij}\dot{\psi}_j - \frac{a}{2}\psi_i\Omega^2_{ij}\psi_j \right]\,. \tag{A.7}$$

As we have discussed in the previous section, the breather solution (A.2) is classically non-disssipative, but not quantumly. In order to study its quantum evaporation, we make use of the techniques developed in Ref. [9]. In the spirit of the CQC, we assume that the ϕ_is are classical degrees of freedom while the ψ_is are quantum. At time $t = 0$ the initial conditions for ϕ_i are such that if λ were to be set to zero, one would recover the non-dissipative breather solution. The quantum harmonic oscillators ψ_i on the other hand are taken to be in their ground state initially. (Since $\phi(t = 0, x) = 0$ this corresponds to the quantum field ψ being in its non-interacting ($\lambda = 0$) vacuum.) Because of the explicit time-dependence induced by the presence of the $\lambda\phi_i^2$ term in Ω^2, their quantum state subsequently evolves and their average energy increases. Within the CQC, this situation can be accurately and quantitatively described by promoting the quantum degree of freedom ψ_i to a classical complex $N \times N$ matrix coefficient Z_{ij}/a. This results in the following substitution at the level of the discretized Lagrangian:

$$L_\psi^{(N)} \to L_Z^{(N)} = \sum_{i,j,k=1}^{N} \left[\frac{1}{2a}\dot{Z}^*_{ij}\delta_{ik}\dot{Z}_{kj} - \frac{1}{2a}Z^*_{ij}\Omega^2_{ik}Z_{kj} \right]\,. \tag{A.8}$$

In addition to the above substitution, the CQC paradigm also requires that we choose very specific initial conditions for the classical variables Z_{ij}. These are most easily written in matrix notation:

$$Z_0 = -i\sqrt{\frac{a}{2}}\sqrt{\Omega_0}^{-1} \quad \text{and} \quad \dot{Z}_0 = \sqrt{\frac{a}{2}}\sqrt{\Omega_0}\,. \tag{A.9}$$

Here the zero subscript denotes initial values while the square root of a symmetric positive definite matrix $S = O.\mathrm{Diag}(\lambda_1, \lambda_2, \ldots, \lambda_N).O^T$ is defined to be $\sqrt{S} = O.\mathrm{Diag}(\sqrt{\lambda_1}, \sqrt{\lambda_2}, \ldots, \sqrt{\lambda_N}).O^T$.

Finally the CQC Lagrangian reads

$$\begin{aligned} L^{(N)}_{CQC} &= \sum_{i=1}^{N} a\left[\frac{1}{2}\dot{\phi}_i^2 + \frac{1}{2a^2}\phi_i(\phi_{i-1} - 2\phi_i + \phi_{i+1})\right. \\ &\qquad \left. -m_\phi^2(1-\cos\phi_i)\right] \\ &+ \sum_{i,j,k=1}^{N}\left[\frac{1}{2a}\dot{Z}^*_{ij}\delta_{ik}\dot{Z}_{kj} - \frac{1}{2a}Z^*_{ij}\Omega^2_{ik}Z_{kj}\right]. \end{aligned} \tag{A.10}$$

Note that the interaction term is present in the very last term because the definition of Ω^2 contains ϕ as in (A.6).

In the next section we will set the problem up for numerical simulation.

4 Numerical setup

To understand how the quantum evaporation of the classical breather proceeds in time we will solve the discretized equations of motion stemming from (A.10). The evolution of ϕ will be described by the ordinary differential equations

$$\begin{aligned} &\ddot{\phi}_i - \frac{1}{a^2}\left(\phi_{i+1} - 2\phi_i + \phi_{i-1}\right) + m_\phi^2\sin(\phi_i) \\ &\qquad +\lambda\left(\frac{1}{a^2}\sum_{j=1}^{N} Z^*_{ij}Z_{ij}\right)\phi_i = 0\,, \end{aligned} \tag{A.11}$$

with initial conditions that would yield the non-dissipative breather solution in the $\lambda = 0$ limit *i.e.*

$$\phi_i(t=0) = 0\,, \tag{A.12}$$

$$\dot{\phi}_i(t=0) = \frac{4\eta\omega}{\cosh\left(\eta\omega a\left(i - \frac{N+1}{2}\right)\right)}\,. \tag{A.13}$$

The Z_{ij} will evolve according to

$$\ddot{Z}_{ij} + \Omega^2_{ik}Z_{kj} = 0\,, \tag{A.14}$$

with initial conditions prescribed by the CQC. More precisely, since $\phi_i(t=0) = 0$, it is easy to diagonalize the tri-diagonal matrix Ω_0^2 and obtain explicit expressions for the initial conditions for

Z_{ij}. Indeed we find that $\Omega_0^2 = ODO^T$, where

$$D_{ij} = \frac{4}{a^2}\sin^2\left(\frac{\pi i}{2(N+1)}\right)\delta_{ij}\,, \tag{A.15}$$

and O is an orthogonal matrix with components,

$$O_{ij} = \sqrt{\frac{2}{N+1}}\sin\left(\frac{\pi ij}{N+1}\right)\,. \tag{A.16}$$

Therefore using (A.9) we can explicitly write

$$Z_{ij}(t=0) = \frac{-ia}{N+1}\sum_{k=1}^{N}\frac{\sin\left(\frac{\pi ik}{N+1}\right)\sin\left(\frac{\pi kj}{N+1}\right)}{\sqrt{\sin\left(\frac{\pi k}{2(N+1)}\right)}}\,, \tag{A.17}$$

$$\dot{Z}_{ij}(t=0) = \frac{2}{N+1}\sum_{k=1}^{N}\sin\left(\frac{\pi ik}{N+1}\right)\sin\left(\frac{\pi kj}{N+1}\right) \times\sqrt{\sin\left(\frac{\pi k}{2(N+1)}\right)}\,. \tag{A.18}$$

The numerical solution to the coupled system of ordinary differential equations (A.11) and (A.14) with respective initial conditions (A.12),(A.13), (A.17) and (A.18) will thus yield the dynamics of the quantum evaporation of the classical breather. In the following we will take $m_\phi = 1$, $\omega = 0.25$ and $L = 100$ (the latter choice thus completely fixing our units). Note that because of the Dirichlet boundary conditions that we used to implement our discretized model, we will only be able to trust our results for maximum integration times T of the order of the size of the lattice L (light crossing time) beyond which spurious reflections are expected to spoil the predictivity of the numerical analysis.

Notice also that because of the matrix nature of the Z variable, the computational complexity of this numerical problem increases as $N^2 \propto 1/a^2$ or in other words as the inverse square of the spatial resolution.

Before going on to discuss our numerical results, we need to address the dependence of our results on the lattice spacing a. Backreaction of the quantum radiation on the classical breather is encoded in the Z^*Z factor in parentheses appearing in Eq. (A.11). The factor diverges logarithmically as $a \to 0$ (for fixed $L = Na$) since, at the initial time we find

$$\frac{1}{a^2}\sum_{j=1}^{N} Z^*_{ij}Z_{ij} \sim \frac{1}{2\pi}\ln N \sim \frac{1}{2\pi}\ln(\mu L) \tag{A.19}$$

where $\mu \equiv 1/a$ is the energy scale corresponding to the lattice cutoff. If we now rescale $\mu \to \zeta\mu$, the Z^*Z factor shifts by $\ln(\zeta)/(2\pi)$. In (A.11), a shift in the Z^*Z factor is equivalent to a shift in the mass term of ϕ. Hence to compare results at different lattice spacings we should ensure that the classical potential $V(\phi)$ is correspondingly adjusted to obtain the same physical mass for ϕ. In other

words, if we rescale $\mu \to \zeta\mu$, we should also change the potential $V(\phi) \to V(\phi) - \lambda \ln(\zeta)\phi^2/(4\pi)$, and then (A.11) is invariant under the rescaling (except for discretization effects in the Laplacian term).

Now that we know how $V(\phi)$ changes with a rescaling of the lattice spacing a, we need a physical input that tells us the potential for some particular value of the lattice spacing, call it a_*. Given that a plays the role of the spatial resolution, we must require that this is enough to resolve the smallest physical object in the simulation box, the breather, whose size is of order 1 (in units where $m_\phi = 1$). For our purposes it will suffice to take $a_* \approx 0.2$ (which corresponds to a lattice with $N_* = 500$ points) and assume that $V(\phi)$ is the classical sine-Gordon potential at this resolution.

The equations of motion (A.11) and (A.14) with initial conditions (A.12),(A.13), (A.17), (A.18) can now be solved numerically using explicit methods in Fortran and also in Mathematica (for smaller values of N). As noted above, the computational costs scale as N^2 and we are effectively limited to $N \leq 1000$.

5 Results

As discussed in the introduction, we expect the classical breather field ϕ to evaporate under the effect of the coupling to the quantum radiation field ψ. This can be explicitly seen in Figs. A.1a and A.1b where we plot snapshots of the breather spatial profile with and without quantum backreaction taken into account: indeed the evaporating breather oscillates at a higher frequency and with decreasing amplitude as compared to the non-evaporating one. The amplitude plots of Figs. A.1c and A.1d confirm these heuristic observations.

We are in particular interested in the breather's decay rate and in how this rate changes with the physical coupling constant λ. As mentioned previously, we would also like to check if our renormalization scheme leads to similar evaporation rates when we change N.

In Fig. A.2 we plot the energy of the breather

$$\begin{aligned} E_{\text{breather}} &= \int dx \left(\frac{1}{2}\dot{\phi}^2 + \frac{1}{2}\phi'^2 + m_\phi^2(1-\cos\phi) \right) \\ &\approx a\sum_{i=1}^{N} \left[\frac{1}{2}\dot{\phi}_i^{\,2} - \frac{1}{2a^2}\phi_i(\phi_{i-1} - 2\phi_i + \phi_{i+1}) \right. \\ &\qquad \left. + m_\phi^2(1-\cos\phi_i) \right], \end{aligned} \tag{A.20}$$

as a function of time for several different values of λ, keeping all other parameters fixed. With $\lambda = 0$, the breather does not decay, as expected. For non-vanishing λ, the breather decays while also undergoing small oscillations. As λ becomes larger, the breather decays faster and the amplitude and frequency of the oscillations grow (which can readily be seen on Figs. A.3 and A.4).

For a more quantitative result we could furthermore find a power law fit of the upper and lower envelopes bounding this oscillatory behavior to estimate the breather lifetime and understand its dependence on λ in particular. Here we only show a linear fit of the large time behavior of the lower envelope in Fig. A.5 for different values of λ. With the exception of the $\lambda = 0.1$ case where the fit is poorer, the slopes increase in absolute value with increasing λ which is consistent with the intuitive idea that the breather lifetime decreases as the coupling becomes stronger.

Finally we check that our renormalization prescription is the correct one for dealing with the small a limit. To do this we plot the breather energy for different values of N for the same L and λ with and without mass renormalization (Figs. A.6a and A.6b). It is clear from these two plots that the dependence on the effective description is dramatically mitigated through the use of our renormalization prescription: the obvious drift in Fig. A.6a is greatly reduced when we shift the value of the bare mass squared by $\lambda \ln(a/a_*)/(2\pi)$ in order for m_ϕ to correspond to the physical mass of the sine-Gordon field. The small residual drift can be attributed to finite N effects *i.e.* contributions to the renormalization that are sub-leading in N and numerical errors due to the coarseness of the lattice. In the $N \to \infty$ limit both these contributions will vanish.

These results, especially Figs. A.2 and A.5, give clear evidence that the breather evaporates by emitting quanta of ψ. In our setup, this comes together with oscillations in the breather energy. In order to understand the origin of these oscillations, note that the vacuum fluctuations of ψ give rise to a nonzero $\langle\psi^2\rangle$, which is affected by the boundary conditions imposed on our simulation box of finite length L as in the Casimir effect.

It is natural to ask how the initial quantum fluctuations of ψ, as measured by $\langle\psi^2\rangle_{t=0}$, affect the breather evolution. This is very simple to answer by considering the SG model perturbed by a constant mass term, $\Box\phi + \sin\phi + m_{\text{eff}}^2\,\phi = 0$, with $m_{\text{eff}}^2 = \lambda\langle\psi^2\rangle_{t=0}$. The energy stored in the breather in this model (without including the m_{eff}^2 perturbation term) exhibits very similar behaviour to that in Figs. A.2 and A.5, including the oscillations with a definite $\lambda-$dependent period. More specifically, taking $m_{\text{eff}}^2 = \lambda \sum Z^* Z/a^2$ evaluated at the center of the box (and at $t = 0$), the plot in Fig. (A.3) is reproduced with better than 10% precision. Note that, the frequency is seen to approach twice the breather frequency at $\lambda \ll 1$, which is readily understood because the perturbation of the SG model at lowest order in λ is proportional to ϕ^2.

This suggests that the oscillatory behaviour in the breather energy can be interpreted as originating from the quantum vacuum fluctuations of ψ. On top of this, there is the quantum creation of ψ particles which leads to the decrease of the average breather energy over time. Thus the CQC scores a double goal, capturing the two kinds of quantum effects at once – as it should.

6 Conclusions

In the previous section we have studied the decay of the breather numerically via the CQC. Backreaction was fully taken into account. A legitimate question that might arise is whether the predictions of the CQC actually correspond to the full quantum solution *i.e.* where both breather and radiation field are treated quantumly. It turns out that in the fixed background approximation the $1/a^2 \sum_{j=1}^{N} Z_{ij}^* Z_{ij}$ term responsible for the backreaction is actually exactly equal to the vacuum expectation value $\langle 0|\psi_i^2|0\rangle$. Therefore the solution of the dynamical system discussed in this paper can be seen to correspond to the limit of a semi-classical iterative procedure where one starts with the classical breather solution, computes the quantum radiation in this background, uses it to calculate the first semi-classical correction to the background and repeats this process *ad infinitum*. To our knowledge this is the first time such a numerical calculation is carried out in full. Usually, the first iteration of this semi-classical procedure is carried out and claimed to give accurate results. However this can lead to relative errors of order 100% as discussed in Ref. [8] in the context of a $0+1$ dimensional toy model. Previous work on the quantum decay of oscillons [7] used methods analogous to

the CQC to calculate the radiation rate on a fixed oscillon background. However the backreaction on the oscillon background was not computed.

The method outlined in this paper can be very powerful in computing quantum backreaction on classical backgrounds but it is important to be aware of its limitations in order to successfully apply it to other field theory models. First of all, it only yields accurate results in the limit where the background can actually be treated classically. This is only true in the limit where the pure sine-Gordon part of the action evaluated for the breather solution dominates the quantum radiation as well as the interaction parts (this can be seen by temporarily restoring the reduced Planck constant $\hbar$). We see that this requirement amounts to [4]

$$E_{\text{breather}} \sim 16 m_\phi \sqrt{1 - \frac{\omega^2}{m_\phi^2}} \gg E_Z - \frac{1}{2}\text{Tr}\,\Omega_0\,, \tag{A.21}$$

where $E_Z = \sum_{i,j,k=1}^{N} [\dot{Z}^*_{ij}\delta_{ik}\dot{Z}_{kj}/2a + Z^*_{ij}\Omega^2_{ik}Z_{kj}/2a]$ and the subtraction in the last term is meant to remove the vacuum energy contribution (which diverges quadratically with N). For our choice of parameters and since total energy is conserved, Fig. A.2 shows that this condition will hold up to times $T \sim L$ as long as $\lambda \ll 1$.

Second, our method also has intrinsic numerical limitations chief among which is its quadratic computational complexity in the size of the lattice. This renders high resolution computations intractable and is a source of numerical error which manifests itself in what could be termed finite N artifacts (such as the residual N-dependent drift in the energy of the breather even after coupling constant renormalization, or the imperfect conservation of total energy). Another source of inaccuracy are the perfectly reflecting boundary conditions chosen in the discretization of the continuous problem which set an upper bound on the meaningful integration time.

However these limitations also suggest new avenues for improvement. In particular parallelizing the code would allow for larger lattices, both potentially increasing the resolution and pushing the spatial boundaries further so as to allow for larger integration times. One could also implement higher order discretization schemes to increase accuracy, or absorbing boundary conditions to reduce spurious reflections.

Finally, it should be mentioned that this technique should be readily applicable to more complicated field theory scenarios such as backreaction of quantum radiation on a gravitationally collapsing background or Schwinger pair creation (recall however that the quantum field cannot have self-interactions). However, gravitational scenarios will necessarily involve more intricate renormalization schemes in particular when dealing with vacuum energy divergences. Another interesting question is whether one can use the CQC to obtain the quantization of the breather spectrum in the full quantum SG theory [4]. By separating the SG field into a classical breather plus quantum fluctuations and treating the latter via CQC one may perhaps reproduce this classic result.

We have thus solved for the quantum evaporation of classical breathers by applying the CQC. This is the first application of the CQC to a field theory problem that has not been solved by traditional methods. The CQC relies on the classicality of the background variable and if the background is quantum there will be deviations from the CQC as seen in the quantum mechanical example in [8]. Thus it will still be useful to solve the breather evaporation problem in full quantum field theory in order to compare to the CQC result and to understand the method's limitations. However, since

the breather is non-perturbative, we expect that a quantum field theory treatment will require new techniques and/or a lattice implementation. In the context of gravity, the CQC may be the only hope to solve important problems such as black hole evaporation because we do not yet have a quantum theory of gravity.

Acknowledgments

TV is supported by the U.S. Department of Energy, Office of High Energy Physics, under Award No. DE-SC0019470 at Arizona State University and GZ is supported by John Templeton Foundation grant 60253.
JO and OP acknowledge support by the Spanish Ministry MEC under grant FPA2017-88915-P, the Severo Ochoa excellence program of MINECO (grant SEV-2016-0588), as well as by the Generalitat de Catalunya under grant 2017SGR1069. We also acknowledge the support of the Centro de Ciencias de Benasque Pedro Pascual for hosting the workshop 'Probes of BSM - from the Big Bang to the LHC' , where this project was initiated.

References

[1] P. B. Umbanhowar, F. Melo, and H. L. Swinney, "Localized excitations in a vertically vibrated granular layer," *Nature*, vol. 382, no. 6594, pp. 793–796, 1996. [Online]. Available: https://doi.org/10.1038/382793a0

[2] M. A. Amin, R. Easther, H. Finkel, R. Flauger, and M. P. Hertzberg, "Oscillons After Inflation," *Phys. Rev. Lett.*, vol. 108, p. 241302, 2012.

[3] M. J. Ablowitz, D. J. Kaup, A. C. Newell, and H. Segur, "METHOD FOR SOLVING THE SINE-GORDON EQUATION," *Phys. Rev. Lett.*, vol. 30, pp. 1262–1264, 1973.

[4] S. Coleman, *Aspects of Symmetry*. Cambridge, U.K.: Cambridge University Press, 1985.

[5] S. W. Hawking, "Particle Creation by Black Holes," *Commun. Math. Phys.*, vol. 43, pp. 199–220, 1975, [,167(1975)].

[6] J. S. Schwinger, "On gauge invariance and vacuum polarization," *Phys. Rev.*, vol. 82, pp. 664–679, 1951, [,116(1951)].

[7] M. P. Hertzberg, "Quantum Radiation of Oscillons," *Phys. Rev. D*, vol. 82, p. 045022, 2010.

[8] T. Vachaspati and G. Zahariade, "Classical-quantum correspondence and backreaction," *Phys. Rev.*, vol. D98, no. 6, p. 065002, 2018.

[9] ——, "Classical-Quantum Correspondence for Fields," 2018.

[10] ——, "Classical Hawking Radiation," 2018.

[11] G. Aarts and J. Smit, "Particle production and effective thermalization in inhomogeneous mean field theory," *Phys. Rev.*, vol. D61, p. 025002, 2000.

[12] S. Borsanyi and M. Hindmarsh, "Semiclassical decay of topological defects," *Phys. Rev.*, vol. D77, p. 045022, 2008.

[13] ——, "Low-cost fermions in classical field simulations," *Phys. Rev.*, vol. D79, p. 065010, 2009.

[14] P. M. Saffin, P. Tognarelli, and A. Tranberg, "Oscillon Lifetime in the Presence of Quantum Fluctuations," *JHEP*, vol. 08, p. 125, 2014.

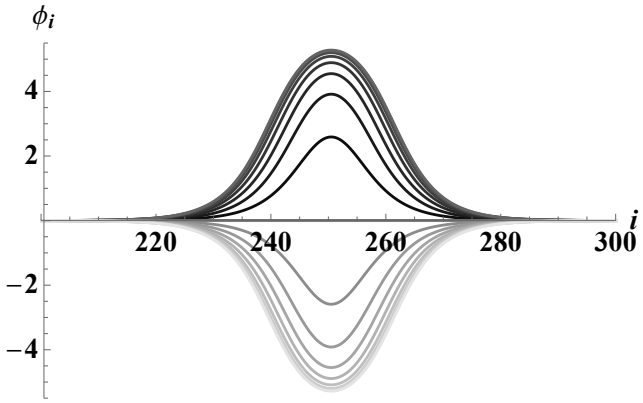

(a) Spatial profile of the breather (ϕ_i as a function of the lattice position i) in the absence of evaporation *i.e.* when $\lambda = 0$. The snapshots are taken every one sixteenth of a period and later times correspond to lighter shades of gray.

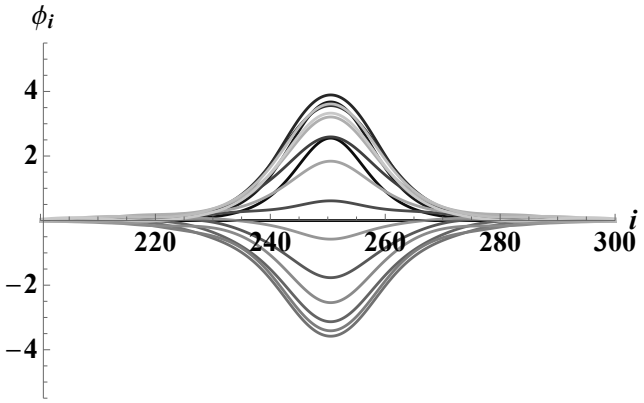

(b) Spatial profile of the breather (ϕ_i as a function of the lattice position i) with evaporation taken into account *i.e.* when $\lambda = 0.1$. The snapshots are taken every one sixteenth of a period (of the non-evaporating breather) and later times correspond to lighter shades of gray.

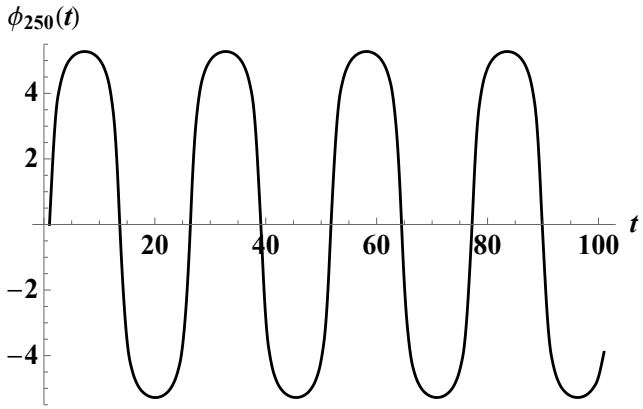

(c) Breather amplitude *i.e.* value of the field at the center of the lattice, as a function of time in the absence of evaporation *i.e.* when $\lambda = 0$.

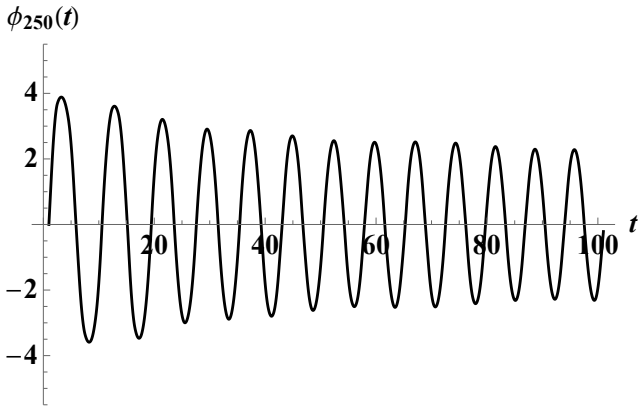

(d) Breather amplitude *i.e.* value of the field at the center of the lattice, as a function of time with evaporation taken into account *i.e.* when $\lambda = 0.1$.

Fig. A.1: Visualisation of the breather dynamics with and without backreaction. Here $N = 500$.

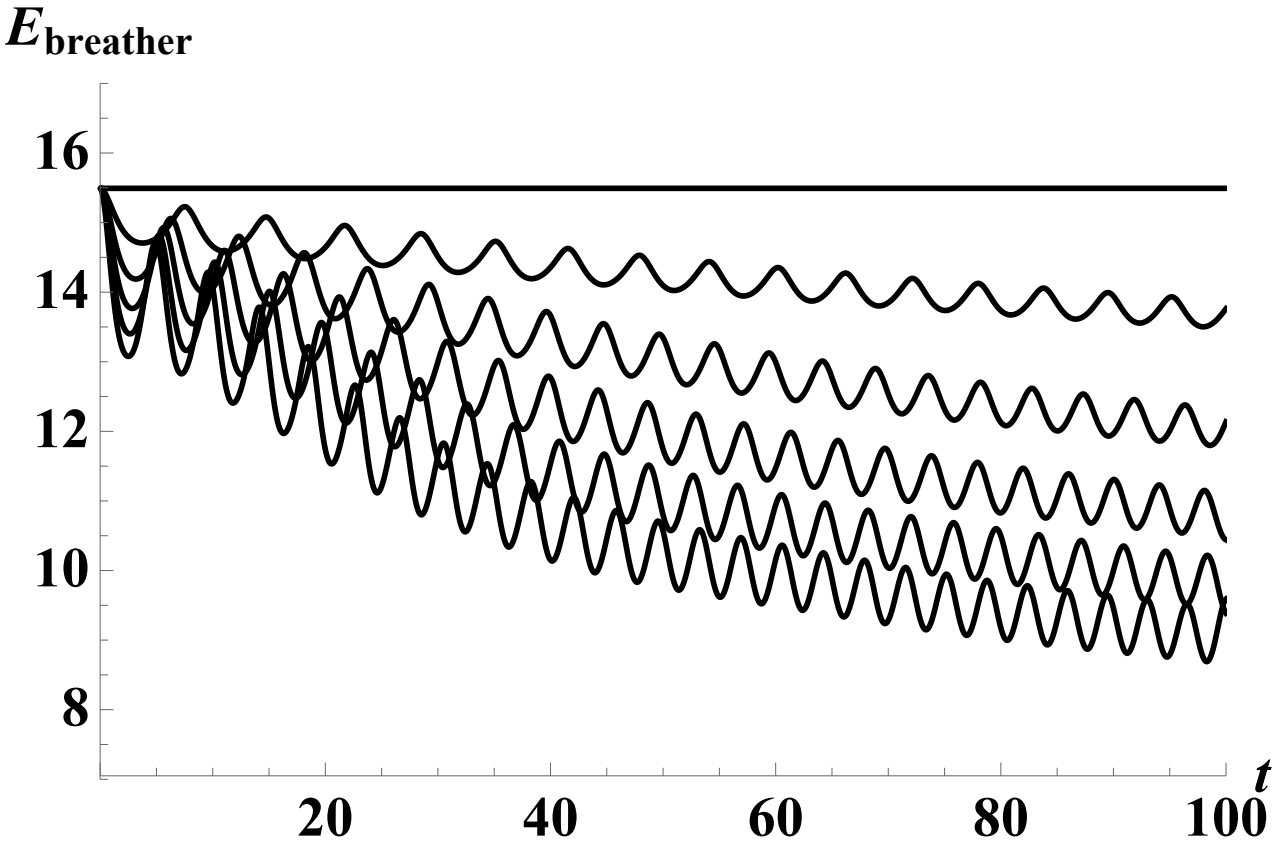

Fig. A.2: Breather energy as a function of time for different values of the physical coupling constant λ. The top (flat) curve corresponds to $\lambda = 0$ while the decaying oscillatory curves correspond, from top to bottom, to λ =0.02, 0.04, 0.06, 0.08 and 0.1. Here $N = 500$.

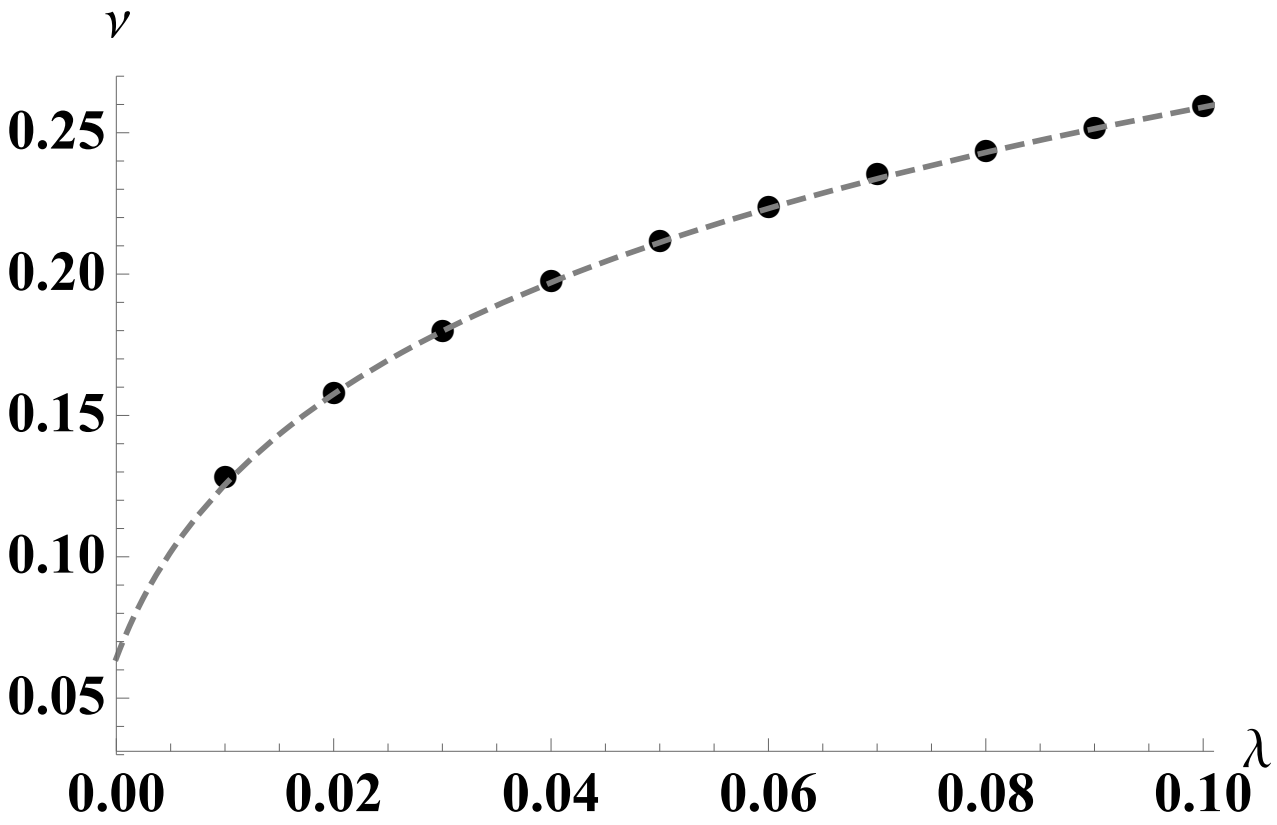

Fig. A.3: Average frequency of oscillation ν of the breather energy as a function of λ. (The oscillation frequency of the breather amplitude is half that of the energy because E is quadratic in ϕ.) The dashed curve represents the best fit power law model: $\nu \approx -0.44 + 0.90(0.01 + \lambda)^{0.11}$. Here $N = 500$.

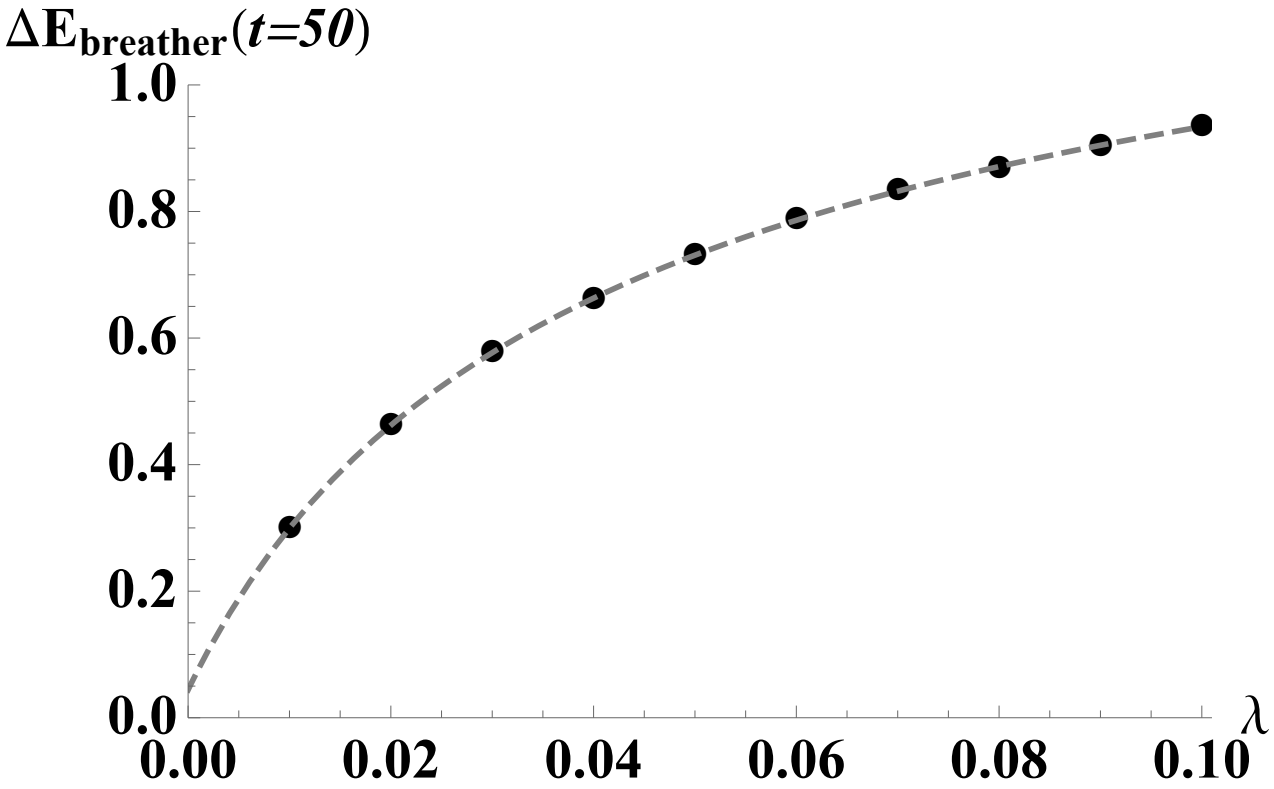

Fig. A.4: Amplitude of oscillation of the breather energy (around time $t = 50$) as a function of λ. The dashed curve represents the best fit power law model: $\Delta E_{\text{breather}}(t = 50) \approx 1.55 - 0.20/(0.03 + \lambda)^{0.56}$. Here $N = 500$.

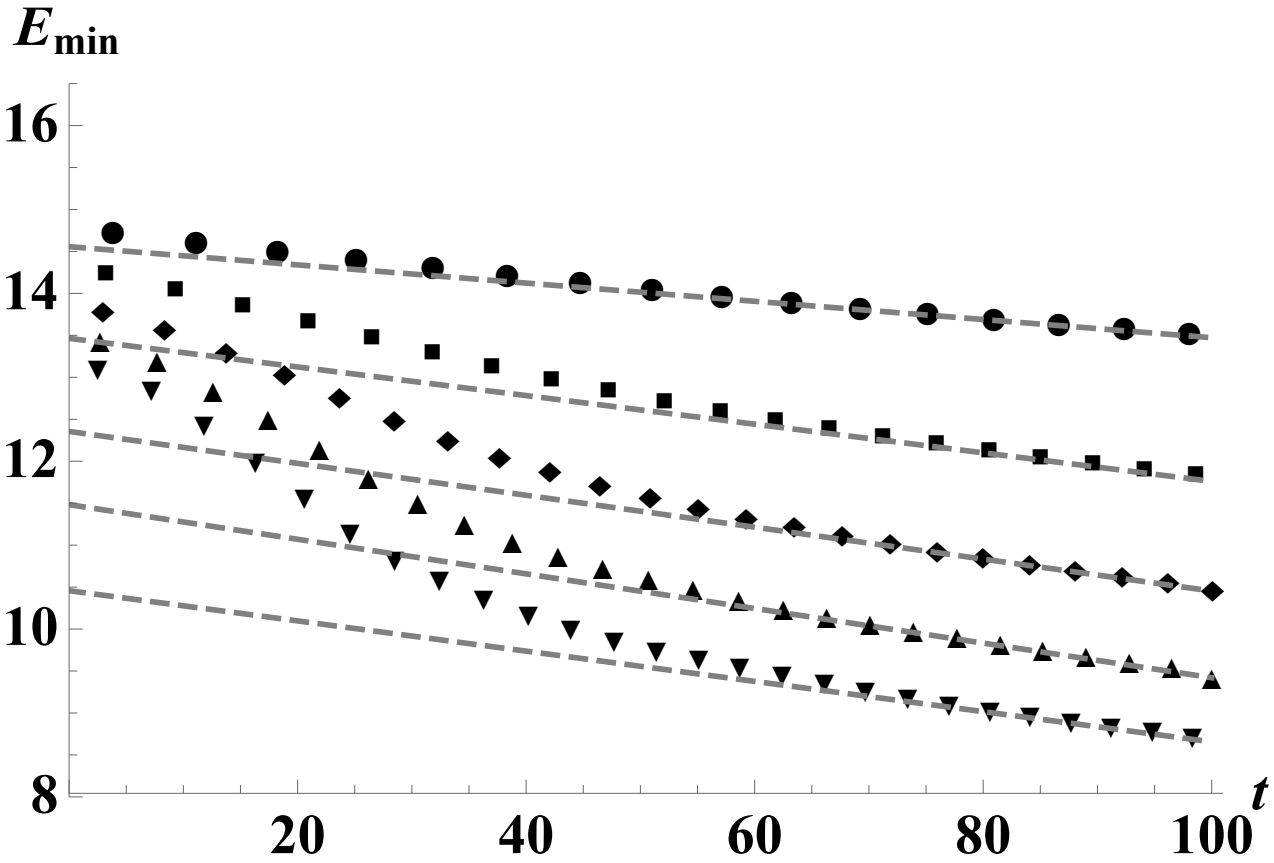

Fig. A.5: Local minima of the breather energy as a function of time for λ =0.02, 0.04, 0.06, 0.08 and 0.1 (corresponding to circle, square, diamond, upper and lower pointing triangles respectively). Also shown are the respective linear fits for late times with slopes of absolute values 0.011, 0.017, 0.019, 0.021, 0.018. Here $N = 500$.

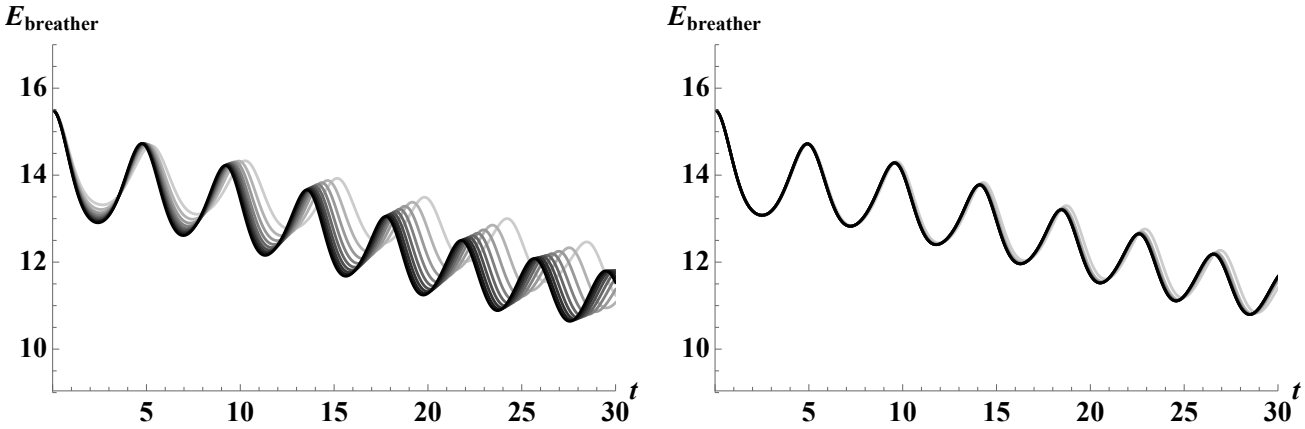

(a) Breather energy as a function of time for different values of N without mass renormalization. N varies from 200 (lightest shade of grey) to 1000 (darkest shade of grey) in increments of 100.

(b) Breather energy as a function of time for different values of N with mass renormalization. N varies from 200 (lightest shade of grey) to 1000 (darkest shade of grey) in increments of 100.

Fig. A.6: Sensitivity of the breather energy on N with and without coupling constant renormalization.

Paper B

Oscillons and Dark Matter

Jan Ollé[1], Oriol Pujolàs[1] and Fabrizio Rompineve[1]

[1] *Institut de Física d'Altes Energies (IFAE)*
The Barcelona Institute of Science and Technology (BIST)
Campus UAB, 08193 Bellaterra (Barcelona) Spain

This paper has been published in *JCAP* 02 (2020) 006.

The layout has been revised.

Abstract

Oscillons are bound states sustained by self-interactions that appear in rather generic scalar models. They can be extremely long-lived and have a built-in formation mechanism – parametric resonance instability. These features suggest that oscillons can affect the standard picture of scalar ultra-light dark matter (ULDM) models. We explore this idea along two directions. First, we investigate numerically oscillon lifetimes and their dependence on the shape of the potential. We find that scalar potentials that occur in well motivated axion-like models can lead to oscillons that live up to 10^8 *cycles or more. Second, we discuss the observational constraints on the ULDM models once the presence of oscillons is taken into account. For a wide range of axion masses, oscillons decay around or after matter-radiation equality and can thus act as early seeds for structure formation. We also discuss the possibility that oscillons survive up to today. In this case they can most easily play the role of dark matter.*

1 Introduction

In our Universe, a variety of visible structures with different length scales form as aggregates of smaller constituents that are kept together by the gravitational force. This is the case for planets, stars, solar systems and galaxies. The formation of bound objects is of course generic to any attractive interaction, and it is natural to wonder what would be the effect of self-interactions in the dark matter sector. Very much like gravity for visible matter, attractive self-interactions must lead to the formation of dark structures which can have important observational consequences.

Nontrivial bound states arise in the simplest field theory that one can imagine: a real scalar field with an attractive self-interaction. The bound objects in this case are then usually called *oscillons*. Interestingly, for very light scalar mass m, this class of models also offers a viable and well motivated dark matter candidate, what is usually dubbed scalar Ultra Light Dark Matter (ULDM) [1–9]. In this framework, then, dark matter can form by itself structures with rather definite properties (mass, size, lifetime). This paper is devoted to the study of how self-interactions affect the usual picture of ULDM, where they are mostly neglected even though in many models they are present or implicit. The most important effect of the attractive self-interactions is that at some point *oscillons* arise as part of the dark sector.

Oscillons are localized and oscillating configurations of a real scalar field, which are sustained solely by self-interactions [10–12]. The most relevant ones are spherically symmetric $\phi = \phi(t, r)$, so one can present them as solutions of the Klein-Gordon equation in flat spacetime with a nonlinear potential,

$$\ddot{\phi}(t, r) - \partial_r^2 \phi(t, r) - \frac{2}{r} \partial_r \phi(t, r) + V'(\phi(t, r)) = 0 \ . \tag{B.1}$$

Since a real scalar field carries no conserved charge, oscillons are unstable[1]: they lose energy even classically by emitting radiation in the form of scalar waves, and eventually decay into a 'wave-packet' that diffuses away (we show the energy density profile of an oscillon with its radiated waves in Fig. B.1). Nevertheless, depending on the strength and type of self-interactions, the radiation

[1] A charged scalar field can also lead to localized non-topological objects, known as Q-balls [13, 14], which can be stable provided self interactions are attractive.

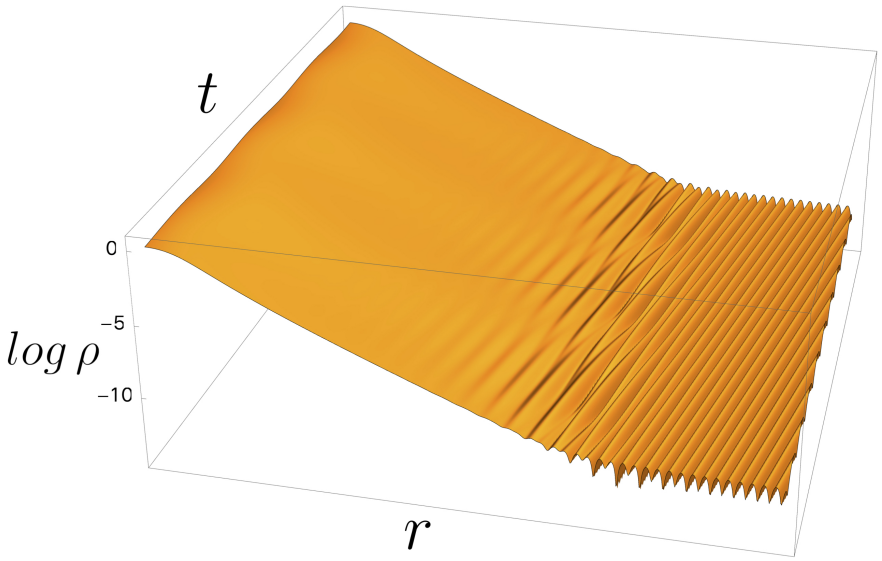

Fig. B.1: *Energy density profile of an oscillon: away from the central core the profile decays exponentially, until radiated scalar waves become relevant. Inside the core, the energy density oscillates in time.*

rate can be extremely slow, thereby leading to large oscillon lifetimes $\tau \gg m^{-1}$ and making them potentially very interesting for cosmology.

There is a considerable amount of literature on the topic of oscillons treating the conditions for them to appear, how can they be understood as attractors of the dynamics and trying to understand what determines their longevity, see e.g. [15–32] for a partial list of relevant work. For the purpose of elucidating their impact on cosmology, there are two basic requirements that guarantee that at some point oscillons will be present. On the one hand, the field needs to start out from a sufficiently inhomogeneous configuration. On the other hand, the scalar potential $V(\phi)$ needs to contain attractive self-interactions; more precisely, it should exhibit regions which are flatter than quadratic, i.e. $V' < m^2\phi$, otherwise self-interactions cannot sustain the localized overdensity. Both conditions are satisfied in a range of well-motivated models. The first example is the QCD axion model with $V(\phi) = m^2F^2(1 - \cos(\phi/F))$, which is known to exhibit oscillon solutions, also referred to as *axitons* [33, 34] (see also [35] for the formation of so-called *miniclusters*, [36, 37] for recent simulations and [38] for *axion stars*). In this model, however, oscillons are not very long-lived: their lifetimes are typically 'only' of order $\tau \sim 10^3\ m^{-1}$.

Still, in the zoo of models that give rise to ultra-light scalars, a much richer variety of potentials has been considered. For instance, in so-called axion monodromy [39, 40] constructions arising from string theory, the scalar potential can asymptote to a power-law behaviour at large field values $V(\phi) \sim \phi^{2p}$, with a variety of exponents p available in the market [41]. Having in mind this class of axion models, we will consider as a benchmark a family of scalar potentials that allows to make contact with these UV models while being simple enough to do a careful numerical study of the

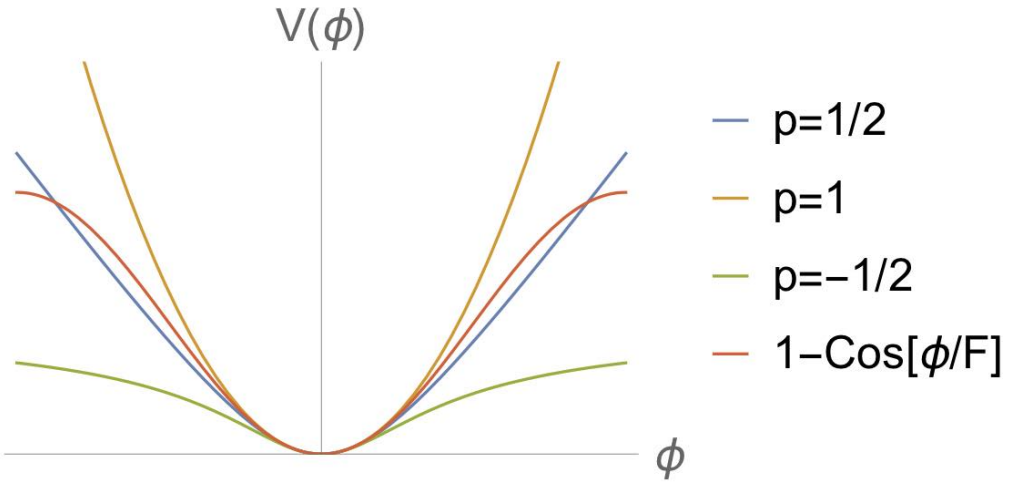

Fig. B.2: *Scalar potentials of the form* (B.2)*, compared to the standard quadratic* ($p = 1$) *and cosine potentials for axions.*

oscillon longevity. Specifically, we will take

$$V(\phi) = \frac{m^2 F^2}{2p}\left[\left(1+\frac{\phi^2}{F^2}\right)^p - 1\right] , \tag{B.2}$$

which is expected to lead to oscillons for $p < 1$. In this parameterization, there are two rather distinct cases. When $0 \leq p < 1$, the potentials are of axion-monodromy form since for $\phi \gg F$ the potential grows as a power law. For $p < 0$ instead, the potential saturates at large field values and exhibits a plateau region, see Fig. C.1.

The requirement to have initially inhomogeneous configurations is also automatically realized in this kind of ULDM model. The mechanism goes as follows: since the scalar is very light, it remains stuck because of Hubble friction during a large portion of the cosmological history. Assuming that the field is already present but subdominant during inflation, then the latter stretches it out to a very homogeneous value which does not need to coincide with the minimum of the potential. Well into the radiation era, the field is then going to roll down its potential and produce a homogeneous but time dependent background $\phi(t)$. Crucially, the homogeneous oscillations following from a potential of the form (B.2) with $p < 1$ lead to a parametric resonance instability of the vacuum fluctuations around $\phi(t)$: certain modes grow exponentially until the field has dumped a large fraction of its energy density into inhomogeneities. The condition that ensures that oscillon solutions form also guarantees that the homogeneous configuration is unstable. Therefore potentials like (B.2) (with $p < 1$) are equipped with a *fragmentation mechanism* whereby the homogeneous configuration is transformed into an admixture of oscillons and scalar radiation. Numerical simulations of this process show that in many cases the initial energy density goes in equal proportions to oscillons and small amplitude scalar waves [42, 43].

These appealing features of ULDM models with potentials (B.2) motivate the present study, which proceeds along two different directions. First, we focus on the formation and evolution of oscillons. To this aim, we perform a linear Floquet analysis of the potentials (B.2) and describe under which

conditions parametric resonance provides the right ground to form oscillons. We then numerically follow the evolution of a single oscillon configuration, according to (B.1). By also adding Hubble friction, we show that oscillons are essentially unaffected by the cosmological expansion, as they form with sizes which are significantly smaller than the Hubble radius at the time of formation. Thus, they can be considered as bound objects which are decoupled from the Hubble flow, very much like any gravitationally bound system in the late Universe. We aim in particular at establishing oscillon lifetimes and their dependence on the exponent p in (B.2). Very interestingly, while we succeed in doing so for $p \geq 0$, we are only able to put a lower bound on the lifetime for $p < 0$, due to our current numerical reach. The oscillons which we investigate are the longest-lived ever encountered, with lifetimes of order $10^8\ m^{-1}$ and even larger in the case $p < 0$.

These findings motivate the second part of our study, which deals with the observational impact of oscillons for dark matter models. Indeed, while oscillons form during the radiation dominated era from scalar field oscillations, for sufficiently small scalar masses they live up to and beyond the epoch of matter-radiation (MR) equality. Thus, they can potentially leave an important imprint on cosmology, either by serving as seeds for early structures or even by possibly making up a significant fraction of the dark matter today. These possibilities are especially likely to occur in the mass range which has been recently investigated in the context of fuzzy DM models [4, 9]. Here, we try to make contact with another peculiarity of this class of DM candidates, by proposing oscillons as early seeds for the well-known solitons of ULDM, which are however sustained by gravity (see [44–47] for more recent studies), in contrast with the objects which we focus on in this work. We thus describe constraints on different scenarios with dark matter made of two components, at least during a part of the cosmological history: field oscillations around the minimum of the potential and MACHO-like oscillons, with masses which increase as F increases and m decreases and span the range $10^{-12}\ M_\odot$ to $10^8 M_\odot$. The energy of these oscillons is concentrated in a region of size set by the inverse scalar mass, ranging between asteroid and galactic core scales as m decreases. One of the main points of this paper is thus that future numerical and analytic studies of scalar DM, and in particular of ULDM (see e.g. the simulations of [8]), should take into account the presence of overdensities on the scales of the oscillon size. This may lead to important changes in current constraints on these scenarios (see e.g. [48]).

Before moving on to the main content, let us put our work into context. The potentials (B.2) with $p > 0$ have been studied in the framework of inflation and arise in string-theoretical constructions of axion inflation [39, 40]. In some cases these potentials can be seen as representing theories with multi-branched potentials (see [49, 50] and [51–54]). Parametric instability and formation of oscillons during reheating after inflation has also been investigated in these setups [23, 25, 42, 55] (see also [56, 57] for the emission of gravitational waves from oscillons). Potentials with a plateau at large field values can also be obtained and are also used for inflation [58–63]. Their instabilities and the generation of oscillons have been studied in [43, 64, 65] and in [66], which also discuss some aspects of plateau-like potentials for ULDM models. Furthermore, in the interesting proposal [67], oscillons play a key role for dark matter, as 'mothers' to primordial black holes: at end of inflation oscillons from the inflaton field may dominate for long enough to form black holes which in the end account for dark matter.

This paper is organized as follows: in Sec. 2 we study the conditions under which parametric resonance is efficient (2.1); we numerically determine oscillon lifetimes (2.2); finally we discuss the

decay of an oscillon and its possible transition to a gravitationally-sustained soliton (2.3). We devote Sec. 3 to the observational implications of long-lived oscillons, separately discussing the cases of decay after (3.1) and before (3.2) MR equality. We discuss the possibility for oscillons to survive until today in Sec. 3.3. Finally, we offer our conclusions in Sec. 4.

2 Life and death of an oscillon

2.1 Birth

Oscillons are born out of inhomogeneous field configurations, which can originate from different mechanisms. On the one hand, one can consider a (pseudo)scalar field which is inhomogeneous from the very beginning of its cosmological history, as a result e.g. of a phase transition which leaves behind topological defects. This is the case of the QCD axion if the PQ symmetry is broken after inflation (see [33, 34]).

Alternatively, the scalar field can originally be homogeneous in the reheated universe and fragment into oscillons later during its evolution. This possibility is particularly relevant for axion fields with very large F, since in this case the PQ symmetry is broken during inflation, and will be the focus of this section. Starting from field values of $O(F)$, the time evolution of the homogeneous field then follows the nonlinear equation

$$\ddot{\phi}(t) + 3\,H\,\dot{\phi}(t) + V'(\phi(t)) = 0. \tag{B.3}$$

The way how the homogeneous field oscillations settle-in depends on the form of $V(\phi)$ (see e.g. [68] and references therein). Let us denote by ϕ_0 the amplitude of oscillations once they start. A good criterium for the Hubble rate at the beginning of the field oscillations is given by [43]

$$H_{\rm osc} \simeq \sqrt{\left|\frac{V'(\phi_0)}{\phi_0}\right|}. \tag{B.4}$$

The latter equation is a natural replacement for the criterium $H_{\rm osc} \simeq m$ for general nonlinear potentials. Notice that for $\phi_0 \gg F$ or for potentials which are very flat beyond $\phi \gtrsim F$, one has $H_{\rm osc} \ll m$. Otherwise, $H_{\rm osc} \lesssim m$, as usual.

Crucially for us, potentials of the form (B.2) support the phenomenon of parametric resonance: fluctuations of the initially homogeneous field can grow exponentially as the background field undergoes slow oscillations. Once a given mode becomes large enough, its further growth is prevented by backreaction of other modes and the resonant phase stops, leaving behind the desired highly inhomogeneous field configuration.

Here we want to assess the conditions under which parametric resonance can be strong enough for the potentials (B.2) (see also [42] for a recent study in the inflationary context). Let us then perform a linear analysis of the fluctuations, defined by $\phi \equiv \phi(t) + \delta\phi(\mathbf{x}, t)$. The equations of motion of the linear fluctuations in Fourier space are

$$\delta\ddot{\phi}_k(t) + 3H\delta\phi_k(t) + \left(\frac{k^2}{a^2} + V''(\phi(t))\right)\delta\phi_k(t) = 0, \tag{B.5}$$

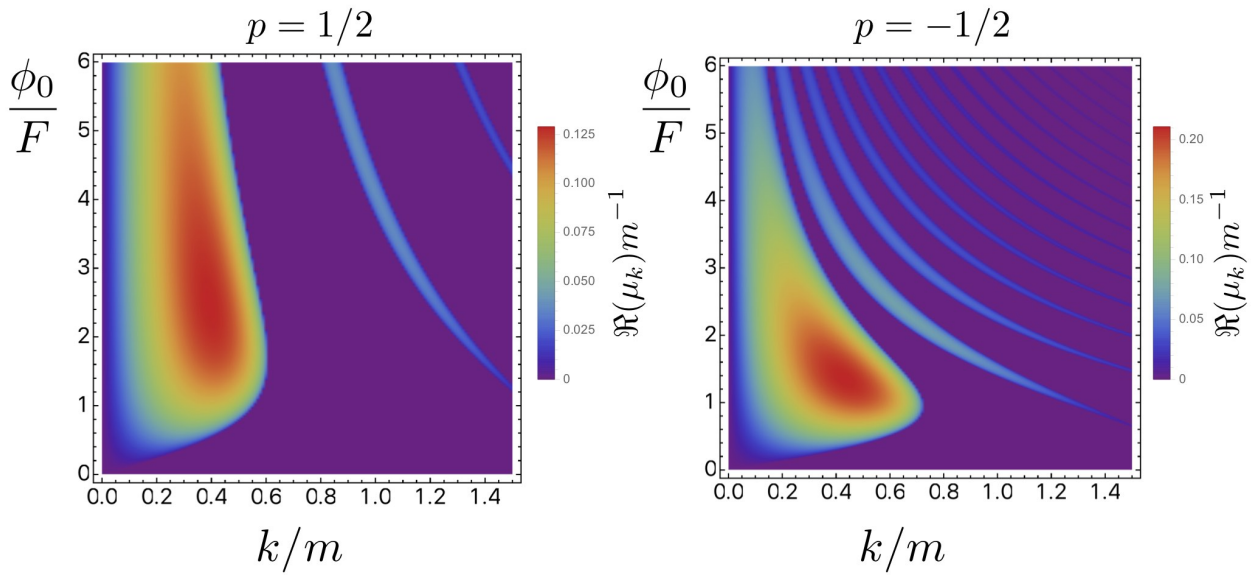

Fig. B.3: *Floquet diagrams for the monodromy potential* (B.2) *with* $p = 1/2$ *(left) and* $p = -1/2$ *(right). These plots are obtained by setting* $H = 0, a = 1$ *in* (B.3) *and* (B.5).

where $k = |\mathbf{k}|$ and $a \equiv a(t) \sim t^{1/2}$. Let us first neglect Hubble friction, setting $H = 0$ and $a = 1$ in (B.3) and (B.5). The motion of the background field in the potential (B.2) is periodic with period T for any value of p and in particular harmonic for $p = 1$. The second derivative of the potential, which acts as source in the equation for the fluctuations, is then also periodic, with period $T/2$. Therefore, (B.5) is in the form of *Hill's equation* (see e.g. [**?**] and the appendix of [69] for a review in the context of reheating). The solution to this equation is of the form $\delta\phi_k \sim e^{\mu_k t} P(t)$, where P is periodic with period $T/2$ and μ_k is in general a complex number. If $\Re(\mu_k) > 0$, then the k-th mode grows exponentially, signaling an instability. This occurs if $V(\phi)$ is flatter than quadratic in some region of field space. Once $\delta\phi_k \sim \phi$, the linear analysis breaks down and one needs to include backreaction of the other modes.

For our purposes, the strength of the resonance can be understood by looking at the values of μ_k as a function of k and ϕ_0 (see the appendix of [69] for a computational method), plotted in Fig. B.3 for $p = \pm 1/2$. In both cases the largest growth occurs in a broad band around $k \simeq m/2$ and $\phi_0 \sim 2F$. The case $p = -1/2$ is characterized by many more bands than $p = 1/2$ and the region of parameter space where μ_k is largest is smaller compared to $p = 1/2$. In both cases, the maximal size of the Floquet exponent is $O(0.1)m$.

Let us now restore Hubble friction in (B.3) and (B.5). This leads to two effects: firstly, it introduces the time scale H^{-1} to which we have to compare μ_k^{-1}. If $\mu_k^{-1}/H^{-1} \ll 1$ then strong resonance can indeed occur. Otherwise, the field remains approximately homogeneous. Secondly, each mode k now redshifts as a^{-1}, thereby moving across the parameter space in Fig. B.3. If a given k spends enough time in the bands of resonant amplification, then the field will be inhomogenized.

Let us first focus on the comparison between μ_k^{-1} and H^{-1}. At the time $t_{\rm osc}$ defined by (B.4), the ratio $\mu_k(\phi_0)/H_{\rm osc}$ may or may not be sufficiently large to induce strong resonance. However, as the

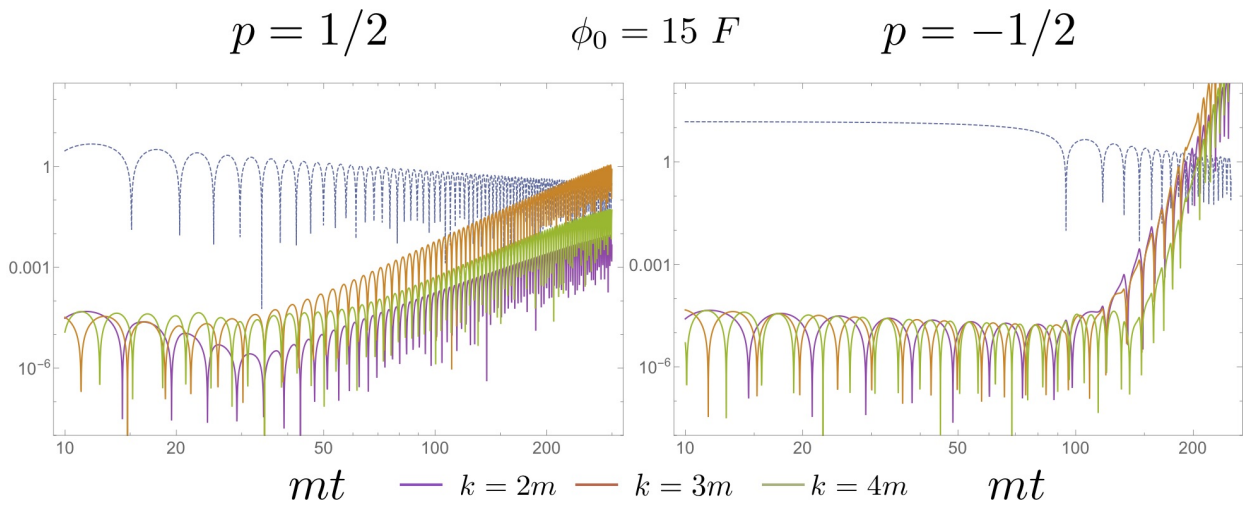

Fig. B.4: *LogLog plot of the absolute value of fluctuations $\delta\phi_k(t)/F$, with $k = 2, 3, 4$ (thick curves) as a function of t. The dashed curve represents the evolution of the homogeneous background. Here we have fixed its initial value $\phi_0 = 15\ F$ and $\delta\phi_k(t_{osc}) = 10^{-5}\phi_0$.*

Universe expands the Hubble rate decreases as t^{-1}, while the background amplitude decreases more slowly, in particular as $\sim a^{-\frac{3}{2}(1+w)} \sim t^{-3/4(1+w)}$ with $w \lesssim 0$. Therefore, the ratio $\mu_k(\phi(t))/H(t)$ can become large and parametric resonance efficient at some time $t_{\rm res} > t_{\rm osc}$. Numerically, we find that for $p = \pm 1/2$, $\mu_k(\phi)/H \gtrsim 10$ in the broad bands of Fig. B.3 for $\phi_0/F \gtrsim 10$, signaling that strong resonance does occur for mildly large initial values of the axion field.[2] This is in contrast with the case of parametric resonance during reheating, where one needs $\phi_0 \gtrsim 100F$ to have efficient resonance [25, 70].

Let us now address the second effect. To this aim, we compute numerically the evolution of some modes according to (B.3) and (B.5). Because of the redshift, we now find that the most amplified modes have $k \gtrsim 2m$ and that $\phi_0 \gtrsim 10$ is indeed enough for these modes to reach $\delta\phi_k \sim \phi$. In Fig. B.4 we show the resonant amplification of three modes with initial amplitude $\delta\phi_k(t_{\rm osc}) = 10^{-5}\phi_0$ for $\phi_0 = 15\ F$ and $p = \pm 1/2$. We observe that strong resonance does indeed occur on a timescale $t_{\rm res} \sim 100\ m^{-1}$. At $mt \sim 200$, multiple modes have reached the same amplitude as the background and the linear analysis ceases to be reliable. The initial condition has been chosen in such a way that fluctuations are amplified to values which are close to F.

This simple linear analysis probably overestimates the final values of the field fluctuations. However, the large values close to F which we find are in principle not necessary to form oscillons, as we now explain. Parametric resonance generically leaves behind localized, approximately spherically symmetric overdensities, whose typical length scale is given by $2\pi/(k/a)$, with $k/a \lesssim m$ at the time of amplification, as can be seen from Fig. B.3. A convenient parametrization of the initial spatial

[2] This means that the field starts its oscillations at ϕ_0, then redshifts due to Hubble friction and crosses the resonance bands shown in Fig. B.3.

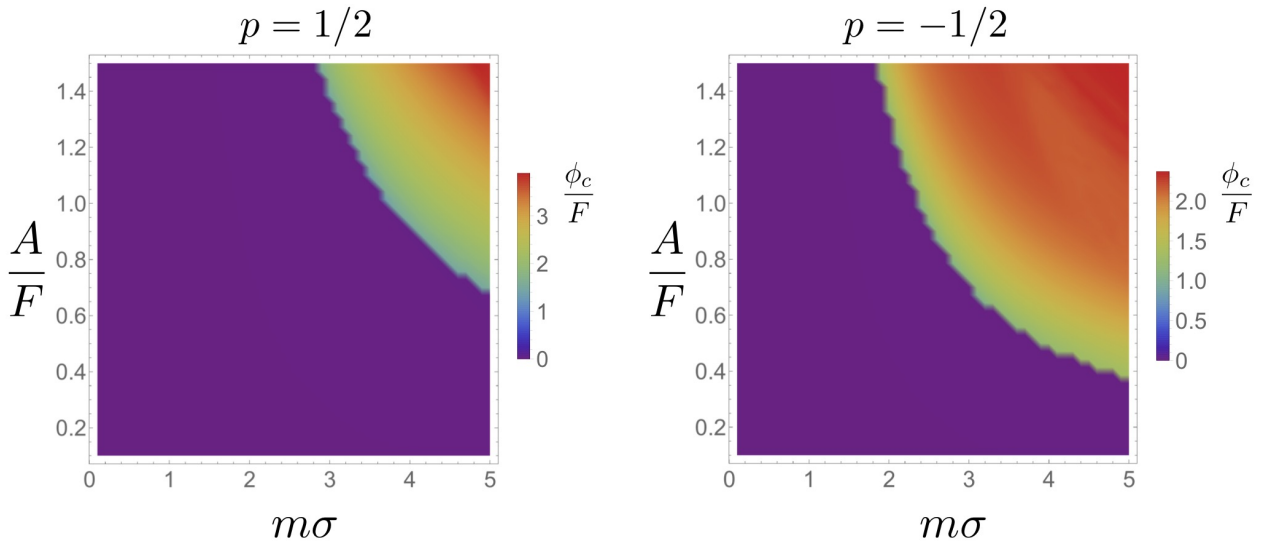

Fig. B.5: *Core amplitude at $t = 10^4\ m^{-1}$ of the localized field configuration initialized with (B.6), as a function of A and σ. The rainbow colored regions correspond to oscillon formation. In the purple region, axion lumps decay away soon after formation.*

profiles of such lumps, which also turns out to match well the final oscillon shapes, is given by

$$\phi(t = t_{\rm res}, r) = \frac{A}{\cosh(r/\sigma)}, \tag{B.6}$$

where $\sigma \sim (k/a)^{-1}$ and $A \sim \delta\phi_k$ at the end of parametric resonance. In order to understand what ranges of A and σ lead to long lived configurations, i.e. oscillons, we have evolved the initial condition (B.6) (with $\dot{\phi}(t_{res}, r) = 0$) according to the full non-linear equation of motion (B.1), scanning over the profile initial amplitude and width. The results are shown in Fig. B.5, where we plot the field amplitude ϕ_c at the lump core at the time $10^4\ m^{-1}$ as we vary A and σ. The crucial point is that localized configurations with sufficiently large initial amplitude and width evolve to new configurations with larger amplitude (and smaller width), which is nothing but the early stage of an oscillon. The exercise shown in Fig. B.5 is a way to track how the parametric resonance instability continues developing during the nonlinear regime for localized overdensities. Strikingly, even with very modest initial amplitudes $A \sim 10^{-1}F$ the tendency to raise the core amplitude and form oscillons is clear (see [31] for a recent study along similar lines). This occurs for sufficiently large values of σ, such as those that we expect from parametric resonance. In the next subsection, we will see that the new overdensity is stable across a time scale which is much larger than the one investigated in Fig. B.5.[3] Therefore, $\phi_0 \sim 10F$ is enough to generate long lived localized field configurations.

[3]Fig. B.5 also makes manifest that the parametric resonance instability and the extreme longevity of oscillons are deeply interconnected: as the oscillon tries to decay it goes to a thicker configuration, which suffers more severely from the instability that tries to make it contract.

2.2 Lifetime

We now focus on the dynamics of a single oscillon, which is characterized by the very slow classical radiation of scalar waves. This can be investigated by numerically evolving the oscillon profile according to the full non-linear equation of motion (B.1). In general oscillons also emit quantum radiation, that is, they can decay by quantum mechanical processes. However, quantum radiation is always suppressed by coupling constants. Assuming that the couplings to any other particles is small, then, one can consistently neglect this radiation. Quantum emission of scalar quanta is also suppressed by m^2/F^2 [24, 71], which is very small in the ULDM setup which we focus on. This justifies our focus on classical processes.

Oscillons can be understood as being attractors of inhomogeneous field configurations [72]. This can already be appreciated in Fig. B.5, where by starting with a profile according to (B.6), one still finds a localized solution after time $t = 10^4\, m^{-1}$. Of special relevance is the fact that the field amplitude at the core ϕ_c after such time is in general $\phi_c > A$, meaning the field has reorganized its energy density until it has found another profile which is preferred by the dynamics. Such a profile is an attractor of the dynamics and is none other than the oscillon. By means of a simple fit, one finds that the shape of this object is very well described by (B.6), albeit with different A and σ than the ones it started with. It is also worth mentioning that the attractor profile is insensitive to specific initial conditions as long as the field is sufficiently inhomogeneous. This result motivates starting our numerical evolution with the profile (B.6).

For random A and σ, however, one would have to spend some computational time until the field relaxes into the real oscillon configuration. In order to reduce this waiting time we use a shooting algorithm that allows us to find the σ closest to an oscillon configuration once an A has been fixed. We are thus left only with the choice of the initial amplitude A, which could result in different lifetimes.

Intuitively, the smaller A, the smaller the lifetime. However, starting with a larger amplitude does not result in a dramatic longevity increase. This is illustrated in Fig. B.6 for the case $p = 1/2$ and manifestly illustrates the existence of a basin of attraction to which inhomoegenous field configurations quickly tend to. Although we have used $p = 1/2$ as a representative example, we have checked that this result is model-independent.

Together with the core field value ϕ_c, the defining properties of an oscillon are its radius $R_{\rm osc}$; its total mass $M_{\rm osc}$; and main oscillating frequency $\omega_{\rm osc}$. Their scalings with the model parameters are:

$$\phi_c \sim F, \quad R_{\rm osc} \sim m^{-1}, \quad M_{\rm osc} \sim V\, R_{\rm osc}^3 \sim F^2/m, \quad \omega_{\rm osc} \sim m. \tag{B.7}$$

Their precise numerical values slowly depend on time and are model dependent. The goal of this section is to estimate these when the oscillon is on the verge of decaying as well as the oscillon lifetime. Again, we will make a distinction between $p < 0$ and $p \geq 0$, picking $p = \pm 1/2$ as representatives.

As it evolves, an oscillon oscillates with a typical main frequency that is very close to but smaller than m. During each oscillation it radiates away a very small amount of axion waves, which makes it lose some energy. The remaining energy gets redistributed by a lowering of ϕ_c and a slow increase in $R_{\rm osc}$. This forces the field to oscillate at a slightly larger frequency, but always below m. This process of radiation emission and energy redistribution continues until the field is forced to oscillate too close to m, at which point all that remains is radiated away in a final burst of axion waves of

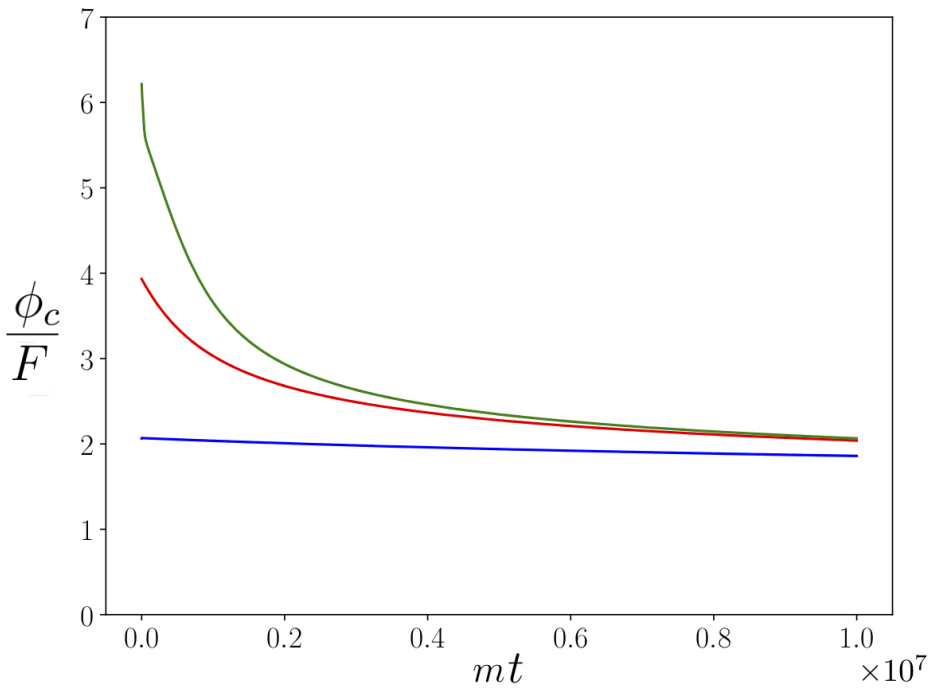

Fig. B.6: *Time evolution of the mean of the absolute value of the field at the center of the oscillon, ϕ_c, for $p = 1/2$ and three different initial conditions.*

frequency $\omega \approx m$. Intuitively, this happens when the field reaches values at which its potential is too close to quadratic, *i.e.* when $\phi_c \approx F$.

In order to qualitatively elucidate the evolution of an oscillon, the latter can also be seen as a non-perturbative object consisting of a large number $N \sim F^2/m^2$ of axion quanta [71]. Because the field at the core explores large values, non-conserving particle number processes take place, the most important being $3 \to 1$, and these allow individual axion quanta to escape from the influence of the rest. This picture matches very well the one in [29, 30], where the extreme longevity of oscillons is understood as arising from a small violation of an effective $U(1)$ symmetry that appears in the non-relativistic limit and corresponding to particle number. This violation is responsible for particle-number violating processes; its smallness implies that such processes are not very frequent and thus that oscillons are very long lived. Numerically, this can be checked by looking at the power spectrum of the waves emitted by an oscillon far away from its core, which we show in Fig. B.9. The dominant peak at $3\omega_{\rm osc}$ clearly signals that axions escape through $3 \to 1$ processes. However, the energy radiated through these processes is a negligible fraction of the total oscillon mass. Nonetheless, once too many axions have escaped, the remaining ones cannot generate a large enough collective coupling that self-sustains the system, at which point the oscillon finally decays.

In what follows, we present numerical results of oscillon evolution, assuming spherical symmetry and neglecting Hubble friction. Before doing so, let us therefore comment on the validity of these

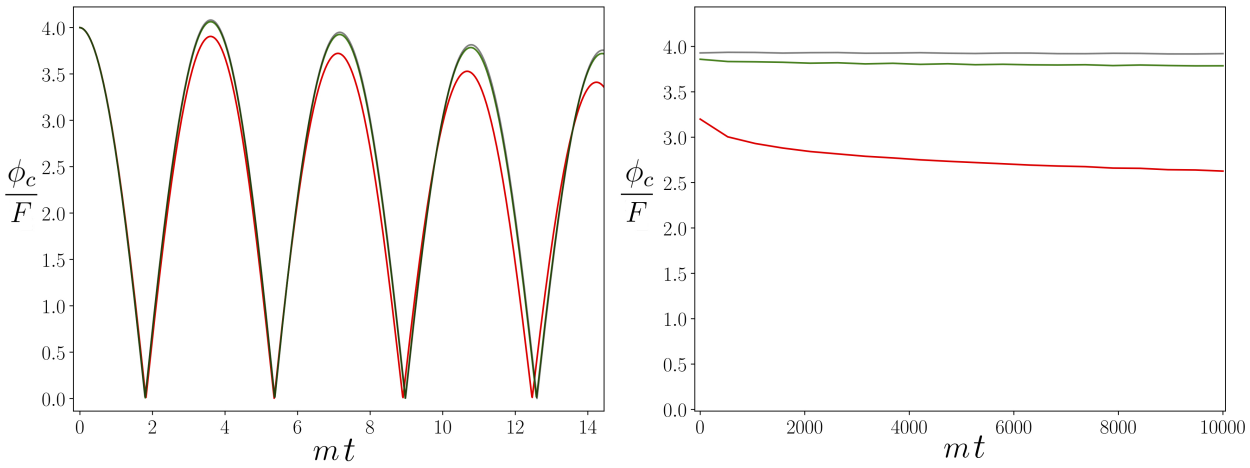

Fig. B.7: *Effect of Hubble friction with initial values of* $H = 10^{-2}, 10^{-3}$ *(red, green) compared to evolution in Minkowski space (gray). On the left, the first few oscillations; on the right, an average of the oscillations over longer timescales. The plots shown here are for* $p = 1/2$*. For the expected value of* $H \lesssim 10^{-3}\, m$ *at oscillon formation, the effect of Hubble friction is negligible.*

approximations.

Regarding the assumption of spherical symmetry, it is true that, in general, parametric resonance will not generate perfectly spherically symmetric profiles. However, there is evidence that those perturbations that break spherical symmetry decay quickly [73]. Since spherically symmetric oscillons are attractors, we do not see any reason why this result should not be general and model-independent.

As for the consistency of neglecting Hubble friction, we have seen in the previous section that parametric resonance produces significant inhomogeneities after $H \lesssim 10^{-2}\, m$. While we have not performed the full numerical analysis of oscillon formation from parametric resonance, recent simulations with similar models [42, 43] suggest that oscillons actually form a bit later, once $H \lesssim 10^{-3}\, m$ [43]. Since the oscillon has a characteristic size at formation $R_{\rm osc} \sim m^{-1} \ll H^{-1}$, one expects that the impact of Hubble friction on the evolution of the oscillon should be minimal. In order to support this expectation, in Fig. B.7 we have plotted the first few oscillations of a $p = 1/2$ oscillon, including Hubble friction in the equations of motion. It is evident from Fig. B.7 that for $H \lesssim 10^{-3}\, m$ the effect of friction on the evolution of the oscillon is quite small and we can thus restrict our simulations to Minkowski space.

Let us now present the results of the numerical evolution of oscillon profiles, according to (B.1). As in the previous sections, we make a distinction between $p \geq 0$ and $p < 0$, choosing $p = \pm 1/2$ as its representatives. We find that the potential with $p = 1/2$ supports oscillons with a lifetime $\tau \approx 3 \times 10^8\, m^{-1}$. For $p = -1/2$ we quote only a lower bound $\tau \geq 6.5 \times 10^8\, m^{-1}$ on the lifetime because we have not seen the oscillons to decay in our simulations after 1200 CPU hours. A snapshot of the lifetime of representative oscillons can be seen in Fig. B.8, where we have also included the $p = 0$ case to show that potentials with $0 \leq p < 1$ lead to comparable oscillon lifetimes. The values of A and σ that we used as initial conditions are $A_{p=1/2} = 2.1\ F$, $\sigma_{p=1/2} = 2.45\ m^{-1}$; $A_{p=0} = 2\ F$,

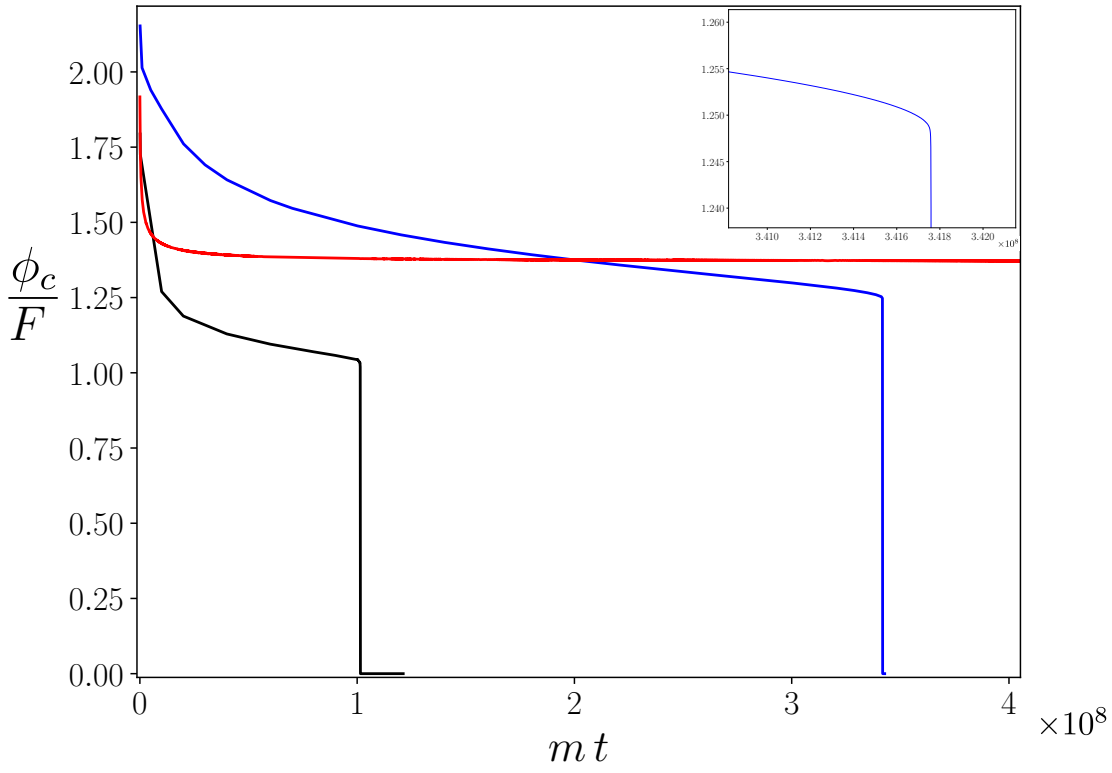

Fig. B.8: *The life of an oscillon in a snapshot. Here we plot the mean of the absolute value of the field at the center of the oscillon, ϕ_c, as a function of time for $p = 1/2$ (blue), $p = 0$ (black) and $p = -1/2$ (red).*

$\sigma_{p=0} = 1.9\ m^{-1}$; $A_{p=-1/2} = 2\ F$, $\sigma_{p=-1/2} = 1.83\ m^{-1}$.

We list the values of $\phi_c, R_{\rm osc}$, $M_{\rm osc}$ and $\omega_{\rm osc}$ at the time of oscillon decay for $p = 1/2$ and at $t = 6.5 \times 10^8\ m^{-1}$ for $p = -1/2$ in Table B.1. Numerically we define $R_{\rm osc}$ as that value of r such that the energy from $r = 0$ to $r = R_{osc}$ is equal to 90% of the total energy in the lattice.

In conclusion, our analysis shows that oscillons supported by the potentials (B.2) have the largest lifetimes ever encountered in the literature. In particular, for $p > 0$ we find $\tau \approx 10^8\, m^{-1}$. Even more intriguing is the case of $p < 0$, for which we have not yet witnessed oscillon decay after $t = 6.5 \times 10^8\, m^{-1}$. As a matter of fact, going beyond $10^9\ m^{-1}$ in lifetime is computationally not feasible. We are fundamentally limited by CPU clock speed, currently at the order of a few GHz. Given that one needs enough time resolution, $dt \sim 10^{-2}\ m^{-1}$, reaching lifetimes $\sim 10^9\ m^{-1}$ requires months of simulation.

In addition, the fact that $\omega_{\rm osc}$ for $p = -1/2$ is still well below m suggests that in this case lifetimes can be several orders of magnitude larger than what we have been able to probe so far. This is further supported by a simple fit of $\phi_c(t)$ to a power law. The exact value of ϕ_c at which the oscillon will decay is not known and giving more precise estimates of the lifetime can be complicated

	ϕ_c/F	$M_{osc}\,F^{-2}m$	$R_{osc}\,m$	$\omega_{\rm osc}\,m^{-1}$	$\tau\,m$
$p=1/2$	1.25	261.05	9.32	0.98	3.4×10^8
$p=-1/2$	1.37	77.38	5.49	0.93	$>6.5\times10^8$

Table B.1: Values of oscillon properties. For $p=1/2$, these are reported at the time of oscillon decay. For $p=-1/2$, we give the values at $t=6.5\times10^8 m^{-1}$.

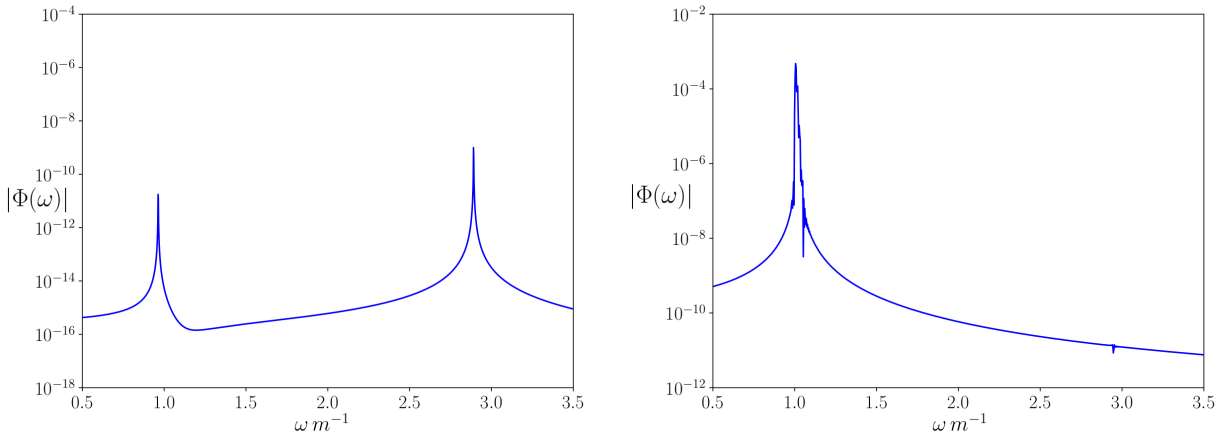

Fig. B.9: *Power spectrum of the field ϕ for $p=1/2$ at a distance $r=80\,m^{-1}$, with arbitrary normalization. Left: Evaluated at $t=10^7 m^{-1}$. Right: At decay, $t\approx3\times10^8 m^{-1}$. Notice that the peak in the right plot at $\omega\sim m$ is much larger than the peaks in the left plot, meaning that indeed most of the energy of the oscillon is lost in moderately relativistic axion waves at its decay.*

and quite probably, wrong. We prefer to remain conservative and quote a lower bound based on what we have achieved to simulate explicitly.

Before moving on to the next chapter of oscillon biography, let us provide details of the numerical method which the results of this subsection are based on. We have evolved an oscillon profile with initial conditions set by (B.6) and $\dot\phi(t=0)=0$, using the full non-linear equations (B.1). We implemented a staggered leapfrog scheme with a three-point spatial Laplacian accurate to $\mathcal{O}(dx^2)$. We kept a fixed ratio between spatial and time discretization $dr=5dt$, and used Neumann boundary conditions at $r=0$ and second order absorbing boundary conditions at the end of the grid. The typical sizes of the grids we have used vary between 50 and 80 units of physical distance, with $dr=0.05$. While these are the typical values, we also have examples with $dr=0.01$ and up to 100 units of physical distance to check stability and robustness of our numerics. Furthermore, we have checked that absorbing boundary conditions remove radiation efficiently from the lattice without introducing significant noise. We used Python to write our code and it has been benchmarked by reproducing the results in [26].

2.3 Legacy

Let us now discuss the fate of oscillons once they decay, having in mind a cosmological setup where they are part of the DM sector.

Oscillons sustain themselves because of the field self-interactions, which are relevant at large field values and require a relativistic treatment. Localized, spherically symmetric field configurations however arise also in the non-relativistic, small amplitude regime of an oscillating axion field. These are commonly referred to as *solitons* and, in contrast with oscillons, are sustained by gravity. Solitons are in fact essential to the proposal of fuzzy dark matter [4, 9] (see also [46, 47] for recent critical takes), since they are supposed to make up the cores of Ultra-Light axion Dark Matter halos. Momentarily neglecting self-interactions, the soliton configuration is obtained as a solution of the non-relativistic Schrödinger-Poisson equations [47]. In fact, a whole family of solutions exist, described by a single parameter λ. The masses and core radii of these solitons are given by

$$M_{\rm sol} = \lambda M_1, \text{ with } M_1 \approx 2.79 \times 10^{12} \left(\frac{m}{10^{-22}\ \text{eV}}\right)^{-1} M_\odot \tag{B.8}$$

$$R_{\rm sol} = \lambda^{-1} R_1, \text{ with } R_1 \approx 0.082 \left(\frac{m}{10^{-22}\ \text{eV}}\right)^{-1} \text{pc}, \tag{B.9}$$

with the additional requirement $\lambda < 1$. In the absence of initial conditions on $M_{\rm sol}$ and/or $R_{\rm sol}$, it is not possible to predict uniquely sizes and masses of axionic gravitational solitons. It is our aim in this section to qualitatively argue that oscillons can indeed work as seeds for the later formation of gravitational solitons, thereby setting the value of $M_{\rm sol}$ and thus of the parameter λ.[4]

The argument is sharper when interactions among oscillons can be neglected. Let us thus first consider such a simplified scenario. The last stages of the oscillon evolution proceed via the emission of axion waves of momentum $k \simeq R_{\rm osc}^{-1} \lesssim m$, where in the last step we have neglected a model-dependent (in particular p-dependent) numerical prefactor of $O(0.1 \div 1)$. Due to Hubble friction, these waves lose energy; eventually they enter the non-relativistic regime and can organize themselves in a soliton structure because of gravity – falling into their own gravitational potential well. Under our simplifying assumption, the total mass carried away by the waves is equal to the original oscillon mass $M_{\rm osc} \simeq O(100) \times F^2/m$. Intuitively, the formation of a soliton of this mass is possible only if the velocity of the radiated waves is not larger than the escape velocity of the soliton itself. Let us estimate how the escape velocity changes with the scale factor, noticing that the initial radius of the overdensity is given by $R_{\rm osc} \sim m^{-1}$. The gravitational escape velocity is then given by

$$v_e(t) = \sqrt{\frac{R_{s,\rm osc}}{R_{\rm osc} a(t)}} \simeq \frac{1}{\sqrt{a(t)}} \left(\frac{F}{M_p}\right), \tag{B.10}$$

where $R_{s,\rm osc}$ is the Schwarzschild radius of the oscillon and $M_p = (8\pi G)^{-1/2}$ is the reduced Planck mass. The group velocity of the radiated waves is initially moderately relativistic and very rapidly

[4] The solitons that obey Eqs. (B.8) and (B.9), are strictly speaking coherent solutions of the Schrödinger-Poisson [47]. The most likely outcome of the oscillon decay can be expected to be a non-coherent but gravitationally bound lump, akin to what is usually referred to as miniclusters/minihalos. It may take a long time for these to settle down to the coherent soliton solution – we thank S. Sibiryakov for pointing this out to us. In this discussion we are interested in estimating how the decaying oscillon can be trapped in its own gravitational potential, regardless of its coherence. To this aim we use Eqs. (B.8) and (B.9) only to obtain rough estimates soliton/miniclusters properties. Henceforth we will also refer as soliton both the coherent and incoherent lumps.

follows the Hubble flow, meaning that it redshifts simply as $v_q \sim k/(ma(t)) \lesssim 1/a(t)$. In other words, the escape velocity decreases more slowly than the velocity of the radiated waves, which implies that indeed eventually the latter are captured by their own gravitational attraction.[5] This occurs of course when $R_{\rm osc}a(t) \simeq R_{\rm sol}$, as can be easily checked, by taking $\lambda = M_{\rm sol}/M_1 \approx (F/M_p)^2$. It is useful to report the corresponding soliton radius, according to (B.9)

$$R_{\rm sol} \simeq \frac{c}{m}\left(\frac{M_p}{F}\right)^2, \tag{B.11}$$

where $c \sim 0.1 \div 1$ is a model-dependent numerical prefactor. We thus see that the soliton is parametrically much larger in size than its parent oscillon.

The analysis that we have just performed is relevant in the case where interactions among oscillons are negligible. This is likely the case during the epoch of radiation domination, since oscillons just keep being further separated from each other. However, during matter domination, overdensities of oscillons grow due to gravity. In this case, gravitational interactions of oscillons can become important: for example, oscillons can merge or disrupt or even lead to the formation of black holes [67] (see Sec. 3.1 for further discussion of this possibility). As a result, it is more challenging to estimate the properties of a soliton which forms out of an overdensity of oscillons without numerical simulations. While this detailed understanding goes beyond the aim of this paper, we expect that a soliton will indeed form, possibly of much larger mass. According to (B.8) and (B.9), the resulting soliton radius can be much smaller than (B.11). We will discuss in more detail how this uncertainty affects constraints on our scenario in Sec. 3.

A comment on the effects of self-interactions is now in order. The soliton solution reviewed here is indeed obtained in the non-relativistic regime of a free massive scalar. The effects of the attractive self-interactions dictated by the potentials (B.2) are negligible as long as they are subdominant compared to the gradient energy of the field. Self-interactions have been properly included in the non-relativistic regime by [44]: the result is that self-interactions may induce a collapse instability of the soliton, if its size is less than

$$R_{\rm min} \simeq 0.1 \text{ pc}\left(\frac{10^{-19}\text{ eV}}{m}\right)\left(\frac{10^{15}\text{ GeV}}{F}\right). \tag{B.12}$$

In most of the parameter space which we will consider in the next section, $R_{\rm sol}$ is generically quite larger than 1 pc, according to (B.11), thus the corresponding soliton lies in the stable branch, where gravity dominates. However, for $m \gg 10^{-19}$eV and $F \gg 10^{15}$ GeV, the soliton size can be smaller than (B.12). Similarly, if multiple oscillons lead to a single soliton, its size can be smaller than (B.11). In these cases the possibility of collapse driven by self-interactions cannot be entirely excluded.

[5] After decay, the oscillon can be understood as a 'wave-packet' of size $\sim$ (few)m^{-1}. Initially, it spreads at a constant speed but one can check that this 'peculiar' speed starts feeling the effect of Hubble friction (and decreasing as $1/a(t)$) on a short time scale. The initial deviation from the Hubble flow may imply that not all of the oscillon mass is actually gravitationally captured in a soliton configuration. The estimate $M_{\rm sol} \simeq M_{\rm osc}$ should nevertheless capture the right order of magnitude.

3 Observational impact

In the previous sections we have established that oscillons can form from an homogeneous scalar field during the radiation dominated era and survive for very long epochs. We now investigate the observational implications of their presence as part of the DM sector.

These certainly strongly depend on the fraction $f \equiv \rho_{\rm oscillons}/\rho_{\rm DM}$ of scalar dark matter in the form of oscillons. As already mentioned, numerical simulations ([25, 74] in the inflationary context for $p = 1/2$ and in [43] for plateau-like potentials) show that a fraction of $O(1)$ of the energy density of the scalar field resides into oscillons after parametric resonance. However, we expect this conclusion to depend on p. In particular, f should decrease as p gets closer to unity, since after all the quadratic potential does not support oscillons. In this work, we thus mostly assume that, after parametric resonance, the energy density of the axion field is equally distributed into two components: the original oscillating homogeneous background and a population of massive oscillons. Both components behave as dark matter, albeit of very different mass.

Implications of our scenario further depend on the typical lifetime of oscillons generated by parametric resonance. In the previous section we argued that attractor configurations exist, with $\tau \gtrsim 10^8\ m^{-1}$ or larger. While we do not know how many of the oscillons produced by parametric resonance are so long-lived, we provided evidence that the precise initial condition provided by the fragmentation is not expected to strongly affect the longevity of oscillons. Therefore, in what follows we assume that their typical lifetime is indeed given by the numerical results discussed in the previous section.

Oscillons decay away via the radiation of scalar waves. This can in principle occur during radiation or matter domination, depending on the field mass and on the oscillon lifetime. In this section we mostly focus on the case $p = 1/2$, which is representative of potentials which support long-lived oscillons with $\tau \sim 10^8\ m^{-1}$. In Fig. B.10, the thick vertical brown line shows the corresponding value of the ULDM mass for which oscillons decay at matter-radiation (MR) equality, while the dashed brown line corresponds to stability until today. On the upper horizontal axis, values of the oscillon radius in kpc are shown. Solid black lines show the corresponding oscillons masses. In Fig. B.11 we plot values of $M_{\rm osc}$ and $R_{\rm osc}$ for larger ULDM masses, for which oscillons decay before MR equality. Different observational constraints arise in the two mass ranges shown in Fig. B.10 and in Fig. B.11. Therefore, we discuss these two scenarios separately. We devote a separate subsection to the observational impact of oscillons which survive across the age of the Universe.

Before moving on however, let us comment on a general constraint which applies in the entire range of scalar field masses which we will be discussing. If we consider a light (pseudo)scalar field which exists already during cosmological inflation, then its fluctuations are of isocurvature type and are thus strongly constrained by CMB observations [75]. The magnitude of these isocurvature fluctuations compared to the scalar adiabatic power spectrum for a light scalar field is simply dictated by the Hubble rate as well as by the value of the field during inflation, which in our case is $\phi_0 \gtrsim 10\ F$. The Hubble rate can be traded for the value of the tensor-to-scalar ratio $r/0.1 \simeq 10^9 (H_I/M_p)^2$, the current upper bound being $r \lesssim 0.07$ [**?**], while future observations can likely probe values down to $r \gtrsim 10^{-3}$. Therefore, the constraint on isocurvature fluctuations translates into an upper bound on H_I or on r, if a given value of $F \gtrsim H_I$ is specified. It turns out that for 10^{14} GeV $\lesssim F \lesssim 10^{16}$ GeV the ULDM scenario which we focus on in this paper requires very small values of r to evade isocurvature

constraints, below the aforementioned observable range.[6] Therefore, if r is eventually measured, the ULDM scenario discussed here, with large F, will be in tension with observations (similarly as in [9]).

3.1 Decay after MR equality

Let us first focus on the scenario in which oscillons live up to or beyond the epoch of MR equality. We fix $p = 1/2$ as a representative example. This scenario then occurs for $m \lesssim 10^{-19}$ eV, which is the typical range of so-called ULDM candidates.

Several constraints exist for such ultra light scalars; however they are mostly derived assuming that the DM is made only by an oscillating homogeneous field with a cosine potential at MR equality. In particular, [47, 76] suggest that masses below $\sim 10^{-22}$ eV are in tension with observations. Interestingly, the presence of oscillons seems to affect significantly these analyses. On the one hand, the constraint from [76] originates from the (otherwise) absence of early galaxies. However, the presence of oscillons means that DM already has large inhomogeneities at MR equality, which are expected to facilitate early structure formation. This suggests that the limit should be revised in this context. On the other hand, the constraint presented in [47] is based on the simulations of [8] that evolve the ULDM configuration starting from MR equality. However, again, the presence of oscillons alters significantly the initial condition at MR, so the analysis does not apply in a straightforward manner. For these reasons we do not show these constraints in Fig. B.10.

ULDM masses below $m \sim 10^{-25}$ eV are strongly constrained by the primary CMB [77], since they alter the expansion rate, thereby affecting the heights of the higher acoustic peaks. This constraint is shown as a shaded red region in Fig B.10. However, in the case of a ULDM with potential (B.2) and initial value $\phi_0 > F$, this region is expected to move to larger masses, since ULDM oscillations are delayed compared to the standard axion DM case.

The allowed values of F and m are certainly constrained by dark matter overproduction. For large initial field values, the axion starts oscillating once the Hubble rate drops to $H_{\rm osc}$ given in (B.4). Shortly afterwards, at $t_{\rm res} \lesssim 100\ m^{-1}$ parametric resonance becomes effective and oscillons are formed. Therefore, the total relic abundance of the axion field can be roughly estimated by redshifting the energy density at $V(\phi_{\rm res})$ from $t_{\rm res}$ to today. For the representative initial value $\phi_0 = 15\ F$, the result of this calculation is given by the thick blue line in Fig. B.10, the shaded blue region above it being excluded by DM overproduction.

In our study of the oscillon evolution we have neglected the effects of gravity on the stability of the oscillon itself. This simplifying assumption is certainly valid at early times, when oscillons do not represent a large density contrast compared to the radiation dominated universe. As the Universe cools down to the epoch of MR equality however, gravity can play an important role because of two different effects:

1 An individual oscillon can be seen as an overdensity $\delta\rho_{\rm osc}$ of dark matter compared to the background homogeneous oscillating field. At formation, the density contrast is

$$\frac{\delta\rho_{\rm oscillon}}{\rho(t_{\rm osc})} \simeq \frac{M_{\rm osc} R_{\rm osc}^{-3}}{0.1\ m^2 F^2} \simeq 1. \tag{B.13}$$

[6] The upper bound on F can in principle relaxed if $\phi_0 \gg 10\ F$, however then the homogeneous oscillations overproduce dark matter.

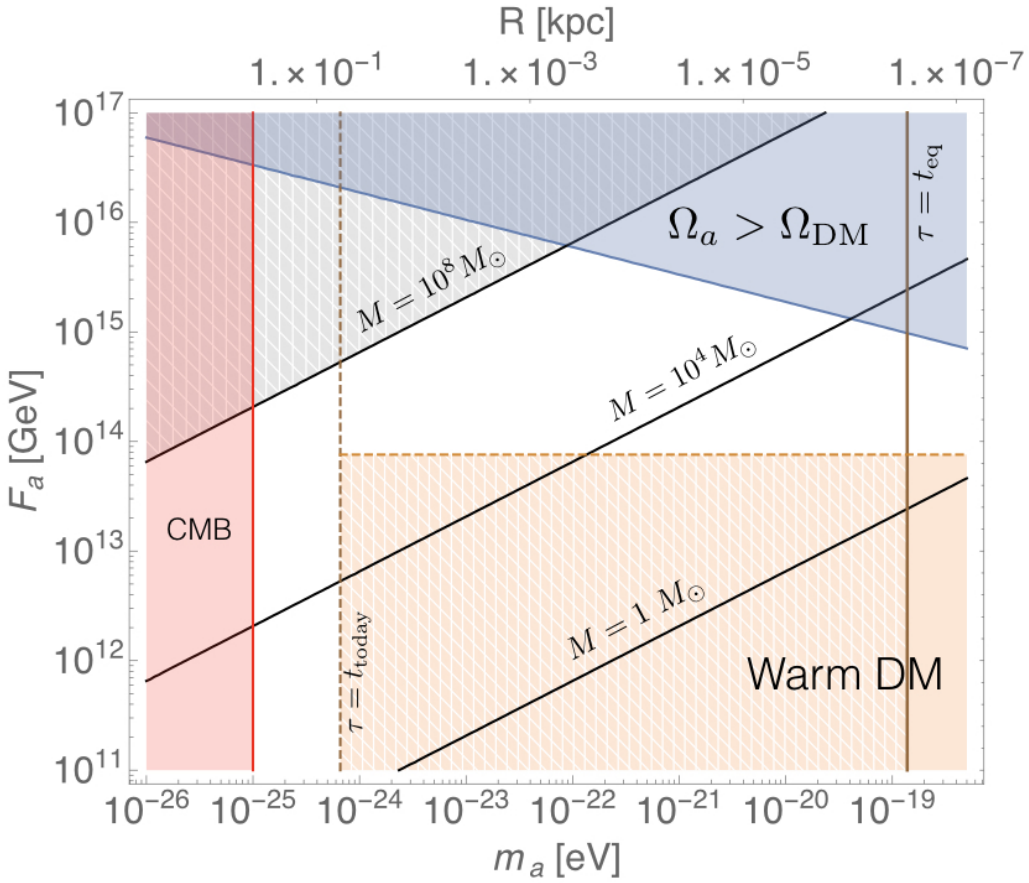

Fig. B.10: *Properties and constraints of oscillons as functions of F and m in the region where they decay after MR equality. We take the representative case $\phi_0 = 15$ F and $p = 1/2$, for which the lifetime is $\tau \simeq 3 \cdot 10^8 m^{-1}$. The red-shaded area is in tension with CMB data and ULDM scalars being most of the DM [48]. The gray-grid-shaded area corresponds to oscillons with masses above $10^8 M_\odot$, which we take as a rough reference exclusion value. In the orange-grid-shaded region the oscillon deaths would warm up DM too much according to the estimate of (B.14). We didn't include here the constraint $m \gtrsim (10^{-23} - 10^{-21})$ eV from [47, 76] because these analyses can be affected by the presence of oscillons.*

Afterwards, the field inside the oscillon is essentially decoupled from cosmological expansion, while the background continues to redshift. Thus the density contrast $\delta\rho_{\rm osc}/\rho_{DM}$ increases with time. Therefore, close to MR equality, oscillons individually start to experience the gravitational force, similarly to what happens in the case of the QCD axion overdensities [33]. Numerical simulations including gravity [78], albeit in a different context, suggest that oscillons are not destabilized by gravity and can in fact have larger lifetimes. This is at least partially supported by intuition, since gravity acts as another source of attractive interaction.

2 Oscillons can also be regarded as a dark matter component, independently of the oscillating background from which they originate. They are weakly interacting among themselves and can

be very massive, (see the solid lines in Fig. B.10). In this respect, they are similar to MACHOs, though not quite as dense since $R_{\rm osc}/R_{s,{\rm osc}} \sim (M_p/F)^2$. Due to their low density, they seem to evade rather generically standard constraints on MACHOs and PBHs. However, at MR equality overdensities of oscillons start to grow (as $a(t)$) and gravitational interactions (e.g. merging of oscillons, tidal disruption) may become relevant and again affect oscillon lifetimes (see [70] for the effects of gravitational interactions in the non-relativistic regime).

The points above can be concretely addressed via including gravity in the evolution of a single oscillon and by simulating the dynamics of a population of oscillons. We leave these detailed studies for future work and focus here on the case in which oscillons simply decay away after a time $\tau \sim 10^8 m^{-1}$, by the radiation of axion waves with momentum $k \simeq R_{\rm osc}^{-1} \lesssim m$.

Further constraints arising from the decay products and legacy of oscillons can restrict the allowed values of F and m in Fig. B.10. However, in the case in which this decay occurs during matter domination, gravitational interactions make precise estimates challenging, as we outlined in Sec. 2.3. Therefore, here we simply point out the physical origin of those constraints, while we leave detailed estimates for future work.

Firstly, axion waves radiated from the oscillon decay are in principle warm enough to affect the good behavior of CDM at and after MR equality. However, as discussed in Sec. 2.3, such waves are likely eventually trapped in a soliton configuration. This should occur rapidly enough not to affect structure formation: one possible constraint to impose is that the transition from oscillon to soliton occurs in less than a Hubble time, i.e. $R_{\rm sol} \lesssim H^{-1}(\tau)$. As argued in Sec. 2.3, it is in fact not clear how large $R_{\rm sol}$ should be. An over-conservative estimate of $R_{\rm sol}$ is given by (B.11) and gives

$$R_{\rm sol} \lesssim H^{-1}(\tau) \simeq \tau \Rightarrow F \gtrsim \frac{M_p}{\sqrt{m\tau}}. \tag{B.14}$$

This constraint is represented in Fig. B.10 for $\tau = 10^8\ m^{-1}$ by the grid-shaded orange region and should be taken with a grain of salt. As we will discuss in the next subsection, the constraint becomes more reliable when oscillons decay before MR equality: accordingly, we show it as an orange shaded region (without grid lines) in Fig. B.10.

A different kind of constraint can arise from galactic observations. One the one hand, if oscillons indeed transition to solitons, the size of the latter today cannot be larger than the typical core of DM halos, that is $R_{\rm sol} \lesssim 1$ kpc. Again, the uncertainty on $R_{\rm sol}$ does not allow more detailed estimates and for this reason we do not show this constraint in Fig. B.10. On the other hand, oscillon or soliton masses much above $10^8 M_\odot$ are likely strongly constrained by observations: accordingly, we grid-shade the corresponding region in Fig. B.10.

Overall, we are thus left with a region of parameter space, roughly centered around $F \simeq 10^{15}$ GeV and $m \sim 10^{-22}$eV, where oscillons survive up to and beyond MR equality and can seed the formation of gravitational solitons and/or of further early structures. Oscillon seeds should thus be considered as part of the initial conditions of numerical simulations of ULDM (see e.g. [8]). In particular, such numerical analyses should be initialized with a significantly non-scale invariant power spectrum, peaked around the scale corresponding to the oscillon radii. This in principle provide the opportunity to test our scenario by comparing the results of simulations with observations of DM halos.

Finally, let us spend some words on the possibility to form black holes from oscillons which decay during matter domination. This mechanism has been recently considered in the context of reheat-

ing after inflation [67]. The basic idea starts from the realization that some initial overdensity of oscillons is statistically possible. Such an overdensity would then grow during matter domination, i.e. $\delta\rho_{\rm oscillon}/\rho_{\rm DM} \sim a$, and can reach the critical threshold for gravitational collapse. If this occurs, a black hole is formed. In our scenario, we can think of this in the language of oscillon-to-soliton transition: in other words, the growth of oscillon overdensities simply corresponds to the fact that several oscillons fuse into a large soliton which approximately captures the total mass of the overdensity. By means of (B.8) and (B.9), we can give a rough estimate of how much mass is required so that (a significant part of) the resulting soliton is a black hole. We need

$$R_{s,\rm sol} = \frac{M_{\rm sol}}{4\pi M_p^2} \gtrsim R_{\rm sol}. \tag{B.15}$$

Let us now write $R_{\rm sol}$ in terms of $M_{\rm sol}$, according to (B.8) and (B.9)

$$\begin{aligned} R_{\rm sol} &= 0.082 \text{ pc} \times \frac{2.8\cdot 10^{12} M_\odot}{M_{\rm sol}} \left(\frac{m}{10^{-22}\text{ eV}}\right)^{-2} \\ &\simeq 3\cdot 10^{49} M_p^{-1} \times \frac{2.8\cdot 10^{12} M_\odot}{M_{\rm sol}} \left(\frac{m}{10^{-22}\text{ eV}}\right)^{-2}, \end{aligned} \tag{B.16}$$

where in the second step we have expressed length scales in units of the inverse reduced Planck mass. Plugging (B.16) in the inequality (B.15), we obtain

$$M_{\rm sol} \gtrsim 10^{12} M_\odot \left(\frac{m}{10^{-22}\text{eV}}\right). \tag{B.17}$$

For $m \lesssim 10^{-19}$ eV, (B.17) gives very large would-be black hole masses $M_{\rm sol} \gtrsim 10^9 M_\odot$. Black holes of these masses are constrained to make up only a small fraction of the DM by different sets of observations, see e.g. [79]. Nevertheless notice that they would form after MR equality, therefore the constraints coming from CMB anisotropies do not apply to this case. We can now also estimate the number and mass of the oscillons which would be necessary to form a black hole soliton with mass (B.17). Taking $m \sim 10^{-19}$eV, we see in Fig. B.10 that close to the solid blue line (where all of the DM comes from the scalar waves and oscillons) the oscillons have masses $M_{\rm osc} \sim 10^3\ M_\odot$. CMB and other constraints on MACHOs do not apply in this case, since oscillons are very dilute objects. Therefore, approximately $\sim 10^6$ oscillons would have to contribute to the formation of the black hole soliton. While we cannot make any further estimate of how likely this scenario is, let us notice that above the orange shaded region in Fig. B.10, the individual oscillon-to-soliton transition takes less than a Hubble time. Therefore, it might not be so implausible to have a very small, but non-negligible fraction of supermassive black holes originating from the growth of oscillon overdensities in our scenario. These estimates are of course very rough and more detailed analyses are required, nevertheless we find this scenario interesting given the potentially important observational impact of such supermassive objects (see e.g. [79]).

3.2 Decay before MR equality

Let us now discuss some peculiarities of the scenario in which oscillons decay before MR equality. Again, we fix $p = 1/2$ as a representative example. Thus this scenario occurs for $m > 10^{-19}$ eV. We limit ourselves to the case which is most interesting for dark matter, and thus focus on $m < H_{\rm QCD}$.

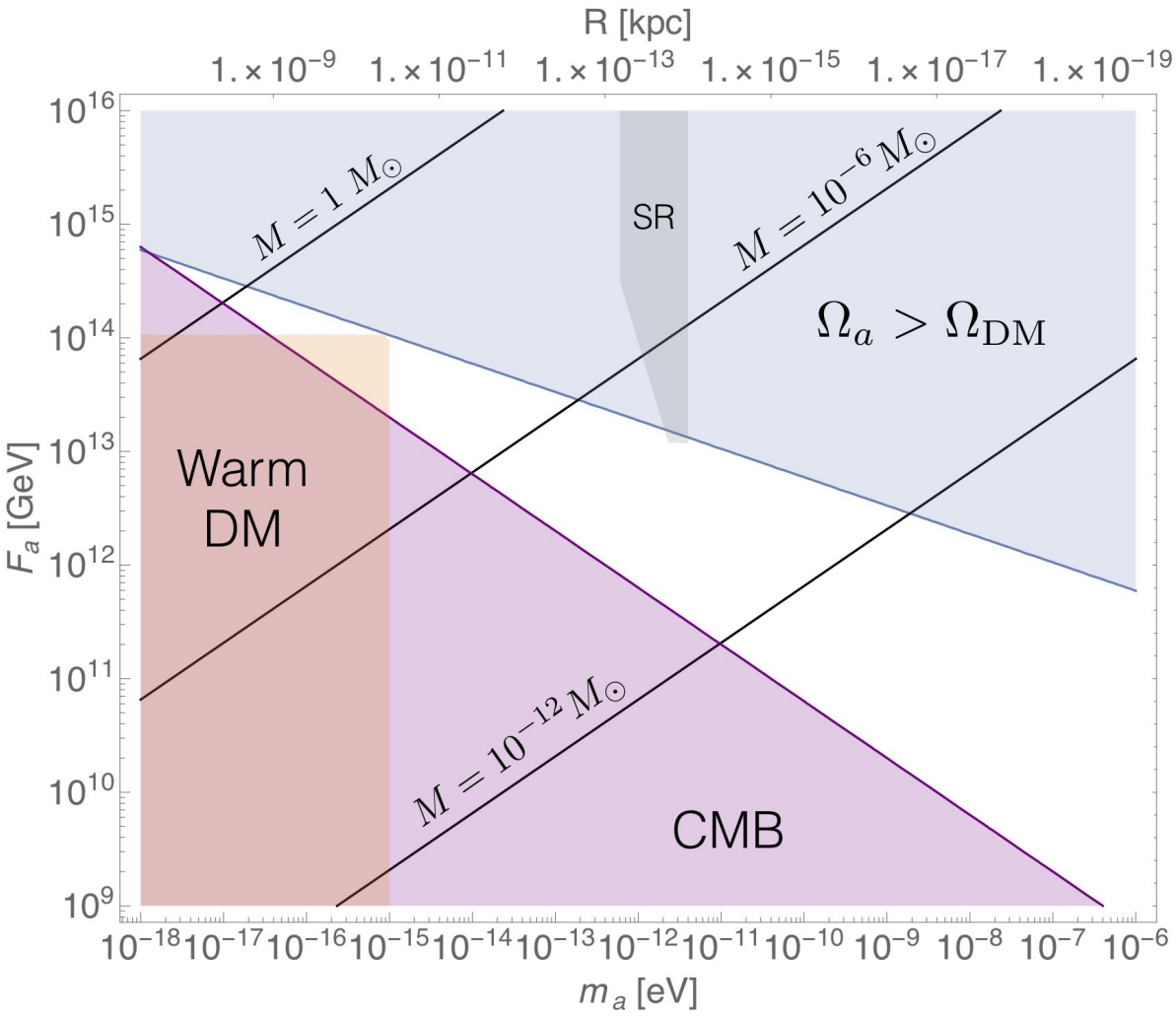

Fig. B.11: *Properties and constraints of long lived oscillons in the case that they decay before MR equality. As before we take the representative case $p = 1/2$ and $\phi_0 = 15$ F, giving $\tau \simeq 3\ 10^8 m^{-1}$. The solid black denote oscillon masses $10^{-12}M_\odot, 10^{-6}M_\odot$ and $1M_\odot$ from the bottom right to the top left corners. Above the solid blue line dark matter is overproduced. The shaded purple region is disfavored by CMB anisotropies and is meant to extend also to the right portion of Fig. B.10, until the brown thick line. The orange shaded region is disfavored by the production of warm dark matter during the decay of the oscillon. The gray shaded region is further constrained by black hole superradiance.*

In order to match the observed abundance of dark matter, smaller values of F are now required. This is shown in Fig. B.11 by the thick blue line. The crucial difference with respect to the previous case is that oscillon overdensities do not significantly grow during radiation domination. After parametric resonance, the typical Hubble patch contains a certain number of separated oscillons. Due to cosmological expansion, the distance between oscillons continues to increase, thus the interactions among them are negligible. Once oscillons decay, their radiated waves are quickly slowed down by Hubble expansion and thus have no possibility to interact with the decay waves of other oscillons. Therefore, the size of the resulting soliton should be well estimated by (B.11) and we expect the

constraint given in (B.14) to hold. The constrained region is shown in shaded orange in Fig. B.10 and Fig. B.11. Notice however that, for large enough axion masses, the waves radiated by the oscillons are redshifted enough at CMB not to affect structure formation. This occurs for $m \gtrsim 10^{-15}$eV: these values of axion masses are thus unconstrained by the production of warm dark matter.

A stronger constraint arises however from requiring that the soliton radius is much smaller than the Hubble patch at CMB, i.e. $R_{\rm sol} \ll H^{-1}(t_{\rm eq})$. In particular, we impose $R_{\rm sol} < 10^{-3} H^{-1}(t_{\rm eq})$, given the current resolution of CMB observations. The disfavored region of parameter space is shaded in purple in Fig. B.11.[7] The thick lines in the same figure show values of soliton/oscillon masses $1 M_\odot, 10^{-6}\ M_\odot$ and $10^{-12}\ M_\odot$ from top to bottom.

Yet another source of constraints is the phenomenon of black hole (BH) superradiance [80, 81], which apply even if the (pseudo)scalar is not all of DM. The affected mass ranges are slightly narrow windows around 10^{-12} eV (from stellar mass BHs), and 10^{-18} eV (from supermassive BHs, $M \sim 10^6$), which do not appear in Fig. B.10. Self-interactions play some role in determining the excluded parameter space [80–83], which translates into cutting the excluded region for low enough F. Doing so, only the stellar mass BHs bound is marginally stronger than the DM overproduction bound, as shown in Figs. B.11. It is natural, however, to ask whether the presence of oscillons can make these bounds more stringent. The oscillon-BH dynamics has been partially studied in previous works. Refs. [84, 85] show that scalar-gravity systems admit solutions of the form of an oscillon with a BH at the center. Also, Ref. [86] showed that BHs can grow a significant (pseudo)scalar hair. It would be interesting to revise superradiance rates for this kind of BH solutions, but we are not in the position of extracting whether this can have an impact on the superradiance constraints.

The parameter space extends to the mass range of the QCD axion. Let us thus spend a word on the possibility to have oscillons from the QCD axion potential. In this case, the latter can be computed in the effective chiral lagrangian approach and turns out not to support long lived oscillons. Furthermore, the initial inhomogeneous conditions are provided by the presence of topological defects in the field, if the PQ symmetry is broken after inflation. Thus significant parametric resonance is not required and indeed may be difficult to achieve [66]. The formation of oscillons from the annihilation of the QCD axion string-wall network is well known [33]. The observational implications are expected to be quite similar to the one we discussed here (see indeed for numerical studies of QCD axitons as seeds of miniclusters [36, 37]).

3.3 Non-decaying oscillons?

Our phenomenological discussion has focused until now on the case in which oscillons have very long lifetimes, which are however quite short compared to the age of the Universe (unless $m \lesssim 10^{-24}$ eV, which is however likely to be in tension with observations). We devote this section to the very intriguing possibility that oscillons can survive until today and thus directly make up a significant fraction of the dark matter.

This speculation is partially supported by two different observations. On the one hand, as mentioned in the previous subsections, the lifetime of oscillons which decay after MR equality may be importantly affected by gravitational dynamics. For example, since oscillon overdensities grow

[7] The beginning of this exclusion region is meant to appear in Fig. B.10 as well, but given the small parameter space and the size of the uncertainties we dismissed it there.

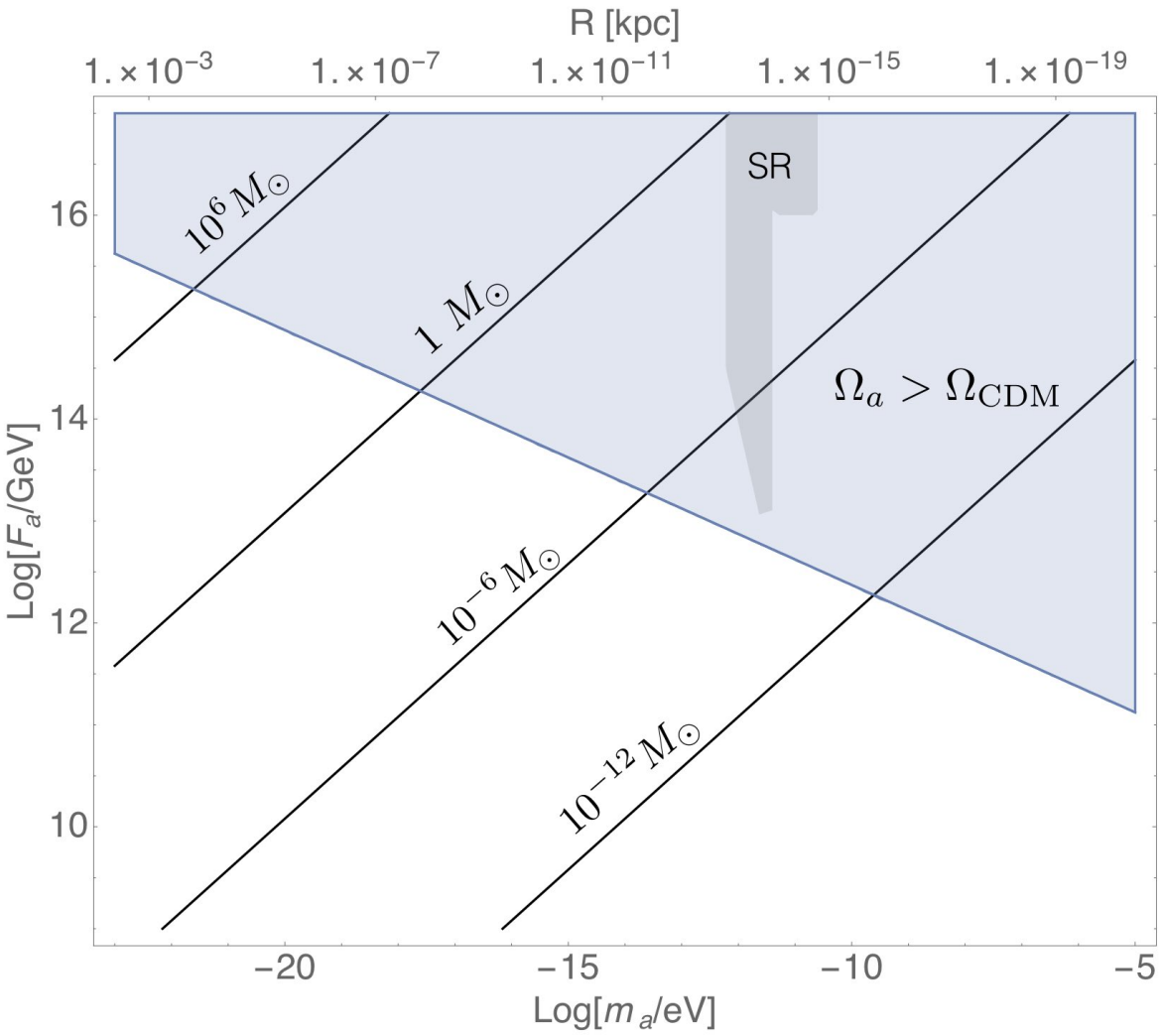

Fig. B.12: *Properties and constraints of long lived oscillons as functions of F and m assuming that they live up to today for any m (which might represent changing p). Above the solid blue line the homogeneous oscillations of the axion field overproduce dark matter, as extracted from the representative case $p = -1/2$, with $\phi_0 = 15\ F$. The solid black lines denote oscillon masses $10^6 M_\odot, 1 M_\odot, 10^{-6} M_\odot$ and $10^{-12} M_\odot$ from the top left to bottom right corners. Observationally disfavored masses ($\gtrsim 10^8 M_\odot$) are not shown since they lie entirely in the blue shaded region, excluded by DM overproduction. The gray shaded region is further constrained by black hole superradiance [82]. The tiny mass window around 10^{-18} eV which is also currently more weakly constrained by supermassive black hole superradiance for $F \gtrsim 10^{16}$ GeV is not shown.*

during matter domination, interactions among oscillons are expected to become more relevant in this epoch. In particular, the radiation of some oscillons may end up feeding neighboring oscillons which may then have extended lifetimes. Alternatively, oscillons may even coexist with the gravitationally-bound solitons and one can envisage hybrid structures with an oscillon at the cores surrounded by a soliton. One can expect a hybrid object of this sort to be much longer lived because the radiation

emitted by the oscillon is trapped inside its own gravitational well, therefore it does not really escape. Hybrid oscillon-soliton objects have indeed been found numerically in [78], with infinite lifetimes in some cases.

On the other hand and more importantly for the present work, the lifetime of oscillons crucially depends on the behavior of the axion potential at large field values, i.e. on the exponent p. Until now we have focused on the representative case $p = 1/2$, for which we know that $\tau \sim 10^8\ m^{-1}$. The same seems to hold true for any $0 \leq p < 1$. However, the situation appears to be different for $p < 0$, i.e. for plateau-like potentials. As discussed in Sec. 2.2, we only have a lower bound on the lifetime for the case $p = -1/2$, i.e. $\tau \gtrsim 6.5\ \cdot 10^8\ m^{-1}$. It is not inconceivable that $\tau_{(p<0)} \gg 10^8\ m^{-1}$. In particular, notice that for $m \lesssim 10^{-22}$ eV, 'just' $\tau_{(p<0)} \gtrsim 7 \cdot 10^{10}\ m^{-1}$ is required to have oscillon stability until the current age of the Universe.

With these motivations in mind, let us consider here the scenario in which oscillons are stable until today for a wide range of phenomenologically interesting axion masses, say 10^{-23} eV $\lesssim m \lesssim 10^{-5}$ eV. In this case, there are essentially no constraints coming from the oscillon decay into warm axions, therefore the available parameter space opens up significantly, as shown in Fig. B.12. In drawing Fig. B.12, we are essentially assuming that $\tau \gtrsim t_{\rm today}$ for every value of m. To be more concrete, the required lifetime in the mass range shown in Fig. B.12 is $10^{10}\ \lesssim (\tau\, m) \lesssim 10^{26}$. While this huge range seems implausible given the much shorter lifetime in the case $p = 1/2$, preliminary numerical results based on a simple extrapolation of numerical data for the case $p = -1/2$ suggest that such long lifetimes may be not so far-fetched [87].

The region where dark matter is overproduced is shown in Fig. B.12 fixing $p = -1/2$ and $\phi_0 = 15\ F$. Its shape does not strongly depend on p, as long as $p < 0$. For $p > 0$, constraints from DM are less rigid, as shown in Figs. B.10 and B.11. The oscillon mass as well as its radius are also obtained for $p = -1/2$ and are slightly smaller than in the case $p = 1/2$, according to Table B.1.

For the masses considered in Fig. B.12, oscillons always remain smaller than approximately 1 pc, therefore they are unconstrained by CMB anisotropies. We should remark that Fig. B.12 is obtained neglecting gravitational interactions among oscillons, which may lead to mergers and solitons as in the previous subsections. Black holes could also form from the growth of oscillon overdensities, as we discussed in the last paragraphs of Sec. 3.1. Interestingly, in the case considered in this section, masses smaller than 10^{-19} eV are allowed which could lead to lighter and observationally more viable black holes, according to (B.17).

While we leave more detailed estimates of oscillon lifetimes for $p < 0$ for future work, we cannot stop ourselves from pointing out that for a wide range of decay constants ALP dark matter may be today characterized by a large number of stable oscillons in our Hubble patch.

4 Conclusions

We have investigated oscillons (long-lived and localized scalar field lumps sustained by self-interactions only) and their implications for cosmology. Our focus has been on very long-lived oscillons because they arise in certain well-motivated models, and they give a significant impact on dark matter.

Oscillons are known to arise in self-interacting massive scalar field theories whenever the potential $V(\phi)$ exhibits regions which are shallower than quadratic. We find very long-lived oscillons whenever

$V(\phi)$ flattens out at large field values[8], with lifetimes reaching out to $\tau \sim (10^8 - 10^9)\, m^{-1}$ or more. Benchmark possibilities are a linear or plateau behavior beyond a critical field value F. Potentials with these properties are known to arise for axion fields in compactifications of string theory and in supergravity.

Another grace of these models is that they have a built-in *oscillogenesis* mechanism: an initial homogeneous field configuration with moderately large field value is enough to end up generating oscillons. The reason is that the homogeneous configuration suffers from parametric resonant instability once the scalar starts to (homogeneously) oscillate: field fluctuations of certain wavelengths can grow exponentially and thus lead to the fragmentation of the scalar field. This mechanism in turn provides the right ground on which oscillons can form (as confirmed by numerical simulations, see [43, 66]). We have studied the condition under which parametric resonance is efficient and we find that the localized overdensities are indeed generated for mildly large initial values of the scalar field, not far from F.

We then numerically evolved a single oscillon configuration, according to the full non-linear equation of motion, assuming spherical symmetry (and ignoring gravity). We provided numerical evidence that oscillons are essentially unaffected by Hubble friction, therefore we performed most of our simulations in flat space. While we confirm that oscillons radiate scalar waves during their evolution, the loss of energy due to this process can be extremely slow and thus makes the objects long-lived on cosmological scales. In particular, for potentials which go linearly at large field values, or as positive power law with exponent smaller than one, we found that oscillons live up to 10^8 oscillations (in units of the inverse scalar field mass m^{-1}). These are the longest lived oscillons ever encountered to our knowledge. Even more dramatic is the case of plateau-like potentials. In this case we have not yet witnessed oscillon death and so we are only able to put a lower bound on their lifetime, $\tau \gtrsim 10^9\ m^{-1}$.

Such long lifetimes make oscillons interesting in the framework of scalar dark matter. In the observationally viable range of m, oscillons are always born during the radiation domination epoch from the oscillations of the (pseudo)scalar field. After formation, these objects can be seen as nothing else than bound states of scalar particles, and thus behave as a separate MACHO-like (albeit much less dense) dark matter component, with masses ranging from 10^{-12} to $10^8 M_\odot$ depending on F and m. The physical radius of these objects at formation ranges from asteroid to galactic-core size and remains essentially constant during the oscillon lifetime, as the object is essentially decoupled from the Hubble flow.

We investigated several observationally interesting implications of oscillons in the context of scalar ULDM. For one thing, if their lifetimes are shorter than the age of the Universe, oscillons can decay before or after matter-radiation (MR) equality. The impact is rather sensitive to model details. Assuming $\tau m \sim 10^8$ as a benchmark value for oscillon lifetimes, then $m \leq 10^{-19}$ eV corresponds to oscillons death happening at or after MR equality. For $m > 10^{-19}$ eV and $\tau m \sim 10^8$, oscillons decay before MR equality. Since at decay oscillons emit a significant amount of warm scalar radiation, this poses some threat to the ULDM model. In this respect, gravity comes to rescue because a decaying oscillon can after all be bound by its own gravitational potential, remaining kept as what

[8] A more quantitative condition on the potential for very long lived oscillons seems to be that the effective mass $V''(\phi)$ is not very negative anywhere in the field space. This can happen whenever i) $V''(\phi) > 0$ for all ϕ, or ii) in case that $V''(\phi) < 0$ somewhere, $|V''(\phi)|/V''(0) \ll 1$. One of these conditions is satisfied the benchmark models (B.2).

is now referred to as a soliton (gravitationally-bound scalar field lump, see e.g. [44–47]). It would be interesting to further study or simulate numerically the oscillon-to-soliton transition, however this (perhaps simplified) picture already allows to estimate the observational bounds.

For $m < 10^{-19}$ eV, oscillons would decay in the matter dominated era, when gravitational effects play an important role in the full evolution of the dark sector itself, therefore it is more challenging to extract clean results. While we have not performed simulations including gravity (see [70] for simulations of non-relativistic ULDM solitons during matter domination), we can speculate that the latter will actually help the stability of oscillons and extend their lifetimes. Indeed, gravity on the one hand can lead to mergers of oscillons, with the possibility of forming heavier, thus longer-lived objects; on the other hand it causes the growth of overdensities, including in the vicinity of the lumps, thereby providing a mechanism to feed the oscillons with the part of the DM that is in the form of scalar waves. Nevertheless, gravity could also induce destructive effects, such as tidal disruption.

Of course the story can be much richer because gravitationally-bound solitonic structures enter into the game. For instance, hybrid objects could form, such as gravitational solitons with oscillon cores [78] that, perhaps, are longer lived than what we can estimate with flat space simulations. While this analysis goes well beyond the scope of this paper, it seems that rather robustly the presence of oscillons (in the past or until today) must be imprinted in the spectrum of DM overdensities as a peak in its spectrum of overdensities at a scale corresponding to the oscillon size, which is roughly the inverse scalar mass $\sim m^{-1}$. This would then alter the initial conditions that need to be assumed for numerical simulations of the ULDM such as the one in [8].

Finally, we cannot resist entertaining the option that oscillons are stable on the scale of the age of the Universe, which might be the case for plateau-like potentials. This scenario would have particularly exciting consequences: namely in this case a significant fraction of the DM today would be in the form of ancient compact objects, similar in a sense to boson stars and solitons, albeit sustained mainly by self interactions. A possible signature would be in pulsar timing arrays observatories, which can be sensitive to ULDM models as described in [88]. The signal is enhanced for denser DM sources, so a larger signal is expected from the galactic centre [89]. In case oscillons live up to today and make up a significant fraction of the DM, nearby oscillons could also lead individually to a sizeable signal. It is also interesting to consider the case of multiple species of axions with different masses and decay constants (i.e. the *axiverse*). The dark matter today could then be simply made up of oscillons of different sizes and masses, in striking similarity to the organization of baryonic structures around us. We presented here some basic constraints on these possibilities, while we leave the important and promising task of figuring out the ultimate fate of these oscillons for future work.

Acknowledgments

We thank R.Z. Ferreira, F. Ferrer, E. Masso and S. Sibiryakov for reading a preliminary draft of this paper and for discussions. We thank F. Ferrer also for helping us in setting up the numerical methods used in this paper. We also thank G. Dvali and D. Gaggero for discussions. We thank Manuel Kreutle for useful earlier collaboration. This work was partly supported by the grants FPA2017-88915-P and SEV-2016-0588 from MINECO and 2017-SGR-1069 from DURSI.

References

[1] M. S. Turner, "Coherent Scalar Field Oscillations in an Expanding Universe," *Phys. Rev. D*, vol. 28, p. 1243, 1983.

[2] W. H. Press, B. S. Ryden, and D. N. Spergel, "Single Mechanism for Generating Large Scale Structure and Providing Dark Missing Matter," *Phys. Rev. Lett.*, vol. 64, p. 1084, 1990.

[3] S.-J. Sin, "Late time cosmological phase transition and galactic halo as Bose liquid," *Phys. Rev. D*, vol. 50, pp. 3650–3654, 1994.

[4] W. Hu, R. Barkana, and A. Gruzinov, "Cold and fuzzy dark matter," *Phys. Rev. Lett.*, vol. 85, pp. 1158–1161, 2000.

[5] J. Goodman, "Repulsive dark matter," *New Astron.*, vol. 5, p. 103, 2000.

[6] P. J. E. Peebles, "Fluid dark matter," *Astrophys. J. Lett.*, vol. 534, p. L127, 2000.

[7] L. Amendola and R. Barbieri, "Dark matter from an ultra-light pseudo-Goldsone-boson," *Phys. Lett. B*, vol. 642, pp. 192–196, 2006.

[8] H.-Y. Schive, T. Chiueh, and T. Broadhurst, "Cosmic Structure as the Quantum Interference of a Coherent Dark Wave," *Nature Phys.*, vol. 10, pp. 496–499, 2014.

[9] L. Hui, J. P. Ostriker, S. Tremaine, and E. Witten, "Ultralight scalars as cosmological dark matter," *Phys. Rev. D*, vol. 95, no. 4, p. 043541, 2017.

[10] I. Bogolyubsky and V. Makhankov, "Lifetime of Pulsating Solitons in Some Classical Models," *Pisma Zh. Eksp. Teor. Fiz.*, vol. 24, pp. 15–18, 1976.

[11] M. Gleiser, "Pseudostable bubbles," *Phys. Rev. D*, vol. 49, pp. 2978–2981, 1994.

[12] E. J. Copeland, M. Gleiser, and H.-R. Muller, "Oscillons: Resonant configurations during bubble collapse," *Phys. Rev. D*, vol. 52, pp. 1920–1933, 1995.

[13] S. R. Coleman, "Q-balls," *Nucl. Phys. B*, vol. 262, no. 2, p. 263, 1985, [Addendum: Nucl.Phys.B 269, 744 (1986)].

[14] A. Kusenko and M. E. Shaposhnikov, "Supersymmetric Q balls as dark matter," *Phys. Lett. B*, vol. 418, pp. 46–54, 1998.

[15] E. P. Honda and M. W. Choptuik, "Fine structure of oscillons in the spherically symmetric phi**4 Klein-Gordon model," *Phys. Rev. D*, vol. 65, p. 084037, 2002.

[16] S. Kasuya, M. Kawasaki, and F. Takahashi, "I-balls," *Phys. Lett. B*, vol. 559, pp. 99–106, 2003.

[17] G. Fodor, P. Forgacs, P. Grandclement, and I. Racz, "Oscillons and Quasi-breathers in the phi**4 Klein-Gordon model," *Phys. Rev. D*, vol. 74, p. 124003, 2006.

[18] P. M. Saffin and A. Tranberg, "Oscillons and quasi-breathers in D+1 dimensions," *JHEP*, vol. 01, p. 030, 2007.

[19] M. Hindmarsh and P. Salmi, "Oscillons and domain walls," *Phys. Rev. D*, vol. 77, p. 105025, 2008.

[20] G. Fodor, P. Forgacs, Z. Horvath, and A. Lukacs, "Small amplitude quasi-breathers and oscillons," *Phys. Rev. D*, vol. 78, p. 025003, 2008.

[21] M. Gleiser and D. Sicilia, "Analytical Characterization of Oscillon Energy and Lifetime," *Phys. Rev. Lett.*, vol. 101, p. 011602, 2008.

[22] G. Fodor, P. Forgacs, Z. Horvath, and M. Mezei, "Radiation of scalar oscillons in 2 and 3 dimensions," *Phys. Lett. B*, vol. 674, pp. 319–324, 2009.

[23] M. A. Amin and D. Shirokoff, "Flat-top oscillons in an expanding universe," *Phys. Rev. D*, vol. 81, p. 085045, 2010.

[24] M. P. Hertzberg, "Quantum Radiation of Oscillons," *Phys. Rev. D*, vol. 82, p. 045022, 2010.

[25] M. A. Amin, R. Easther, H. Finkel, R. Flauger, and M. P. Hertzberg, "Oscillons After Inflation," *Phys. Rev. Lett.*, vol. 108, p. 241302, 2012.

[26] P. Salmi and M. Hindmarsh, "Radiation and Relaxation of Oscillons," *Phys. Rev. D*, vol. 85, p. 085033, 2012.

[27] E. A. Andersen and A. Tranberg, "Four results on ϕ^4 oscillons in D+1 dimensions," *JHEP*, vol. 12, p. 016, 2012.

[28] P. M. Saffin, P. Tognarelli, and A. Tranberg, "Oscillon Lifetime in the Presence of Quantum Fluctuations," *JHEP*, vol. 08, p. 125, 2014.

[29] K. Mukaida, M. Takimoto, and M. Yamada, "On Longevity of I-ball/Oscillon," *JHEP*, vol. 03, p. 122, 2017.

[30] M. Ibe, M. Kawasaki, W. Nakano, and E. Sonomoto, "Decay of I-ball/Oscillon in Classical Field Theory," *JHEP*, vol. 04, p. 030, 2019.

[31] M. Gleiser and M. Krackow, "Resonant configurations in scalar field theories: Can some oscillons live forever?" *Phys. Rev. D*, vol. 100, no. 11, p. 116005, 2019.

[32] I. Dymnikova, L. Koziel, M. Khlopov, and S. Rubin, "Quasilumps from first order phase transitions," *Grav. Cosmol.*, vol. 6, pp. 311–318, 2000.

[33] E. W. Kolb and I. I. Tkachev, "Nonlinear axion dynamics and formation of cosmological pseudosolitons," *Phys. Rev. D*, vol. 49, pp. 5040–5051, 1994.

[34] ——, "Large amplitude isothermal fluctuations and high density dark matter clumps," *Phys. Rev. D*, vol. 50, pp. 769–773, 1994.

[35] C. J. Hogan and M. J. Rees, "AXION MINICLUSTERS," *Phys. Lett. B*, vol. 205, pp. 228–230, 1988.

[36] A. Vaquero, J. Redondo, and J. Stadler, "Early seeds of axion miniclusters," *JCAP*, vol. 04, p. 012, 2019.

[37] M. Buschmann, J. W. Foster, and B. R. Safdi, "Early-Universe Simulations of the Cosmological Axion," *Phys. Rev. Lett.*, vol. 124, no. 16, p. 161103, 2020.

[38] L. Visinelli, S. Baum, J. Redondo, K. Freese, and F. Wilczek, "Dilute and dense axion stars," *Phys. Lett. B*, vol. 777, pp. 64–72, 2018.

[39] E. Silverstein and A. Westphal, "Monodromy in the CMB: Gravity Waves and String Inflation," *Phys. Rev. D*, vol. 78, p. 106003, 2008.

[40] L. McAllister, E. Silverstein, and A. Westphal, "Gravity Waves and Linear Inflation from Axion Monodromy," *Phys. Rev. D*, vol. 82, p. 046003, 2010.

[41] X. Dong, B. Horn, E. Silverstein, and A. Westphal, "Simple exercises to flatten your potential," *Phys. Rev. D*, vol. 84, p. 026011, 2011.

[42] K. D. Lozanov and M. A. Amin, "Self-resonance after inflation: oscillons, transients and radiation domination," *Phys. Rev. D*, vol. 97, no. 2, p. 023533, 2018.

[43] N. Kitajima, J. Soda, and Y. Urakawa, "Gravitational wave forest from string axiverse," *JCAP*, vol. 10, p. 008, 2018.

[44] E. D. Schiappacasse and M. P. Hertzberg, "Analysis of Dark Matter Axion Clumps with Spherical Symmetry," *JCAP*, vol. 01, p. 037, 2018, [Erratum: JCAP 03, E01 (2018)].

[45] M. P. Hertzberg and E. D. Schiappacasse, "Scalar dark matter clumps with angular momentum," *JCAP*, vol. 08, p. 028, 2018.

[46] H. Deng, M. P. Hertzberg, M. H. Namjoo, and A. Masoumi, "Can Light Dark Matter Solve the Core-Cusp Problem?" *Phys. Rev. D*, vol. 98, no. 2, p. 023513, 2018.

[47] N. Bar, D. Blas, K. Blum, and S. Sibiryakov, "Galactic rotation curves versus ultralight dark matter: Implications of the soliton-host halo relation," *Phys. Rev. D*, vol. 98, no. 8, p. 083027, 2018.

[48] D. J. E. Marsh, "Axion Cosmology," *Phys. Rept.*, vol. 643, pp. 1–79, 2016.

[49] E. Witten, "Large N Chiral Dynamics," *Annals Phys.*, vol. 128, p. 363, 1980.

[50] ——, "Theta dependence in the large N limit of four-dimensional gauge theories," *Phys. Rev. Lett.*, vol. 81, pp. 2862–2865, 1998.

[51] G. Dvali, "Three-form gauging of axion symmetries and gravity," 7 2005.

[52] N. Kaloper and L. Sorbo, "A Natural Framework for Chaotic Inflation," *Phys. Rev. Lett.*, vol. 102, p. 121301, 2009.

[53] N. Kaloper, A. Lawrence, and L. Sorbo, "An Ignoble Approach to Large Field Inflation," *JCAP*, vol. 03, p. 023, 2011.

[54] K. Yonekura, "Notes on natural inflation," *JCAP*, vol. 10, p. 054, 2014.

[55] S. Antusch, F. Cefala, S. Krippendorf, F. Muia, S. Orani, and F. Quevedo, "Oscillons from String Moduli," *JHEP*, vol. 01, p. 083, 2018.

[56] S.-Y. Zhou, E. J. Copeland, R. Easther, H. Finkel, Z.-G. Mou, and P. M. Saffin, "Gravitational Waves from Oscillon Preheating," *JHEP*, vol. 10, p. 026, 2013.

[57] M. A. Amin, J. Braden, E. J. Copeland, J. T. Giblin, C. Solorio, Z. J. Weiner, and S.-Y. Zhou, "Gravitational waves from asymmetric oscillon dynamics?" *Phys. Rev. D*, vol. 98, p. 024040, 2018.

[58] R. Kallosh and A. Linde, "Universality Class in Conformal Inflation," *JCAP*, vol. 07, p. 002, 2013.

[59] R. Kallosh, A. Linde, and D. Roest, "Universal Attractor for Inflation at Strong Coupling," *Phys. Rev. Lett.*, vol. 112, no. 1, p. 011303, 2014.

[60] ——, "Superconformal Inflationary α-Attractors," *JHEP*, vol. 11, p. 198, 2013.

[61] Y. Nomura, T. Watari, and M. Yamazaki, "Pure Natural Inflation," *Phys. Lett. B*, vol. 776, pp. 227–230, 2018.

[62] Y. Nomura and M. Yamazaki, "Tensor Modes in Pure Natural Inflation," *Phys. Lett. B*, vol. 780, pp. 106–110, 2018.

[63] A. Landete, F. Marchesano, G. Shiu, and G. Zoccarato, "Flux Flattening in Axion Monodromy Inflation," *JHEP*, vol. 06, p. 071, 2017.

[64] J.-P. Hong, M. Kawasaki, and M. Yamazaki, "Oscillons from Pure Natural Inflation," *Phys. Rev. D*, vol. 98, no. 4, p. 043531, 2018.

[65] K. D. Lozanov and M. A. Amin, "Gravitational perturbations from oscillons and transients after inflation," *Phys. Rev. D*, vol. 99, no. 12, p. 123504, 2019.

[66] H. Fukunaga, N. Kitajima, and Y. Urakawa, "Efficient self-resonance instability from axions," *JCAP*, vol. 06, p. 055, 2019.

[67] E. Cotner, A. Kusenko, and V. Takhistov, "Primordial Black Holes from Inflaton Fragmentation into Oscillons," *Phys. Rev. D*, vol. 98, no. 8, p. 083513, 2018.

[68] E. Masso, F. Rota, and G. Zsembinszki, "Scalar field oscillations contributing to dark energy," *Phys. Rev. D*, vol. 72, p. 084007, 2005.

[69] M. A. Amin, P. Zukin, and E. Bertschinger, "Scale-Dependent Growth from a Transition in Dark Energy Dynamics," *Phys. Rev. D*, vol. 85, p. 103510, 2012.

[70] M. A. Amin and P. Mocz, "Formation, gravitational clustering, and interactions of nonrelativistic solitons in an expanding universe," *Phys. Rev. D*, vol. 100, no. 6, p. 063507, 2019.

[71] G. Dvali and S. Zell, "Classicality and Quantum Break-Time for Cosmic Axions," *JCAP*, vol. 07, p. 064, 2018.

[72] M. Gleiser and D. Sicilia, "A General Theory of Oscillon Dynamics," *Phys. Rev. D*, vol. 80, p. 125037, 2009.

[73] M. Hindmarsh and P. Salmi, "Numerical investigations of oscillons in 2 dimensions," *Phys. Rev. D*, vol. 74, p. 105005, 2006.

[74] J. Liu, Z.-K. Guo, R.-G. Cai, and G. Shiu, "Gravitational wave production after inflation with cuspy potentials," *Phys. Rev. D*, vol. 99, no. 10, p. 103506, 2019.

[75] Y. Akrami *et al.*, "Planck 2018 results. X. Constraints on inflation," *Astron. Astrophys.*, vol. 641, p. A10, 2020.

[76] B. Bozek, D. J. E. Marsh, J. Silk, and R. F. G. Wyse, "Galaxy UV-luminosity function and reionization constraints on axion dark matter," *Mon. Not. Roy. Astron. Soc.*, vol. 450, no. 1, pp. 209–222, 2015.

[77] R. Hlozek, D. Grin, D. J. E. Marsh, and P. G. Ferreira, "A search for ultralight axions using precision cosmological data," *Phys. Rev. D*, vol. 91, no. 10, p. 103512, 2015.

[78] T. Ikeda, C.-M. Yoo, and V. Cardoso, "Self-gravitating oscillons and new critical behavior," *Phys. Rev. D*, vol. 96, no. 6, p. 064047, 2017.

[79] B. Carr and J. Silk, "Primordial Black Holes as Generators of Cosmic Structures," *Mon. Not. Roy. Astron. Soc.*, vol. 478, no. 3, pp. 3756–3775, 2018.

[80] A. Arvanitaki and S. Dubovsky, "Exploring the String Axiverse with Precision Black Hole Physics," *Phys. Rev. D*, vol. 83, p. 044026, 2011.

[81] A. Arvanitaki, M. Baryakhtar, and X. Huang, "Discovering the QCD Axion with Black Holes and Gravitational Waves," *Phys. Rev. D*, vol. 91, no. 8, p. 084011, 2015.

[82] A. Arvanitaki, M. Baryakhtar, S. Dimopoulos, S. Dubovsky, and R. Lasenby, "Black Hole Mergers and the QCD Axion at Advanced LIGO," *Phys. Rev. D*, vol. 95, no. 4, p. 043001, 2017.

[83] A. Gruzinov, "Black Hole Spindown by Light Bosons," 4 2016.

[84] T. Helfer, D. J. E. Marsh, K. Clough, M. Fairbairn, E. A. Lim, and R. Becerril, "Black hole formation from axion stars," *JCAP*, vol. 03, p. 055, 2017.

[85] K. Clough, T. Dietrich, and J. C. Niemeyer, "Axion star collisions with black holes and neutron stars in full 3D numerical relativity," *Phys. Rev. D*, vol. 98, no. 8, p. 083020, 2018.

[86] K. Clough, P. G. Ferreira, and M. Lagos, "Growth of massive scalar hair around a Schwarzschild black hole," *Phys. Rev. D*, vol. 100, no. 6, p. 063014, 2019.

[87] J. Olle, O. Pujolas, and F. Rompineve, "Recipes for Oscillon Longevity," *JCAP*, vol. 09, p. 015, 2021.

[88] A. Khmelnitsky and V. Rubakov, "Pulsar timing signal from ultralight scalar dark matter," *JCAP*, vol. 02, p. 019, 2014.

[89] I. De Martino, T. Broadhurst, S. H. Henry Tye, T. Chiueh, H.-Y. Schive, and R. Lazkoz, "Recognizing Axionic Dark Matter by Compton and de Broglie Scale Modulation of Pulsar Timing," *Phys. Rev. Lett.*, vol. 119, no. 22, p. 221103, 2017.

Paper C

Recipes for Oscillon Longevity

Jan Ollé[1], Oriol Pujolàs[1] and Fabrizio Rompineve[2]

[1] *Institut de Física d'Altes Energies (IFAE)*
The Barcelona Institute of Science and Technology (BIST)
Campus UAB, 08193 Bellaterra (Barcelona) Spain

[2] *Institute of Cosmology, Department of Physics and Astronomy,*
Tufts University, Medford, MA 02155, USA

This paper has been published in
JCAP 09 (2021) 015.

The layout has been revised.

Abstract

Oscillons are localized states of scalar fields sustained by self interactions. They decay by emitting classical radiation, but their lifetimes are surprisingly large. We revisit the reasons behind their longevity, aiming at how the shape of the scalar potential $V(\phi)$ determines the lifetime. The corpuscular picture, where the oscillon is identified with a bound state of a large number of field quanta, allows to understand lifetimes of order of 10^3 cycles in generic potentials. At the non-perturbative level, two properties of the scalar potential can substantially boost the lifetime: the flattening of $V(\phi)$ and the positivity of $V''(\phi)$. These properties are realized in the axion monodromy family of potentials. Moreover, this class of models connects continuously with an exceptional potential that admits eternal oscillon solutions. We check these results with a new fast-forward numerical method that allows to evolve in time to stages that cannot be otherwise simulated on a computer. The method exploits the attractor properties of the oscillons and fully accounts for nonlinearities. We find lifetimes up to 10^{14} cycles, but larger values are possible. Our work shows that oscillons formed in the early Universe can be stable on cosmological time scales and thus contribute to the abundance of (ultra)light scalar dark matter.

1 Introduction

Real scalar fields can exhibit a variety of dynamical phenomena in the early Universe, which makes them interesting and useful for inflationary and dark matter model building. Among these, a quite peculiar one can occur in the presence of attractive self interactions: the formation of localized, oscillating field configurations, known as *oscillons* [1–3] and also referred to as *axitons* when the scalar field potential is periodic, e.g. in the QCD axion case [4, 5].

Since particle number is not a conserved quantity in a real scalar field theory, oscillons are necessarily subject to decay. In very weakly coupled theories, such as is the case of axions, this occurs very slowly via the classical radiation of scalar waves. Oscillon lifetimes then vary dramatically with the shape of the potential, and so does their observational impact. Understanding the causes of an oscillon's longevity is thus an important task, to which a lot of work has been devoted (see e.g. [6–24]).

In this paper, we approach this problem in two directions: First, we provide an analytical understanding behind the longevity of large-amplitude oscillons aiming to identify the properties of the scalar potential $V(\phi)$ that can enhance longevity from a quantum field theory point of view. Secondly, we present a new numerical method by which one can reliably estimate the lifetime of an oscillon even when its evolution is too long to be entirely simulated on a computer. We thus obtain evidence of oscillons which can survive until today and constitute an interesting dark matter component.

Our analytical approach is anchored on the properties of an *exceptional* scalar potential, $V(\phi) \sim \phi^2 + \epsilon\phi^2 \log\phi$, that is almost quadratic across an exponentially large field range when $\epsilon \ll 1$. It is known that this potential leads to (classically) infinitely long lived oscillons, both in $1+1$ [25] and $3+1$ dimensions [26]. This largely explains the longevity of oscillons supported by "monodromy" potentials [27, 28] that behave like some power-law ϕ^{2p} at large field values, and which we have shown in our previous work [20] to have the largest lifetimes ever computed before. Indeed, in the

$p \to 1$ limit, these potentials closely resemble the exceptional potential at large field values and it is then possible to analytically estimate the lifetimes of the associated oscillons by perturbing the exact solution. This shows that, in contrast to our previous expectations, monodromy oscillons with $1/2 < p \lesssim 1$ can be extremely long-lived, much beyond what can be simulated on a computer.

Our analytical findings then motivate the search for a novel numerical strategy to probe such large lifetimes. Recently, a new method in this direction has been proposed [18] (and applied to monodromy potentials in [21]), which takes advantages of two key concepts. First, the time evolution can be *fast-forwarded* by means of a clever trick: rather than numerically evolving the whole field configuration in a discretized lattice, one just computes the emitted power in scalar radiation from a given oscillon-like configuration. A simple idea then is to just *assume* a certain profile with a single oscillation frequency, and obtain the energy loss rate $\Gamma(\omega)$ for an "oscillon" of that frequency. The result can then be easily integrated and gives an estimate of the lifetime. The second ingredient in [18, 21] was the computation of $\Gamma(\omega)$ by linearizing the field equation for the radiation field. This simplifies the computation at the expense of neglecting some nonlinearities which might be important.

In this work, we propose what we believe is an improvement on this method by adopting the fast forward strategy of computing the energy loss $\Gamma(\omega)$ but keeping the full nonlinear equation (see also [22] for progress in this direction). Starting from quite random initial conditions, one can populate real oscillons in a range of frequencies by giving a sufficient (but realizable) relaxation time. Even in the most extreme cases when the lifetimes are very long, the relaxation time needed to see the trajectory of the true oscillon in the $\Gamma - \omega$ plane is much smaller than the actual lifetime. This strategy still 'buys' a lot of time, and for this reason we call the method *relax and fast forward*.

Our method, while more costly to implement, offers the great advantage of dealing always with the full nonlinear problem, basically with no assumptions on the oscillon shape and power spectrum at a given time. This exploits the attractor property of the true oscillon configuration, which drives many different initial conditions into the same oscillon (the same trajectory in the $\Gamma - \omega$ plane), in a rather short relaxation time.

Equipped with our numerical strategy, we are able to extract oscillon lifetimes for any value of p and confirm our analytical estimates. In particular, this allows us to complete our investigation of potentials with $p < 0$. In contrast to our previous expectations [20], we find that flattening the potential with $p < -1/2$ does not lead to increased lifetimes with respect to the case $p \lesssim 1$.

The rest of this paper is structured as follows: In Sec. 2 we present qualitative criteria to obtain long-lived oscillons, while we provide analytical estimate for generic, exceptional and monodromy-like potentials in Secs. 2.1, 2.2 and 2.3 respectively. We then introduce our numerical strategy in Sec. 3.1 and present numerical results for oscillon lifetimes in Sec. 3.2. We offer a final discussion and conclusions in Sec. 4 and provide more details about our numerical method in the Appendix.

2 Understanding Longevity

In this section we discuss oscillons and their longevity in the context of quantum field theory, in which oscillons can be understood as bound states of field quanta that are held together by the attractive self-interaction encoded in the potential $V(\phi)$. To set the stage, we consider a single real

scalar field of mass m with lagrangian $\mathcal{L} = (\partial\phi)^2/2 - V(\phi)$ and with a generic potential,

$$V(\phi) = \frac{1}{2} m^2\phi^2 + \sum_{n=2}^{\infty} g_{2n}\, \phi^{2n} \,, \tag{C.1}$$

with a negative quartic coupling $g_4 < 0$. For axions, it is convenient to write $V = m^2\, F^2\, v(\phi/F)$ with v a dimensionless function $v(x) = x^2/2 + \ldots$ and with F the axion decay constant. The quartic coupling is then naturally of order $g_4 \sim (m/F)^2$ (in general, $g_{2n} \sim m^2/F^{(2n-2)}$) and the weak coupling regime maps to $m \ll F$.

Despite the smallness of the couplings in the Lagrangian, a strong collective interaction arises when a large occupation number of axion scalar quanta N is considered, as can be understood by defining a *collective coupling* $\lambda = N g_4$ [29]. For $N \sim 1/g_4 \gg 1$, the system can be treated classically and in particular when $\lambda \sim 1$ one expects the formation of bound states held together by attractive self interactions, i.e. oscillons. However, since particle number is not conserved for a real scalar field, such bound states are metastable. For $g_4 < 0$, higher dimensional operators in (C.1) need to be important at large field values, otherwise the potential would be unstable. These operators can then play an important role in determining the longevity of the scalar bound state.

While the lifetime of oscillons depends crucially on the higher dimensional operators in $V(\phi)$, it is possible to qualitatively understand the features that can lead to large lifetimes in a model-independent (and non-perturbative) way. First, let us consider the quantity

$$\Delta\omega \equiv m - \omega_{\rm osc}, \tag{C.2}$$

where $\omega_{\rm osc}$ is the frequency of oscillations of the field ϕ in the oscillon configuration. The quantity $\Delta\omega$ can be thought of as the binding energy per particle: each corpuscle decreases the total energy of a set of N quanta by $\Delta\omega$ by being in the lump, therefore the very existence of an oscillon requires a significant $\Delta\omega$. While the dependence of $\Delta\omega$ on $V(\phi)$ may be complicated, in the classical field theory limit with $N \sim 1/g_4 \gg 1$, it is very reasonable to expect that this quantity is directly controlled by the deviation of $V(\phi)$ from the free part in the oscillon core

$$\Delta V(\phi) \equiv \frac{1}{2} m^2\phi^2 - V(\phi). \tag{C.3}$$

We will refer to ΔV as the *binding potential*: in order to form and persist, an oscillon should experience a significant gain in potential by exploring large field values, and therefore it can be characterized by a significant $\Delta V(\phi)$ in its core. This in turn leads to a rough criterion to estimate the oscillation amplitude in the core, ϕ_0, for any given $V(\phi)$, i.e.

$$\Delta V(\phi_0) = \delta\, \frac{m^2\, \phi_0^2}{2} \tag{C.4}$$

with δ a sizeable fraction of 1 namely, $\delta \sim O(0.1)$. For later use, we shall refer to δ as the binding potential 'fraction'. Its precise value is expected to depend on the shape of the potential, therefore further computations are needed to find it. In practice, what we will do below is to find numerically

the oscillon configurations in a class of potentials, and then use (C.4) as a definition for δ (with ϕ_0 the field amplitude at the center) to check that the criterion that we are presenting here works.[1]

Secondly, once an oscillon has formed, its lifetime is dictated by its (in)efficiency to radiate classical scalar waves. In this respect, it is well known that fluctuations of an homogeneous oscillating field can undergo resonant enhancement. The same can happen in the localized oscillon configuration, i.e. the amplitude of modes whose wavelength is smaller than the oscillon size can be potentially enhanced. When this happens, the oscillon configuration is quickly disrupted. In analogy with the homogeneous case, the efficiency of such a resonant enhancement is on general grounds expected to be controlled by the effective mass, $V''(\phi_{\rm osc}(t,r))$, experienced by the field fluctuations over the oscillon background. In particular, we expect that potentials with negative $V''(\phi)$ for some large enough field values will be characterized by efficient resonant decay of oscillon configurations. The same logic suggests that, generically, negative but small effective mass, $|V''(\phi)|/m^2 \ll 1$, at the core can be 'tolerated' because both the length- and time- scales of the oscillons are of order $\sim 1/m$, so the naively tachyonic instability can be inefficient.

In sum, a qualitative criterion for the presence of long-lived oscillons is that the potential $V(\phi)$ satisfies these 2 conditions:

1) $\Delta V(\phi)$ is maximized.

2) $V''(\phi)$ (including the sign) is maximized.

Interestingly, the two conditions above are somewhat antagonistic. For instance the obvious way to increase the binding potential $\Delta V(\phi)$ is by "bending" $V(\phi)$ so that it decreases with ϕ past some value. However, this means that there is a maximum, with $V''(\phi) < 0$, so that radiation would be efficient in this case. In turn, requiring that $V''(\phi)$ is bounded from below limits the size of the binding potential $\Delta V(\phi)$.

At first, it is not immediate to tell which of the conditions above is more important, nor what combination of the two should one optimize in order to maximize the lifetime. It is rather obvious that plateau-shaped potentials are good at satisfying **1**), while potentials very close to ϕ^2 are good at satisfying **2**).

It turns out that condition **2**) plays a stronger role in enhancing longevity. One way to understand this is that even if $V(\phi)$ deviates from $m^2\phi^2/2$ only slowly, one can still find a large enough amplitude ϕ_0 such that condition (C.4) (sizeable binding potential) is met. If this happens while the potential is still close to quadratic (therefore $V''(\phi)/m^2$ close to 1) then one does not expect much radiation, which therefore leads to a long lifetime.

This logic is further confirmed by the fact that the binding potential $\Delta V = -\phi^2 \log\phi$ (which incarnates precisely the limit of being close to a quadratic potential) turns out to admit *exact* non-dissipative oscillons, as we discuss below (see Sec. 2.2). Oscillons in close-to-quadratic potentials, then, are expected to have a boosted lifetime.

[1] This criterion is actually supported by our numerical studies with monodromy-like potentials, as we shall see below. For instance, as shown in Fig. C.5, there is a clear correlation between $\Delta\omega$ and δ as defined through (C.4) with ϕ_0 the amplitude at the oscillon center. Moreover, typical values of δ extracted in this way in simulations for different potentials give a range of δ from 0.2 to 0.85. This supports the criterion suggested above that δ must be a sizeable fraction of unity. Moreover, another result from Fig. C.5 is that in the $p \to 1$ limit, δ is of order $0.15 - 0.2$.

The oscillons for $\Delta V = -\phi^2 \log \phi$ are classically eternal for any amplitude. However, this potential displays a maximum at high enough ϕ (with order-1 negative V''), which seems to go against condition **2**) above. The crack in the argument is that the oscillons that explore the maximum in fact decay because they have unstable resonant modes [30]. Therefore our logic still applies. A similar thing happens with breathers in 1+1 sine-Gordon theory: at the quantum level the spectrum of amplitudes is quantized [31], and the 'ground state' breather does not probe the maximum.

We now discuss separately the longevity for the 3 relevant types of potentials: of generic form, exceptional form, and finally we go to the family of monodromy potentials.

2.1 Lifetime estimates

In this section we follow the corpuscular description of bounds states [32, 33] (devised to understand generic localized objects like black holes or solitons) to obtain estimates of the oscillon lifetime in terms of the couplings appearing in the potential. The starting point of the corpuscular picture is that classical field solutions can be re-interpreted as mean-field descriptions of the (bosonic) quantum field in the Bose-Einstein condensate limit, that is when there is a large occupation number of the same state. This picture is well suited for oscillons when the couplings in the Lagrangian are small. First, this is because in a weakly coupled theory it makes sense to view the bound states as being composed of approximately free field quanta. Second, the oscillon mass typically scales like $E \sim m/g_4 \gg m$ so indeed one can view it as composed of a large number $N \sim 1/g_4$ of quanta, which is consistent with the large occupation number picture.

Since the N quanta basically occupy the same state, one can identify the wavelength of the occupied quantum state with the oscillon radius, R, which is around $1/m$, but often slightly bigger. A heuristic way to obtain R is to picture that the scalar field quanta are trapped (dynamically) inside a spherical box of radius R. The lowest energy modes should then exhibit a relation between the oscillation frequency and the radius of the form

$$\omega = \sqrt{m^2 - R^{-2}} \ . \tag{C.5}$$

Since the oscillation frequency indeed satisfies $\omega < m$, one can use this equation as a definition for the oscillon radius (the numerical simulations show that this is a good estimate for the radius) once the oscillon frequency is 'measured'.

The departure of ω from m is an important property of oscillons, as it leads to a notion of binding energy $\Delta\omega$ according to

$$\omega_{osc} = m - \Delta\omega \ . \tag{C.6}$$

This $\Delta\omega$ represents the gain in energy (per quantum) in forming the localized bound state. In numerical simulations, $\Delta\omega/m$ is measured to be in the $10^{-2} - 10^{-1}$ range.[2] For small binding energy $\Delta\omega/m \ll 1$, one obtains the usual non-relativistic relation between $\Delta\omega$ and the momentum $1/R$,

$$\Delta\omega \simeq \frac{1}{2mR^2} \ . \tag{C.7}$$

[2]The lower end of the window can be understood from the requirement of stability of the oscillon in the non-relativistic approximation, see [17, 21].

With this corpuscular picture in mind we are now ready to estimate the oscillon lifetime from the form of the potential (C.1). We are now viewing the oscillon as a finite density concentration of $N \sim 1/g_4$ particles, therefore one can attempt to estimate the lifetime by means of the usual formula

$$\Gamma \sim v\,\sigma\,n, \tag{C.8}$$

where σ is the scattering cross section associated to the processes that generate radiation, n is the number density and v the typical velocity of particles. The number density is

$$n = \frac{N}{V} \sim \frac{1}{g_4 R^3}$$

with R the typical oscillon size, which is related to the frequency of oscillation. The typical speed of the quanta in the soliton can be estimated as $v \sim p/E$ with $E = \omega$ and $p \sim 1/R$. Using (C.6), this reduces to approximately $1/(mR)$ for small $\Delta\omega$. The cross section for individual $3 \to 1$ conversion processes from the quartic coupling is estimated as $\sim g_4^2 m^{-2}$. Since there are $1/g_4$ quanta in the bound state, the total cross section is enhanced by a $1/g_4$ factor. Collecting all terms, one arrives at

$$\Gamma \sim \frac{1}{g_4 R^3}\,\frac{1}{Rm}\,\frac{g_4}{m^2} = \left(\frac{\Delta\omega}{m}\right)^2 m \tag{C.9}$$

where we used (C.7) in the last step.

There are 3 important features of this estimate: First, oscillons in simplest potentials (including the sinusoidal, which is relevant for the QCD axion) exhibit a rather small binding energy (per quantum)

$$\frac{\Delta\omega}{m} \sim 10^{-2}$$

and this according to (C.9) leads to a considerably long lifetime, of the order of 10^3 oscillations. This naive estimate actually matches the lifetime which is determined by numerical computations for quartic and sinusoidal potentials.

Second, (C.9) does not depend on the magnitude of the coupling g_4, as expected. In the $g_4 \ll 1$ limit, where the dynamics simplifies to mean field theory, the field can always be rescaled at will in order to fix the magnitude of *one* coupling, which we can take to be g_4. This also makes manifest that oscillon properties such as its binding energy $\Delta\omega$ or its lifetime must depend exclusively on the set of higher order self-interactions, g_n with $n \geq 6$.

Third, the estimate (C.9) is based on looking only at the quartic self-coupling so this implicitly assumes that higher order couplings, g_n with $n \geq 6$, do not give rise to cancellations that would significantly change the estimate. This is what we mean by *non-exceptional* potentials. Note that *all* couplings $n \geq 6$ contribute to processes where the emitted particle has energy $\sim 3m$, which can compete with the $3 \to 1$ channel from g_4, therefore it is conceivable that higher order couplings may affect the rate. In the introduction of Sec. 2, we discussed in an intuitive way the possible ways by which the final rate can be suppressed, based on the shape of $V(\phi)$ (and $V''(\phi)$). In the next subsections we show this more explicitly.

By the same logic, one expects that lifetimes (identified with $1/\Gamma$) substantially differing from (C.9) should correspond to the situation where there is destructive interference between different

channels (from different couplings). This should also translate into having enhanced emitted power in the different multiples of the fundamental frequency ($3w_{\rm osc}$, $5w_{\rm osc}$, etc). We shall not show results for the power spectra of the radiation from oscillons, but we have checked that this is indeed the case: for potentials with longer lived oscillons, the power spectra in higher harmonics become more comparable, which further confirms this picture.

Finally, let us take a brief detour as we want to emphasize that the kind of reasoning presented here is strictly parallel to the way of understanding a more familiar yet nontrivial bound state appearing in a very simple theory: namely, positronium in QED. Even though in this case we are dealing with fermions, and there are only two particles in the bound state, the same use of (C.8) also allows to compute the positronium decay rate. As is well known, the decay rate differs for the two spin states. The singlet state (para-positronium) decays by emitting 2 photons ($\sigma \sim \alpha^2$), while the triplet (ortho-positronium) emits 3 photons ($\sigma \sim \alpha^3$). The rate picks 3 more powers of α from the number density which is obtained from the Bohr radius $1/(m_e\alpha)$, reproducing the usual values of the lifetime $\alpha^5 m_e$ or $\alpha^6 m_e$ for (para- or ortho-) positronium. Perhaps this makes one more confident with the estimate (C.9) above.

2.2 Exceptional potential

Let us now discuss an exceptional potential that escapes the logic presented in the previous section. It consists in the special form "$V_{\log}(\phi)$"$\propto \phi^2 - \phi^2 \log\phi$. In the context of oscillons, [26] showed that this potential supports eternal oscillons in 3 spatial dimensions and moreover it is the unique one with this property. Previous work [25] had established the same properties in 1 space dimension. Heuristically, it is somewhat unsurprising that this potential leads to non-radiative localized solutions because the effective mass-squared at the origin blows up and so it is energetically impossible to emit scalar radiation. Still, this potential stores an additional surprise: the resulting oscillon solutions can be obtained analytically.

For later use, we perform an arbitrary rescaling and introduce a parameter ϵ to write the potential in the form

$$V_{\log}(\phi) = \frac{1}{2}(1+\epsilon)m^2\phi^2 - \frac{1}{2}\epsilon\, m^2\phi^2 \log\left(\frac{\phi^2}{F^2}\right) . \tag{C.10}$$

This potential has 2 somewhat 'unwanted' features: i) it is not exactly analytic around ϕ due to the $\log\phi$; ii) it is unbounded from below – clearly at $\phi \geq e^{\frac{1}{2}(1+\frac{1}{\epsilon})}F$ it becomes negative.

The potential (C.10) leads to an equation of motion of the form

$$\frac{\partial_r^2\phi}{\phi} + \frac{2}{r}\frac{\partial_r\phi}{\phi} - \frac{\partial_t^2\phi}{\phi} = \frac{V'_{\log}(\phi)}{\phi} = m^2 - \epsilon m^2 \log(\phi^2/F^2). \tag{C.11}$$

Despite being nonlinear, this equation is factorizable [25, 26] – which is at the very root of the exceptional properties of $V_{\log}$. Indeed, the factorized ansatz

$$\phi_i(t,r) = A(t)B(r) \tag{C.12}$$

leads to an immortal localized solutions with a Gaussian profile

$$B(r) = e^{-(r/R)^2} \qquad \text{with} \qquad R = \sqrt{\frac{2}{\epsilon}}\frac{1}{m} \tag{C.13}$$

provided that the overall amplitude A satisfies the ODE

$$\ddot{A} = -m^2 A \left(1 + 3\epsilon - \epsilon \log(A^2/F^2)\right) ,$$

that is, it oscillates according to the same logarithmic potential. Since the equation above can be solved by quadratures, the evolution of $A(t)$ is periodic, and therefore this is a non-radiating everlasting oscillon. Solutions with any oscillation amplitude A_0 exist, however one expects that only those that do not reach the maximum will be stable, as was indeed found in [30]. This limits the amplitude of stable oscillons to at most $A_0 \sim e^{\frac{1}{2\epsilon}} F$.

Two comments are in order. First, the potential $\phi^2 \log \phi$ is encountered in some supersymmetric models (see e.g. [25, 34] and [35] in a different context). Second, the mere fact that the theory admits exact stable localized excitations suggests that this might be due to some kind of integrability property. Indeed the potential $\phi^2 \log \phi$ is a member of a class of potentials with the property [36] that they contain static localized 'lump' field configurations, whose stability leads to a reflectionless Schrödinger potential [36–38]. Interestingly, for the $\phi^2 \log \phi$ potential the 'lump' (the above solution with $A_0 = e^{1/2\epsilon} F$) leads to a Schrödinger problem with a purely quadratic potential, so it has an infinite number of evenly-spaced bound states.

2.3 *Monodromy* potentials

We now consider the 1-parameter family of potentials:

$$V(\phi) = \frac{1}{2p} m^2 F^2 \left[\left(1 + \frac{\phi^2}{F^2}\right)^p - 1\right] = \frac{m^2\phi^2}{2} - \frac{1-p}{4}\frac{m^2}{F^2}\phi^4 + \ldots , \tag{C.14}$$

which was our focus in [20]. Oscillons form for $p < 1$, which is when both **1**. the quartic coupling is negative and **2**. the potential is smaller than the free part, $V(\phi) < m^2\phi^2/2$. It is useful to analyze certain limiting cases of this class of potentials.

I) $\mathbf{p \to -\infty}$

The potential becomes

$$V(\phi) \simeq \frac{m^2 \tilde{F}^2}{2}\left(1 - e^{-\phi^2/\tilde{F}^2}\right) + \mathcal{O}\left(\frac{1}{p}\right) \tag{C.15}$$

with $\tilde{F} = F/\sqrt{1-p}$. Therefore, at large negative p the potential is insensitive to the value of p as should be the oscillon properties.

II) $\mathbf{p \to 1}$

Expanding around $p = 1$, the potential becomes

$$V(\phi) \simeq \frac{1}{2} m^2 \left\{\phi^2 - (1-p)\left[\left(F^2 + \phi^2\right)\log\left(1 + \frac{\phi^2}{F^2}\right) - \phi^2\right] + \ldots\right\} \tag{C.16}$$

the dots denoting corrections of order $\mathcal{O}\left[(1-p)^2 \log^2(1 + \phi^2/F^2)\right]$. This potential is of course smooth at the origin, where $V = m^2\phi^2/2 - \ldots$, whereas at large field values it is very similar

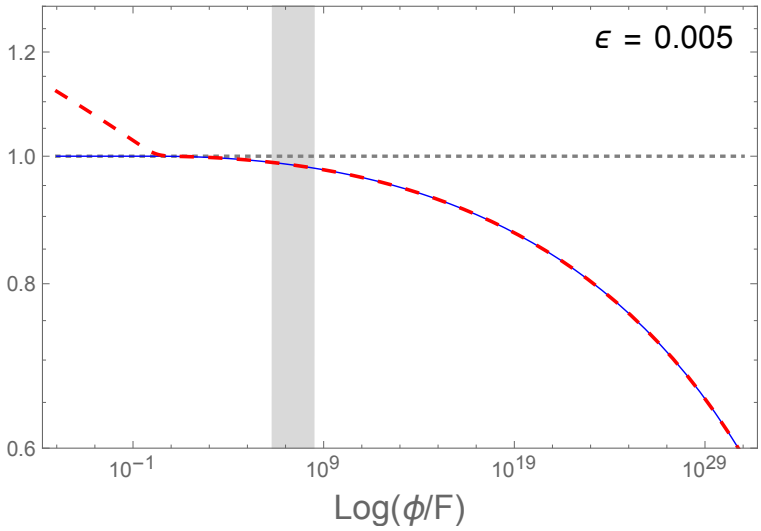

Fig. C.1: Ratio of the truncated potential (C.16) to the full monodromy potential (C.14) (blue solid line) and of the exceptional (C.10) to the monodromy potentiald (red dashed line) as a function of ϕ, for $\epsilon = 0.005$. Clearly, there is a (C.16), (C.10) are very similar (and close to (C.14)) for many orders of magnitude. The vertical band represents the value of $\phi_0 \sim e^{\delta/2\epsilon}$.

to the exceptional potential (C.10). Indeed, one recovers (C.16) by replacing $\phi^2 \to \phi^2 + F^2$ in the $\phi^2 \log \phi$ term of (C.10), with the identification

$$\epsilon \equiv 1 - p \ll 1 \ . \tag{C.17}$$

Given that the series expansion near $p = 1$ is really an expansion in $(1-p)\log\phi$, the potential (C.14) can be safely truncated as (C.16) in a rather large range in field space, $\phi \lesssim \tilde{\phi}$, with

$$\tilde{\phi} \equiv e^{\frac{1}{2\epsilon}} \ F \gg F \ . \tag{C.18}$$

Therefore, in the $1 - p \ll 1$ limit (C.14) reduces to the exceptional potential $V_{\log}$ (C.10) in a large range of field space, except for small values $\phi \lesssim F$.

As explained above, the field amplitude ϕ_0 in the oscillon core must be large enough to have a significant binding potential, expressed as the condition (C.4) with δ of order of, say, $\sim 1/10$. Applied to the potential (C.16), this condition gives (since $\phi_0 \gg F$ we are confronting $\Delta V \simeq -\epsilon m^2 \phi_0^2 \log(\phi_0/F)$ with $\delta\, m^2\phi_0^2/2$)

$$\phi_0 \simeq e^{\frac{\delta}{2\epsilon}+\frac{1}{2}} \ F \tag{C.19}$$

which in the $\epsilon \ll 1$ limit is large but smaller than $\tilde{\phi} \sim \phi_0^{1/\delta}$ (in units of F).

In sum, in the $\epsilon \equiv 1 - p \ll 1$ limit, the approximation (C.16) is well justified and the oscillon amplitude is expected to lie in the window

$$F \ll \phi \ll \tilde{\phi}$$

where the potential is very close to the exceptional one (C.10), see Fig. C.1. This class of potentials is then expected to lead to oscillons with enhanced longevity is the limit $p \to 1$.

Scaling of the lifetime for $p \to 1$

The expectation above is confirmed by numerical simulations, which we will present in Sec. 3. In particular, when p is very close to 1, oscillon lifetimes increase seemingly without bound, and certainly to values that cannot be simulated in present day computers.

In the limit $\epsilon = 1 - p \to 1$, however, we can exploit the similarity of the monodromy potential with the form $\sim \phi^2 \log \phi$. Indeed, $V \simeq V_{\log}$ for a very large range in field space $F \ll \phi \ll \tilde{\phi}$ in the $\epsilon \ll 1$ limit. The oscillon lifetime then can be estimated by assuming that oscillons supported by (C.14) should be very close to the 'immortal' oscillons (C.12).

This suggests to split the solution as

$$\phi = \phi_i + \delta\phi \tag{C.20}$$

where ϕ_i is the 'immortal' solution (C.12) and we assume $\delta\phi$ is a small deviation from it in a large space-time region.[3] Plugging (C.20) into the equation of motion one arrives at

$$\Box\delta\phi + V''(\phi_i(t,r))\ \delta\phi = -\left(\Box\phi_i + V'(\phi_i)\right) \equiv j(t,r) \tag{C.21}$$

where terms of order $\delta\phi^2$ have been dropped. Using the equation of motion that ϕ_i satisfies, the source $j(t,r)$ is identified as

$$j(t,r) = -\left(V' - V'_{\log}\right)\Big|_{\phi=\phi_i} = \epsilon\, m^2\ \phi \left[\log\left(1 + \frac{\phi^2}{F^2}\right) - \log\left(\frac{\phi^2}{F^2}\right)\right]\Bigg|_{\phi=\phi_i} \tag{C.22}$$

The function $V'_{\log}(\phi) - V'(\phi)$ has a maximum at around $\phi \simeq 0.5\, F$, where it takes the value $\simeq 0.8\, \epsilon\, m^2\, F$. For small field values, $\phi \ll F$, it goes like $\sim -2m^2\epsilon\phi \log(\phi/F)$, and at large ϕ it decays like $\sim \epsilon\ m^2\ F^2/\phi$. Having in mind large amplitude oscillons with $\phi_0 \sim e^{\frac{\delta}{2\epsilon}+\frac{1}{2}}\ F$ as given in (C.19), this implies that the source term j is tiny. Compared to V' in the full solution, it is suppressed by a factor (neglecting logarithms)

$$\frac{|\, V' - V'_{\log}\,|}{V'} \lesssim \frac{F^2}{\phi_0^2} \sim e^{-\frac{\delta}{\epsilon}}\ . \tag{C.23}$$

While the characteristic size of the oscillon (where, say, most of the energy is concentrated) is $R \simeq \sqrt{2/\epsilon}\ m^{-1}$, the Gaussian approximation holds up to much larger distances. With the amplitude in the core $\phi_0 \sim e^{\delta/2\epsilon} F$, one expects the Gaussian profile to hold all the way up to $\phi \sim F$. Let us denote by $\tilde{R}$ the radius up to which the Gaussian profile is expected to hold,

[3] Of course, this assumption must break down asymptotically far away but still it is possible to see that there is a 'radiation zone' where $\delta\phi$ is small and takes energy from the oscillon core.

which is when $\phi \sim F$. Since at the origin the amplitude is (C.19) and we have the Gaussian profile, this is simply obtained from the condition $\exp\left(\frac{\delta}{2\epsilon} - \frac{\tilde{R}^2}{R^2}\right) \sim 1$, that is

$$\tilde{R} \sim \sqrt{\frac{\delta}{\epsilon}} R = \frac{\sqrt{\delta}}{\epsilon\, m} \ . \tag{C.24}$$

Note from the definition of $j(t,r)$ that this radius is where j is expected to be localized (a shell around the oscillon considerably far from its core radius R).

This relation also clarifies the main condition for the validity of the approximation (C.20): a well defined approximately Gaussian-shaped oscillon profile requires that there is a clear separation between R and $\tilde{R}$. This translates into the condition

$$\epsilon \ll \delta \ . \tag{C.25}$$

More quantitatively, a factor 10 in $\tilde{R}/R$ translates into

$$\epsilon \sim 10^{-2}\delta$$

Numerically one finds that δ is around 0.2 for $\epsilon \to 0$ (see Sec. 3.2), therefore the Gaussian approximation should be reliable for $\epsilon \lesssim$ few 10^{-3}.

Let us then proceed to estimate the lifetime of an oscillon in this regime. The effective scalar mass at the core $V''(\phi(t,0))$ is around $\simeq m^2(1-\delta-3\epsilon)$ (with spikes going up to m^2 when $|\phi| \lesssim F$). In the crudest approximation one can neglect the space- and time- variation in (C.21), and estimate the radiation from the massive KG equation with a source (C.22). Barring the potential resonant effects from the time dependent mass and source, one can then estimate the size of $\delta\phi$ upon integration of (C.21) as $\delta\phi \simeq j/m^2$. The emitted power can then estimated as $\dot{E} = 4\pi r^2 T^{0r} \simeq \tilde{R}^2 \partial_r \delta\phi\, \partial_t \delta\phi \sim \tilde{R}^2 \partial_r j\, \partial_t j/m^4$. Recalling that the maximal magnitude is $j \lesssim \epsilon F^2 m^2/\phi \sim \epsilon F m^2$ and using $\partial_t \sim \omega_{osc}$, $\partial_r \sim 1/\tilde{R}$, we arrive at the estimate

$$\dot{E} \sim \tilde{R}^2 \frac{w_{osc}}{\tilde{R}} \epsilon^2 F^2 \sim \sqrt{\delta}\epsilon F^2 \ . \tag{C.26}$$

On the other hand, the oscillon energy can be estimated as

$$E \sim R^3 m^2 \phi_0^2 \sim \epsilon^{-3/2} e^{\frac{\delta}{\epsilon}} \frac{F^2}{m} \ . \tag{C.27}$$

Combining (C.26) and (C.27) we arrive at the following estimate for the decay rate,

$$\Gamma = \frac{\dot{E}}{E} \ \sim \ \epsilon^2 \, \frac{F^2}{\phi_0^2} \, \frac{w_{osc}\, \tilde{R}}{m^2\, R^3} \ \sim \ \epsilon^{\frac{5}{2}} \, e^{-\frac{\delta}{\epsilon}} \, \sqrt{\delta}\, m \tag{C.28}$$

where we used $R \sim m^{-1}/\sqrt{\epsilon}$, and $\omega_{osc} \sim m$. We thus find an exponentially large lifetime as $\epsilon \to 0$, i.e. $p \to 1$. In Sec. 3.2 we will see that this simple formula correctly captures the magnitude and behavior of oscillon lifetimes.

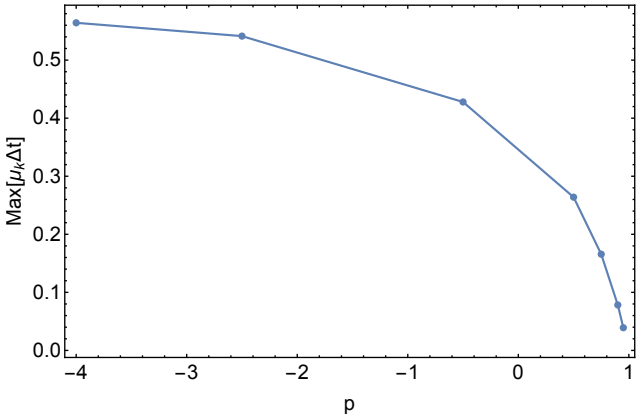

Fig. C.2: Maximal values of the resonance efficiency parameter $\mu_k \Delta t$ as functions of p for monodromy potentials.

Until now we have neglected gravity in our calculations. This is only valid if the oscillon is not particularly compact, i.e. as long as

$$\frac{R_S}{R} = \frac{2GM}{R} \sim \epsilon^{-1} e^{\frac{\delta}{\epsilon}} \frac{F^2}{M_P^2} \ll 1. \tag{C.29}$$

This translates into the upper bound $F \ll \sqrt{\epsilon}\ e^{-\delta/(2\epsilon)} M_p$, which is particularly strong for $\epsilon \ll 0.01$. However, for phenomenological applications an even stronger bound on F arises from dark matter overproduction, since the typical initial amplitude of the scalar field background required to form such oscillons also grows exponentially with ϵ^{-1}. This latter constraint is discussed in Sec. 4.

2.4 Floquet analysis

As argued at the beginning of this section, one of the conditions to ensure that oscillons can have long lifetimes is that resonant enhancement of short wavelength modes is suppressed. The aim of this subsection is to argue qualitatively that this is indeed the case for the monodromy potentials introduced in Sec 2.3.

We start by considering the Floquet diagram of an homogeneous oscillating scalar field with potential (C.14). Some examples of such diagrams have been presented in our previous work [20]. Their crucial feature is the existence of a broad resonance band at $k \lesssim m$, whereas only very narrow bands arise for $k > m$. The distance in k-space between these bands increases with p: in particular bands are denser for $p < 0$ than they are for $0 < p < 1$. Similarly, the values of the Floquet exponent μ_k are largest in the broad resonance band and increase with decreasing p, until they reach an approximately constant value for $p \ll -1$.

In analogy with the homogeneous case, we can understand the relevance of resonant enhancement for oscillons by considering the approximately spherical region of space $r \lesssim R$. Inside this region the localized field configuration is oscillating with amplitude $\phi_0 > \phi_{\rm out}$, where $\phi_{\rm out}$ is the amplitude of the field outside the lump (here we neglect the dilution of this amplitude due to Hubble friction).

The precise relation between ϕ_0 and $\phi_{\rm out}$ can be obtained numerically; for monodromy potentials (C.14) one finds that $\phi_0 \simeq 3\phi_{\rm out}$ during most of the oscillon lifetimes. Of course, only modes with $k \gtrsim R^{-1}$ can be enhanced, since those with $k < R^{-1}$ have wavelengths larger than the oscillon size, thus they cannot notice the presence of localized oscillations. Therefore, this implies that only modes with $R^{-1} \lesssim k \lesssim m$ can potentially undergo significant resonance.

Additionally, those modes are actually enhanced only while they remain inside the oscillon configuration. Each mode propagates through space with a phase velocity $v = \nu/k = \sqrt{m^2+k^2}/k$, thus it exits the lump after a time $\Delta t \sim R/v \sim R\ k/\sqrt{m^2+k^2}$. Therefore, modes are actually strongly enhanced only if $r = \mu_k\ \Delta t \gtrsim 1$.[4] Since the oscillon size R depends on ϕ_0 (through ϵ in the Gaussian approximation considered above), one can compute values of $\mu_k\ \Delta t$ as a function of ϕ_0 and k by means of standard Floquet methods, and extract its maximal size to understand the behavior of resonance with p.

The result of this analysis is shown in Fig. C.2 for some representative values of p, for which we have also numerically computed R as a function of ϕ_0. One can appreciate that $\mu_k\ \Delta t$ is always smaller than 1 for any value of $-4 < p < 1$. This suggests that resonance does not threaten the longevity of oscillons supported by the potentials (C.14) for those values of p, as confirmed by the numerical simulations which we present in the next section. Interestingly, resonance is shut off for $p \to 1$ and becomes more relevant for $p \ll -1$: as we will see, oscillon lifetimes will follow the opposite trend, with a notable exception around $p \simeq -1/2$.

3 Numerical Simulations

We now turn to a numerical investigation of oscillon lifetimes. We start by presenting a novel numerical strategy, then present results for different values of p.

3.1 Relax and Fast-Forward

In this section we focus on a numerical method to compute $\Gamma = \dot{E}/E$, which then controls the lifetime τ of oscillons. It is convenient to treat Γ as a function of ω so that we can write the differential equation

$$\Gamma(\omega) = \frac{\dot{E}}{E} = \frac{1}{E}\left(\frac{dE}{d\omega}\right)\frac{d\omega}{dt}, \tag{C.30}$$

which can be easily inverted to give

$$\tau = \int_{t_0}^{t_f} dt = \int_{\omega_0}^{\omega_f} \frac{d\omega}{\Gamma(\omega)}\ \frac{1}{E(\omega)}\left(\frac{dE}{d\omega}\right), \tag{C.31}$$

where $\omega_{0,f} \equiv \omega(t_{0,f})$ are some particular initial and final values for the frequency. In general, this equation can be numerically integrated to obtain the lifetime, and this is what we do in practice. However, as we will see in Fig. C.3, for certain values of p the function $\Gamma(\omega)$ shows a pronounced dip at some frequency ω_* where the oscillon will spend most of its lifetime. Here, both E and $dE/d\omega$

[4] Very much like in the early Universe parametric resonance is effective only if $\mu_k H^{-1} \gtrsim 1$.

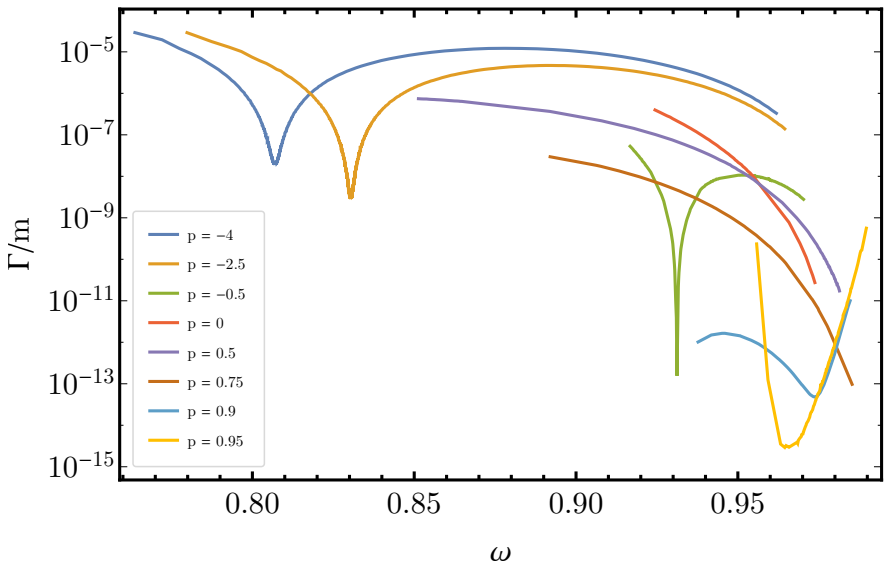

Fig. C.3: Numerical results for the decay rate $\Gamma(\omega)$, obtained using the relax and fast-forward method, for various values of p.

are constants to very good approximation. Calling $\Gamma_* = \Gamma(\omega_*)$, we can then write

$$\Gamma(\omega) \approx \Gamma_* \left[1 + \frac{\beta}{\omega_*^2} (\omega - \omega_*)^2\right], \tag{C.32}$$

where β is a dimensionless quantity. Insertion of (C.32) and $E \approx E_*$, $dE/d\omega = (dE/d\omega)_*$ into (C.31) allows us to obtain the following analytic expression for τ:

$$\tau \approx 2 \left(\frac{\omega}{E}\frac{dE}{d\omega}\right)_* \frac{\arctan\left(\sqrt{\beta}\right)}{\Gamma_* \sqrt{\beta}}, \tag{C.33}$$

where we have chosen $\omega_{0,f} \approx \omega_*$. This expression makes manifest that the expectation $\tau \sim \Gamma_*^{-1}$ can receive important corrections due to the other terms appearing in (C.33), a feature which is also maintained in the general calculation (C.31). Even though we will not be using this expression to estimate the lifetimes, we have nonetheless checked that the order of magnitude is still correctly predicted.

The next step is to generate data points $\{\omega_i, \Gamma(\omega_i), E(\omega_i)\}$. Recently, similar methods have been proposed [21–23]. In [21, 23], the authors assumed a certain profile with a single oscillation frequency and computed $\Gamma(\omega)$ by linearizing the field equation of the perturbations around such profile and computing the emitted power perturbatively in the small scalar waves. These (semi-analytic) results were then improved by the authors in [22] and were benchmarked against a full numerical simulation. Given that the single frequency approximation tends to overestimate the actual Γ [22], we choose to numerically solve the full relativistic non-linear equation of motion for ϕ (see Appendix A for details and [22] for a similar approach). The decay rate Γ is then obtained by numerically computing the outgoing flux at a position far away from the oscillon core (see Appendix B).

We parametrize initial conditions using

$$\phi(t=0,r)=\frac{A}{\cosh(r/\sigma)},\quad \dot{\phi}(t=0,r)=0, \tag{C.34}$$

where A, σ are free parameters that we vary. As one initializes the field according to (C.34) two things can happen: either the field quickly goes to the configuration $\phi=0$ or it settles into an oscillon configuration after a mild relaxation time $t_{\rm relax}$. Whether the former or the latter happens depends strongly on the choice of A,σ in (C.34), which is something that makes manifest both the chaotic and attractor nature of oscillons.

This is very useful because one can then trade time evolution with sampling of initial conditions. The strategy is to choose a set of N different initial configurations parametrized by (C.34) and evolve each of them a time $t_{\rm relax}$[5] until the oscillon configuration is found. Every initial configuration will find a different oscillon configuration, i.e. $\{A_i,\sigma_i\}\to\{\text{oscillon}(\omega_i)\}$ after a time $t_{\rm relax}$, with these configurations being related to each other by time evolution. All in all, this results in a huge numerical advantage since $Nt_{\rm relax}\ll\tau$. We refer the interested reader to Appendix C for a more in-depth explanation of this strategy, which we dub the *relax and fast-forward* method.

3.2 Results

In this section we present the numerical results that we have obtained with the numerical strategy outlined above. In particular, we give a complete picture of the lifetimes of oscillons in monodromy potentials, which has remained somewhat elusive until now, and we perform a dedicated analysis of the regime $1-p\ll 1$.

The first result is the shape of the function $\Gamma(\omega)$ for several values of p, which can be found in Fig. C.3. One can see that a dip appears for certain values of p. The tendency is to start from a shallow dip at small frequencies for negative large p that becomes deeper and closer to m as one approaches $p=0$. At $p=0$ the dip is lost and Γ tends to be a bit larger than at small negative p. This is followed by Γ getting increasingly smaller as p starts to get closer to 1, recovering a dip very close to m. In all cases, the trajectories terminate at some frequency close to m where we see the core amplitude collapse to $\phi=0$, corresponding to the death of the oscillon.

From the results shown in Fig. C.3 we can compute oscillon lifetimes using (C.31). Results are shown in Fig.C.4. The obtained lifetimes depend only mildly on the chosen initial frequency w_0 provided it isn't too close to the end of the Γ-w curve. The results shown in Fig. C.4 are obtained by integrating in the whole range depicted in Fig. C.3, for each p. For values of p corresponding to small enough lifetimes, the *relax and fast-forward* results have been benchmarked against the explicit time evolution of the corresponding oscillons during their whole lifetimes, whose values are reported in Table C.1. In particular, we find a maximum relative error of 7 %, which shows the quality of our method. We have also checked that these results are mildly sensitive to the choice of the initial profile (the order of magnitude of the lifetime isn't affected). This indicates that such long lifetimes are not artefacts related to fine-tuned initial conditions of [39].

The lifetimes shown in Fig. C.4 follow the dependence on p expected from our analysis of Sec. 2. In particular, the lifetime becomes insensitive to p as $p\to-\infty$ and approaches $\tau\sim 10^5/m$, that is the

[5]The exact value for $t_{\rm relax}$ depends on the particular initial condition and p.

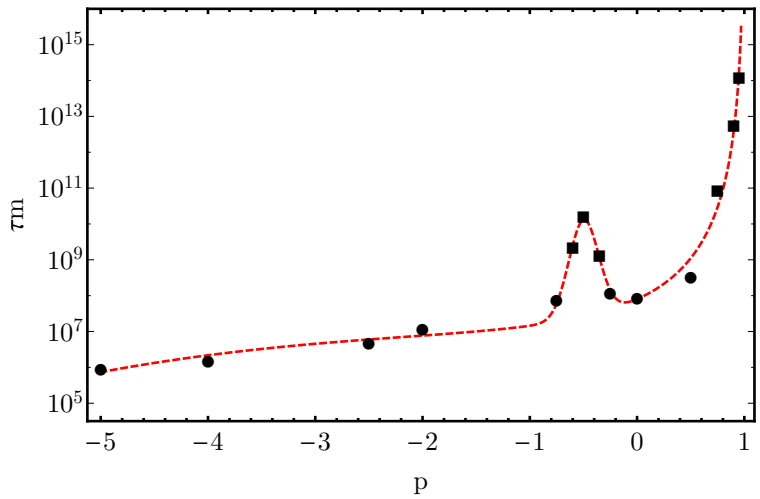

Fig. C.4: Lifetime τ of oscillons that we have studied (dots) in the family of potentials (C.14) as a function of p. Round dots have been benchmarked against an explicit numerical time evolution of the oscillon's whole lifetime, while square markers are results from the *relax and fast-forward* method only. Dashed line is merely an eye guide.

lifetime of oscillon supported by the potential (C.15). Secondly, the lifetime increases exponentially as $p \to 1$. Finally, we unexpectedly find a bump in the region $-1 \leq p \leq 0$, which appears to arise from an interplay between having a small and negative $V''(\phi)$ and being efficient in minimizing the binding potential. The power of our method is clear from our results for $p = 0.95$: we find $\tau \sim 10^{14}/m$, while following the oscillon evolution for such a huge lifetime would have taken $O(10^5)$ years using present day computers.

As we have argued in Section 2, the first step to understand oscillon longevity comes from the notions of *binding energy per particle*, encoded in $\Delta\omega$, and the binding potential 'fraction', δ, defined by (C.4). From the data of our simulations these quantities can be easily extracted and are shown in Fig. C.5, where we see a clear correlation between the binding frequency $\Delta\omega$ and the binding potential fraction δ. In particular, the tendency is that both $\Delta\omega$ and δ decrease as p increases. Typical values in simulations for different p give a range of δ from 0.1 to 0.85. This supports the criterion suggested above that δ must be a sizeable fraction of unity. Moreover, another result from Fig. C.5 is that in the $1 - p \ll 1$ limit, δ is of order 0.1 - 0.2.

Finally, obtaining the $\Gamma(\omega)$ curve becomes particularly challenging for $0.95 < p < 1$, due to

p	τm estimated	τm real	Relative Error (%)
-5	8.45×10^5	9×10^5	6.11
-4	1.39×10^6	1.5×10^6	7.33
-2.5	4.74×10^6	5×10^6	5.20
-2	1.13×10^7	1.2×10^7	5.83

Table C.1: Comparison between estimated lifetimes based on (C.31) and actual lifetimes for oscillons evolved with an explicit numerical time evolution (real) for some values of p.

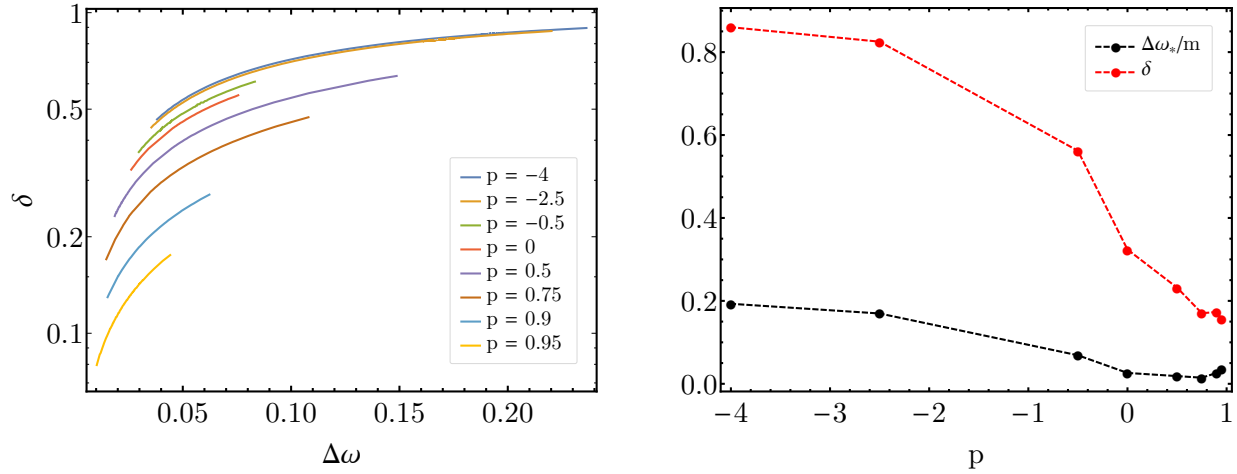

Fig. C.5: Extraction from the numerical simulations of the binding frequency $\Delta\omega \equiv m - w_{osc}$ and the binding potential 'fraction' $\delta \equiv 1 - \frac{V(\phi_0)}{m^2\phi_0^2/2}$ as defined by Eq. (C.4) with ϕ_0 the amplitude of oscillation at the core. The left panel shows the relation between δ and $\Delta\omega$ at each time (frequency) of the evolution. The right panel shows the relation obtained by selecting the typical frequency ω_* where the oscillon spends most time (corresponding to the minimum of $\Gamma(w)$ shown in Fig.C.3).

the fact that we must substantially increase the size of our lattice. Instead, switching to the (ϵ, δ) language with potential (C.16) allows us to test our analytic result (C.28) for Γ. We thus numerically solve the equation of motion with potential (C.16) by initializing the field with a Gaussian profile with parameters determined by (C.13). We evolve such configuration for a time $\sim (\epsilon\, m)^{-1}$ and show the results for Γ in Fig. C.6. From that, we see that Γ is only slightly overestimated by the analytic result (C.28), which however correctly captures the behavior with ϵ. This gives further numerical evidence that the lifetime of oscillons increase exponentially as $p \to 1$. Also, notice that even though we show really tiny values for Γ in Fig. C.6, the numerics are under control since the largest values for ϕ_0 that we explore are $O(10^8)\, F$.

It is instructive to look at the main numerical result summarized in Fig. C.4, from the perspective of the corpuscular picture. The lifetime τ turns out to be significantly larger than the estimate in 2.1 ($\tau \sim 10^4 m^{-1}$). Monodromy potentials are expected to enhance τ from classical field theory intuition, due to properties of the potential (flattening V and not too negative V''). Still, the dependence of τ on p seems quite remarkable. In particular there are two salient features: the extreme growth at $p \to 1$ and the peak near $p = -1/2$. The reason for the former is clear, the closeness to the $\phi^2 \log\phi$ exceptional potential. The origin of the peak is less clear to us at present, and seems more accidental.

4 Discussion and Conclusions

The observational impact of oscillons crucially depends on their lifetime. In this paper, we provided some analytical understanding for the observed extraordinary longevity of large amplitude oscillons as well as a novel numerical strategy to reliably compute their lifetimes.

We derived estimates from a simple corpuscular picture, which is valid at small coupling/large

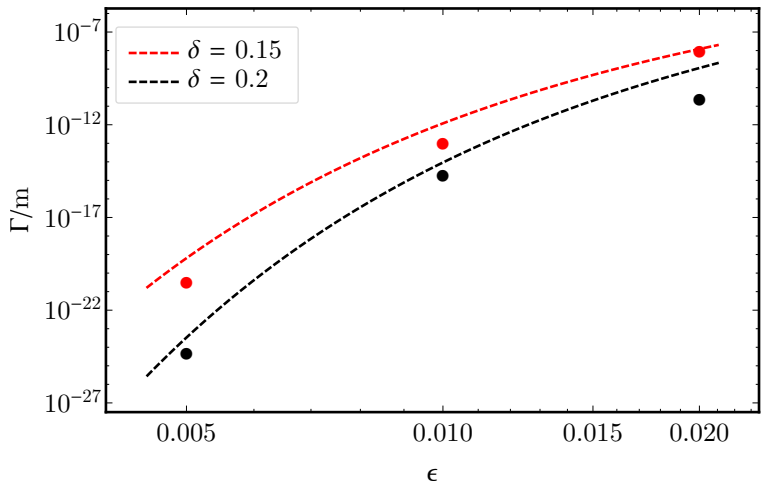

Fig. C.6: Decay rate Γ of oscillons for $\epsilon \equiv 1 - p \to 0$. Markers are data from numerics while dashed lines correspond to the analytic prediction (C.28).

occupation numbers and admits a classical field theory limit, to qualitatively reproduce the lifetime of oscillons supported by generic potentials, such as $\sim \phi^4$ or sine-Gordon $\sim \cos(\phi/f)$. The estimates assume no cancellations amongst various possible channels (encoded in the different self-couplings), but do not exclude that these cancellations might occur. Oscillons that are much longer lived than these estimates are supported by "monodromy"-like potentials, which at large field values behave as $V \sim \text{const.} + \phi^{2p}$ with $p < 1$. Despite several efforts in recent years, the ultimate reason for such long lifetimes and their behavior with p were not fully transparent.

In this work, we have argued that one way how these cancellations can occur is with potentials that flatten at large ϕ while keeping the effective mass $V''(\phi)$ as close as possible to the mass in vacuum, $m^2 = V''(0)$ (with negative but small $V''(\phi)/m^2$ being tolerated). The monodromy family of potentials satisfies this property and the numerical results, summarized in Fig. C.4, indeed show long lifetimes. This is most dramatic in the $p \to 1$ limit, as they approach the *exceptional* form $V_{\log} \sim \phi^2 \log \phi$. This logarithmic potential is known to admit eternal (non-decaying) oscillons [25, 26] so, in a way, the extreme longevity is inherited by 'proximity' with this exceptional theory.

Oscillons supported by monodromy potentials with $p \to 1$ can be studied both analytically and numerically, and our analysis shows that they are extremely long-lived (see Fig. C.6), with lifetimes many orders of magnitude larger than their cousins with $p \leq 1/2$, which were previously believed to be the most longeve oscillons [20]. Moreover, we presented a new numerical method to compute oscillon lifetimes, which is particularly useful when the evolution of a single oscillon is too long to be fully simulated on a computer.

Our results can have very interesting observational implications for light scalar dark matter. Let us briefly discuss some of them, while leaving a detailed study for future work (see e.g. [41] for a detailed analysis of observational consequences of oscillons in axion models). Fig. C.7 summarizes our findings for monodromy-like potentials. For $p \leq 0.95$ (left figure), we find that oscillons formed during the radiation-dominated epoch can survive until matter-radiation equality for masses as large as $m \sim 10^{-14}$ eV when p is close to unity. These overdensities may then act as seeds for the formation

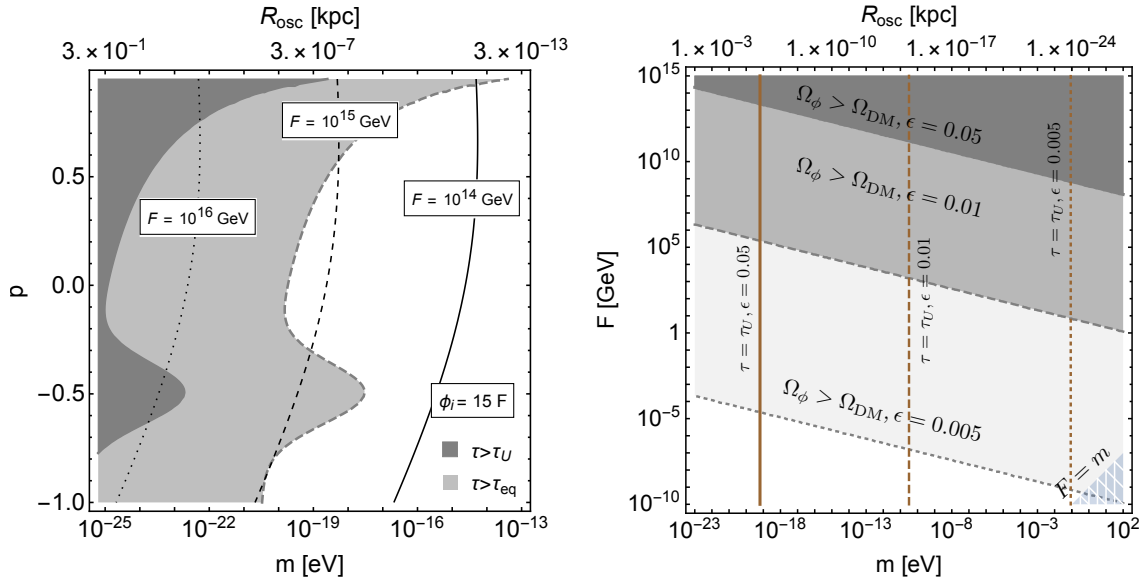

Fig. C.7: Left: values of p and m for which oscillons supported by monodromy-like potentials with $p \leq 0.95$ are stable until today (dark gray) or until matter-radiation equality (light gray). Contours of values of F for which the background scalar reproduces the dark matter abundance are also shown, when the initial field value is fixed to $\phi_i = 15\ F$. **Right:** Constraints on F and m for monodromy-like potentials with $\epsilon \equiv 1 - p \leq 0.05$ from dark matter overproduction. Values of the scalar mass for which oscillons are stable until today are denoted with vertical lines, which move to the right as ϵ decreases. In the lower right corner of the figure $F \sim m$ and the theory becomes strongly coupled. Close to this line, quantum annihilations in the oscillon core become important and alter oscillon lifetimes (see e.g. [13, 40]).

of structures. For $m \sim 10^{-19}$ eV and p close to unity, we find that oscillons can actually survive until today and thus potentially constitute a part of the dark matter. We confirmed that a window of negative values of p around $p = -1/2$, corresponding to plateau-like potentials, with longer lifetimes than their cousins with $0 < p \leq 1/2$ exists. However, in contrast to the expectations in our previous work [20], we found that decreasing p further decreases, rather than increases, an oscillon's lifetime. The origin of this window is still unclear to us and deserves further work.

Values of the scale F for which the oscillating background scalar field explains the observed dark matter abundance are also shown in the left plot in Fig. C.7 for an example choice of initial background field amplitude $\phi_i \sim 15\ F$, taking into account the delay in the onset of oscillations as p decreases. This choice is guided by requiring that self-resonance is efficient in the radiation dominated Universe (see e.g. [20]), so that the homogeneous field can undergo fragmentation, which would then provide initial conditions for oscillon formation.[6] Oscillon masses in this case can be extremely large when m is very small, the precise value depending also on p. In particular, for $p = -1$ we find $M > 10^8 M_\odot$ when $m \sim 10^{-25}$ eV, whereas for $p = 0.95$ we find that the same oscillon mass is obtained for $m \sim 10^{-22}$ eV. This can be used to constrain the left most region of the

[6] In general, the value of ϕ_i required to have efficient fragmentation increases as p increases. In particular, for $p \simeq 0.9$, a larger value of ϕ_i is required than in our example choice. Nonetheless, we find that for those large values of p the required ϕ_i is only a $O(1)$ factor larger than in our example choice.

left plot in Fig. C.7 (see e.g. [42, 43]), which is also further disfavored by galactic [44] and Lyman-α observations [45].

Nonetheless, we find that for $p \simeq -1/2$ and $p \lesssim 0.9$ oscillons with masses smaller than $10^8\ M_\odot$ can be stable today and contribute to the abundance of scalar dark matter when $F \sim 10^{15} - 10^{16}$ GeV and $m \sim 10^{-23} - 10^{-19}$ eV. Very interestingly, this is the mass range of Ultra-Light Scalar Dark Matter, where other bound structures (held together by gravity rather than by self interactions) can form at late times.

The observational impact of models with p very close to unity, which may be motivated by other frameworks (e.g. supersymmetry), is dramatically different, since oscillon lifetimes and core amplitudes increase exponentially with $1/\epsilon = 1/(1-p)$. Our results for this case are shown in the right plot of Fig. C.7. Oscillons can then be stable until today for scalar masses up to $m \lesssim 0.1 - 1$ meV, when $\epsilon \sim 0.005$. In order to understand the viability of this scenario, we fix the background amplitude required to obtain these oscillons from fragmentation to be equal to the core amplitude. The right plot in Fig. C.7 then shows that very large longevity comes at the expense of a much smaller scale F, since otherwise the background scalar field would overclose the Universe. For $\epsilon \sim 0.01$ the mass window extends to $m \lesssim 10^{-12}$ eV and larger values of $F \lesssim 10^4$ GeV are allowed.

Overall, our work presents evidence that the observational implications of self-interacting (ultra)light scalar dark matter may be even richer than what has been considered so far, due to the extreme longevity of oscillons supported by certain well-motivated potentials. A comprehensive study of these consequences is a promising task for future work.

Acknowledgments

We thank G. Dvali and M. Hertzberg for discussions and A. Arvanitaki, S. Sibiryakov and H. Zhang for helpful comments on the first version of this paper. The work of FR is supported in part by National Science Foundation Grant No. PHY-2013953. This work was partly supported by the grants FPA2017-88915-P and SEV-2016-0588 from MINECO and 2017-SGR-1069 from DURSI. IFAE is partially funded by the CERCA program of the Generalitat de Catalunya.

A Numerical Time Evolution

Time evolution of field configurations is generated by numerically solving the Euler-Lagrange equation of motion for ϕ with potential (C.14) and spherical symmetry,

$$\partial_t^2\phi(t,r) - \partial_r^2\phi(t,r) - \frac{2}{r}\partial_r\phi(t,r) + V'(\phi(t,r)) = 0. \tag{C.35}$$

It is convenient to rescale ϕ, t and r so that they become dimensionless. This can be achieved by doing $\phi \to \phi/F$ and $t, r \to mt,\ mr$. In the remainder of this section, ϕ, t and r will be understood to be dimensionless.

Discretizing the equation of motion in a lattice $0 \leq r_i \leq r_{\rm max}$ with spatial resolution $\Delta r \equiv$

$r_{i+1} - r_i$, the field configuration at time $t + \Delta t$ is given by

$$\phi(t+\Delta t, r_i) = 2\phi(t, r_i) - \phi(t-\Delta t, r_i) + (\Delta t)^2 \left[\frac{\phi(t, r_{i+1}) - 2\phi(t, r_i) + \phi(t, r_{i-1})}{(\Delta r)^2} + \frac{\phi(t, r_{i+1}) - \phi(t, r_{i-1})}{r_i \Delta r} - \phi(t, r_i) \left[1 + \phi(t, r_i)^2\right]^{p-1} \right], \tag{C.36}$$

where we have introduced the specific form of the potential (C.14). This equation is valid for all r_i except the first and last points of the lattice: $r_i = 0, r_{\max}$. For $r_i = 0$ we impose Neumann boundary conditions, while for $r_i = r_{\max}$ we implement second order absorbing boundary conditions following [14]. The typical sizes and resolutions that we use are $r_{\max} = 80$, $\Delta r = 0.05 = 5\Delta t$. We have written the code in Python.

B Computing Γ numerically

Oscillons slowly decay by emitting scalar waves, so we consider the outgoing flux at a position $r = r_d$ far away from the core and larger than the oscillon size R,

$$\Phi(t) = 4\pi r_d^2 \, \dot{\phi}(t, r_d) \, \phi'(t, r_d), \tag{C.37}$$

where derivatives of ϕ are computed numerically as

$$\dot{\phi}(t, r_d) = \frac{\phi(t, r_d) - \phi(t - \Delta t, r_d)}{\Delta t}, \quad \phi'(t, r_d) = \frac{\phi(t, r_d + \Delta x) - \phi(t, r_d - \Delta x)}{2\Delta x}. \tag{C.38}$$

This function will be oscillatory in time, so we will be interested in averaging it over a sufficient long period T, which we typically choose to be $T = N\Delta t \sim 10^2/\omega$. The decay rate Γ will then be

$$\Gamma = \frac{4\pi r_d^2 \left| \sum_{i=0}^{N} \dot{\phi}(t_i, r_d) \, \phi'(t_i, r_d) \right|}{NE}, \tag{C.39}$$

where $\dot{\phi}$, ϕ' are computed using (C.38) and $t_i = t + i\Delta t$. As for the energy E, it is computed using SciPy's *integrate.cumtrapz* method and is also replaced by an average in the period T.

C More Details of the Relax and Fast-Forward Method

The working principle of this method is that one can buy computing time from time evolution by sampling initial conditions. This is only an advantage if the relaxing time to reach the oscillon configuration when starting from a somewhat random initial configuration is much smaller than the total oscillon lifetime, $t_{\text{relax}} \ll \tau$. This happens due to the attractor nature of oscillons. As one can see in Fig. C.8, several different initial conditions as parametrized by C.34 cluster in parameter space after a mild relaxation time.

The second important observation is that the different configurations that are found after time t_{relax} are all part of the same oscillon and are related by time evolution. This is illustrated in Fig. C.9,

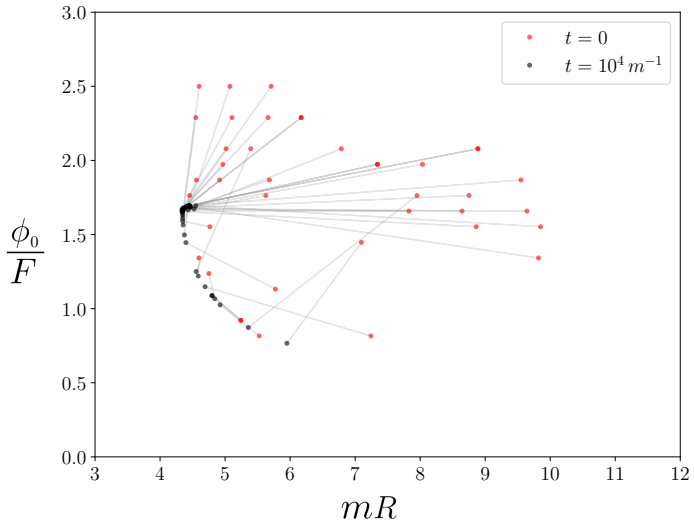

Fig. C.8: Different initial conditions evolved for a time $t = 10^4 m^{-1}$ for $p = -2.5$. ϕ_0 is the field amplitude at $r = 0$ and R is the oscillon size. One can see how different initial conditions cluster into the oscillon configuration. Lines connecting initial to final states are meant to be for identifying purposes, they are not the actual trajectories in parameter space. Here R is numerically computed as the position where 90 % of the energy in the lattice lies.

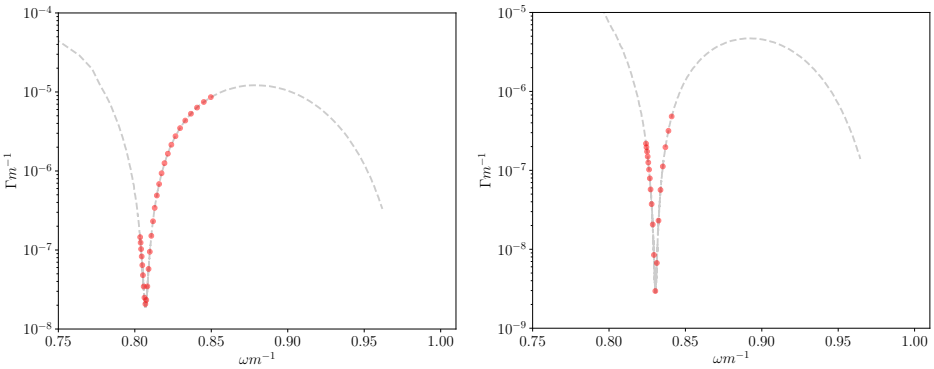

(a) p = -4 (b) p = -2.5

Fig. C.9: Comparison between points generated by the *Relax and Fast-Forward* method (red dots) and the full time evolution (black dashed). Each red dot comes from a *different* initial condition that is evolved for a time $t_{\text{relax}} = 10^4 m^{-1}$, while the black dashed lines are generated from a single initial condition by applying numerical time evolution.

where we see that different initial conditions all find the oscillon trajectory after a mild relaxation time $t_{\text{relax}} = 10^4 m^{-1}$ at different configurations (different values of ω).

In some cases, the lifetimes will be so large that the oscillon trajectory in parameter space will not be easily computable. What this means is that there will be some p's for which the black dashed curves of Fig. C.9 will not be known, and by exploring several initial conditions we will have to reconstruct them. This problem reduces to checking that the relaxation time is large enough, and this can depend not only on p, but also on the initial condition. Nevertheless, once one sees that a configuration barely moves in parameter space after a period of relatively fast movement, we can be sure that the configuration has relaxed into the oscillon. This is illustrated for a particular initial condition of $p = 0.9$ in Fig. C.10, where we have added the reconstructed trajectory.

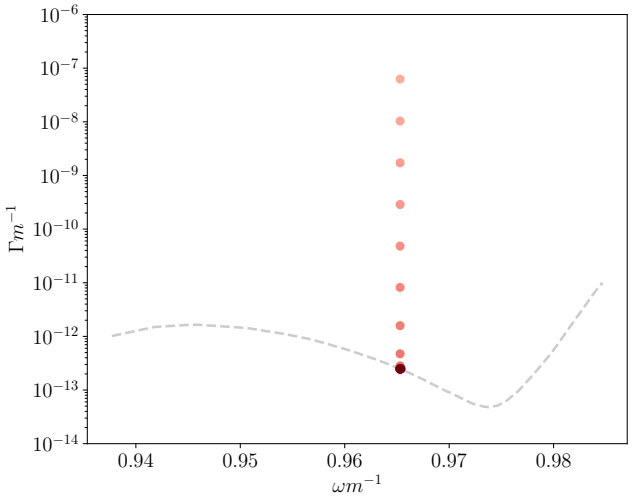

Fig. C.10: Example of relaxation of a particular initial condition for $p = 0.9$. Increasingly darker markers determines the direction of time. After a period of rapid evolution, the configuration ends in the attractor oscillon configuration.

References

[1] I. Bogolyubsky and V. Makhankov, "Lifetime of Pulsating Solitons in Some Classical Models," *Pisma Zh. Eksp. Teor. Fiz.*, vol. 24, pp. 15–18, 1976.

[2] M. Gleiser, "Pseudostable bubbles," *Phys. Rev. D*, vol. 49, pp. 2978–2981, 1994.

[3] E. J. Copeland, M. Gleiser, and H.-R. Muller, "Oscillons: Resonant configurations during bubble collapse," *Phys. Rev. D*, vol. 52, pp. 1920–1933, 1995.

[4] E. W. Kolb and I. I. Tkachev, "Nonlinear axion dynamics and formation of cosmological pseudosolitons," *Phys. Rev. D*, vol. 49, pp. 5040–5051, 1994.

[5] ——, "Large amplitude isothermal fluctuations and high density dark matter clumps," *Phys. Rev. D*, vol. 50, pp. 769–773, 1994.

[6] S. Kasuya, M. Kawasaki, and F. Takahashi, "I-balls," *Phys. Lett. B*, vol. 559, pp. 99–106, 2003.

[7] G. Fodor, P. Forgacs, P. Grandclement, and I. Racz, "Oscillons and Quasi-breathers in the phi**4 Klein-Gordon model," *Phys. Rev. D*, vol. 74, p. 124003, 2006.

[8] P. M. Saffin and A. Tranberg, "Oscillons and quasi-breathers in D+1 dimensions," *JHEP*, vol. 01, p. 030, 2007.

[9] G. Fodor, P. Forgacs, Z. Horvath, and A. Lukacs, "Small amplitude quasi-breathers and oscillons," *Phys. Rev. D*, vol. 78, p. 025003, 2008.

[10] M. Gleiser and D. Sicilia, "Analytical Characterization of Oscillon Energy and Lifetime," *Phys. Rev. Lett.*, vol. 101, p. 011602, 2008.

[11] G. Fodor, P. Forgacs, Z. Horvath, and M. Mezei, "Radiation of scalar oscillons in 2 and 3 dimensions," *Phys. Lett. B*, vol. 674, pp. 319–324, 2009.

[12] M. A. Amin and D. Shirokoff, "Flat-top oscillons in an expanding universe," *Phys. Rev. D*, vol. 81, p. 085045, 2010.

[13] M. P. Hertzberg, "Quantum Radiation of Oscillons," *Phys. Rev. D*, vol. 82, p. 045022, 2010.

[14] P. Salmi and M. Hindmarsh, "Radiation and Relaxation of Oscillons," *Phys. Rev. D*, vol. 85, p. 085033, 2012.

[15] E. A. Andersen and A. Tranberg, "Four results on ϕ^4 oscillons in D+1 dimensions," *JHEP*, vol. 12, p. 016, 2012.

[16] P. M. Saffin, P. Tognarelli, and A. Tranberg, "Oscillon Lifetime in the Presence of Quantum Fluctuations," *JHEP*, vol. 08, p. 125, 2014.

[17] K. Mukaida, M. Takimoto, and M. Yamada, "On Longevity of I-ball/Oscillon," *JHEP*, vol. 03, p. 122, 2017.

[18] M. Ibe, M. Kawasaki, W. Nakano, and E. Sonomoto, "Decay of I-ball/Oscillon in Classical Field Theory," *JHEP*, vol. 04, p. 030, 2019.

[19] M. Gleiser and M. Krackow, "Resonant configurations in scalar field theories: Can some oscillons live forever?" *Phys. Rev. D*, vol. 100, no. 11, p. 116005, 2019.

[20] J. Ollé, O. Pujolàs, and F. Rompineve, "Oscillons and Dark Matter," *JCAP*, vol. 02, p. 006, 2020.

[21] M. Kawasaki, W. Nakano, and E. Sonomoto, "Oscillon of Ultra-Light Axion-like Particle," *JCAP*, vol. 01, p. 047, 2020.

[22] H.-Y. Zhang, M. A. Amin, E. J. Copeland, P. M. Saffin, and K. D. Lozanov, "Classical Decay Rates of Oscillons," *JCAP*, vol. 07, p. 055, 2020.

[23] M. Kawasaki, W. Nakano, H. Nakatsuka, and E. Sonomoto, "Oscillons of Axion-Like Particle: Mass distribution and power spectrum," 10 2020.

[24] H.-Y. Zhang, "Gravitational effects on oscillon lifetimes," 11 2020.

[25] G. Dvali and A. Vilenkin, "Solitonic D-branes and brane annihilation," *Phys. Rev. D*, vol. 67, p. 046002, 2003.

[26] M. Kawasaki, F. Takahashi, and N. Takeda, "Adiabatic Invariance of Oscillons/I-balls," *Phys. Rev. D*, vol. 92, no. 10, p. 105024, 2015.

[27] E. Silverstein and A. Westphal, "Monodromy in the CMB: Gravity Waves and String Inflation," *Phys. Rev. D*, vol. 78, p. 106003, 2008.

[28] L. McAllister, E. Silverstein, and A. Westphal, "Gravity Waves and Linear Inflation from Axion Monodromy," *Phys. Rev. D*, vol. 82, p. 046003, 2010.

[29] G. Dvali and S. Zell, "Classicality and Quantum Break-Time for Cosmic Axions," *JCAP*, vol. 07, p. 064, 2018.

[30] M. Ibe, M. Kawasaki, W. Nakano, and E. Sonomoto, "Fragileness of Exact I-ball/Oscillon," *Phys. Rev. D*, vol. 100, no. 12, p. 125021, 2020.

[31] T. Vachaspati, *Kinks and domain walls: An introduction to classical and quantum solitons*. Cambridge University Press, 4 2010.

[32] G. Dvali and C. Gomez, "Black Holes as Critical Point of Quantum Phase Transition," *Eur. Phys. J. C*, vol. 74, p. 2752, 2014.

[33] ——, "Quantum Compositeness of Gravity: Black Holes, AdS and Inflation," *JCAP*, vol. 01, p. 023, 2014.

[34] P. Moxhay and K. Yamamoto, "Peccei-Quinn Symmetry Breaking by Radiative Corrections in Supergravity," *Phys. Lett. B*, vol. 151, pp. 363–366, 1985.

[35] B. Von Harling, A. Pomarol, O. Pujolàs, and F. Rompineve, "Peccei-Quinn Phase Transition at LIGO," *JHEP*, vol. 04, p. 195, 2020.

[36] J. A. Minahan and B. Zwiebach, "Field theory models for tachyon and gauge field string dynamics," *JHEP*, vol. 09, p. 029, 2000.

[37] B. Zwiebach, "A Solvable toy model for tachyon condensation in string field theory," *JHEP*, vol. 09, p. 028, 2000.

[38] F. Cooper, A. Khare, and U. Sukhatme, "Supersymmetry and quantum mechanics," *Phys. Rept.*, vol. 251, pp. 267–385, 1995.

[39] E. P. Honda and M. W. Choptuik, "Fine structure of oscillons in the spherically symmetric phi**4 Klein-Gordon model," *Phys. Rev. D*, vol. 65, p. 084037, 2002.

[40] M. P. Hertzberg, F. Rompineve, and J. Yang, "Decay of Boson Stars with Application to Glueballs and Other Real Scalars," 10 2020.

[41] A. Arvanitaki, S. Dimopoulos, M. Galanis, L. Lehner, J. O. Thompson, and K. Van Tilburg, "Large-misalignment mechanism for the formation of compact axion structures: Signatures from the QCD axion to fuzzy dark matter," *Phys. Rev. D*, vol. 101, no. 8, p. 083014, 2020.

[42] B. J. Carr and M. Sakellariadou, "Dynamical constraints on dark compact objects," *Astrophys. J.*, vol. 516, pp. 195–220, 1999.

[43] B. Carr and J. Silk, "Primordial Black Holes as Generators of Cosmic Structures," *Mon. Not. Roy. Astron. Soc.*, vol. 478, no. 3, pp. 3756–3775, 2018.

[44] N. Bar, D. Blas, K. Blum, and S. Sibiryakov, "Galactic rotation curves versus ultralight dark matter: Implications of the soliton-host halo relation," *Phys. Rev. D*, vol. 98, no. 8, p. 083027, 2018.

[45] T. Kobayashi, R. Murgia, A. De Simone, V. Iršič, and M. Viel, "Lyman-α constraints on ultralight scalar dark matter: Implications for the early and late universe," *Phys. Rev. D*, vol. 96, no. 12, p. 123514, 2017.